MCR-69-436   Copy No.

ADVANCED PROPELLANT
MANAGEMENT SYSTEM FOR
FOR
SPACECRAFT PROPULSION SYSTEMS

PHASE II - DETAIL DESIGN

SEPTEMBER 1969

N69-38172

FACILITY FORM 602

(ACCESSION NUMBER)

140

(PAGES)

NASA CR 101913

(NASA CR OR TMX OR AD NUMBER)

(THRU)

/

(CODE)

27

(CATEGORY)

MARTIN MARIETTA CORPORATION

MCR-69-436

Contract NAS9-8939

ADVANCED PROPELLANT MANAGEMENT SYSTEM
FOR
SPACECRAFT PROPULSION SYSTEMS

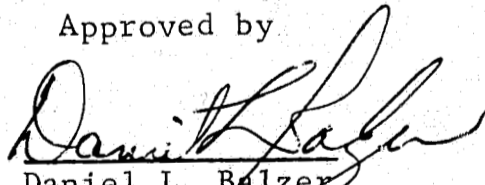## PHASE II -- DETAIL DESIGN

September 1969

Prepared for

NASA Manned Spacecraft Center

Houston, Texas

Prepared by

Daniel L. Balzer
Thomas R. Barksdale
Thomas E. Bowman
Dennis E. Gilmore
David N. Gorman
Ralph E. Hise

Approved by

Daniel L. Balzer
Program Manager

Martin Marietta Corporation
Denver Division
Denver, Colorado

FOREWORD

This document is submitted in accordance with Appendix A of Contract NAS9-8939, dated 21 November 1968. The report contains the results of the Phase II effort and represents the completion of the two-phase program.

This work was performed by the Martin Marietta Corporation under the technical direction of Mr. Larry Rhodes, NASA Technical Monitor.

CONTENTS

I. INTRODUCTION

During Phase I of this program, various techniques for positioning and retaining spacecraft propulsion system propellants for engine restart in the presence of upsetting body forces from the vehicle maneuvers were studied. The primary goal of the propellant control scheme was to provide gas-free liquid feed to the engine without the use of auxiliary propulsion for propellant settling maneuvers.

The reference configuration used for the study was the Apollo spacecraft propulsion tankage. A sketch of the tank envelope is shown in **Fig. I-1**. The guideline operating characteristics of the system are presented in Table I-1. The design goals for the advanced propellant management system designs are presented in Table I-2. The evaluation was divided into two different areas, subject to the following limitations:

1) No **hardware** changes to the system as outlined in Table I-1 and Fig. I-1;

2) No hardware limitations (any change to the configuration is permissible within the existing tankage envelope).

As **discussed** in the Phase I report (Ref I-1), six categories of propellant management systems were evaluated: nonmetallic bladders and diaphragms, metallic bladders and diaphragms, capillary forces, sliding seal pistons, metallic bellows, and miscellaneous systems. A summary of the results of the evaluation are presented in Table I-3. Based on these results, a capillary propellant management system was selected as the only technique of sufficient merit to be recommended for further study.

Capillary propellant management systems were selected for the Phase II detail design study for both the no-hardware-change and the no-hardware-limitation conditions. This report presents the results of this design study. Both analytical and experimental results are included.

The resultant capillary system designs are lightweight, versatile, and provide completely passive propellant control capability.

Table I-1 Propulsion System Characteristics

Oxidizer	Nitrogen Tetroxide, N_2O_4
Fuel	50% N_2O_4 - 50% $(CH_3)_2$ N_2H_2 (b.w.)
Pressurant Gas:	Helium
Entering Temperature	$-50 \rightarrow +120°F$
Tank Volume	161.3 ft^3 (see Fig. 1)
Operating Pressure	175 to 200 psia (nominal)
Oxidizer Flowrate	39.26 lb_m/sec
Fuel Flowrate	24.54 lb_m/sec
Feed Line Diameter	3.0 in.
Acceleration Levels:	
+g boost	$0 \rightarrow 7.35$
operation	$0.33 \rightarrow 0.94$
-g	$0 \rightarrow 0.2$
Transverse g	$-0.009 \rightarrow +0.009$
Roll g	$-0.001 \rightarrow +0\ 001$ (5 deg/sec)
Restart Condition	$\leq 10^{-5}g$ 5 sec prior to restart
Pitch Rate	5 deg/sec
Vibration Levels	10 to 1000 cps at 3 db/octave increase
	1000 to 1500 cps at 0.3 g^2/cps spectral density
	Decrease at 6 db/octave
	Time: 700 sec in each of three axes
Engine Duty Cycle:	
Number of Restarts	$0 \rightarrow 50$
Burn Duration	1 sec $\rightarrow$ propellant depletion

Fig. I-1 Oxidizer and Fuel Tanks

Table I-2 System Design Goals

<u>Priority I</u>

    1)   Passive operation (no auxiliary propulsion settling required);

    2)   99.5 percent expulsion efficiency (by volume);

    3)   10 lb/tank;

    4)   No pressurant gas ingestion at tank outlet.

<u>Priority II</u>

    1)   Not affected by propellant slosh;

    2)   Operation in either negative or positive acceleration field;

    3)   No hardware changes to the propulsion system as outlined in Table I-1 and Fig. I-1;

    4)   No engine duty cycle limitations;

    5)   No off-load propellant limitations;

    6)   Multicycle capability;

    7)   Propellant exposure tolerance of system in the range of one year without replacement;

    8)   Series tankage capability.

Table I-3 Propellant Control Systems Evaluation Summary

Technique / Criteria	Nonmetallic		Metallic*		Capillary Retention	Sliding Seal Pistons	Metallic Bellows
	Bladders	Diaphragms	Design A Cylindrical Rolling Diaphragm	Design B-2 Conospheroid Reversing Diaphragm			
Expulsion Efficiency, % (99.5% Goal)	98	99.5	99.5	99.5	99.5	99.5	97 - 99
Volumetric Efficiency Within Tank Envelope, % (Fig. 1)	99.8	99.9	99	66	99.9	75	75
Weight, lb (10-lb Goal)	32	38	104	$32^\dagger$	10.7 - 18.7	$94^\dagger$	$91^\dagger$
Pressurant Ingestion	Permeation of Pressurant	Permeation of Pressurant	None	None	Dissolved Pressurant	None with Good Seal Performance	None
Hardware Changes	Minimal Tank Redesign	Modest Tank Redesign	Modest Tank Redesign	Extensive Rank Redesign	Retrofit Possible	Extensive Tank Redesign	Extensive Tank Redesign
Duty Cycle Limitations	None	None	None	None	No. Restarts Constrained	None	None
Off-Load Propellant Limitations	Off-Load Not Desirable	Off-Load Not Desirable	Off-Load Not Desirable	Off-Load Not Desirable	None	None	None
Cycle Life	≈20	≈20	1 Reversal	≈6	>1000	1 Cycle	>1600
Propellant Exposure Tollerance, Yr (1-Year Goal)	1	1	>1	>1	1	1	>1
Series Tankage Capability	No	No	No	No	Yes	No	No
State-of-the Art[‡]	1	1	5	4	1	3	2
Development Time and Cost[‡]	2	2	4	3	1	4	3

*All metallic systems are rated based upon titanium construction.

[†]Tank weight additions due to configuration change not included.

[‡]Relative Ratings - 1 through 5 where 1 represents best rating and 5 poorest. No absolute value significance is intended.

II. DESIGN CONFIGURATIONS

Although a primary objective of the propellant management system designs considered was to be adaptable to the propulsion system configuration as outlined in Fig. I-1 without any hardware changes, the evaluation also included designs that were not restricted to any hardware limitations. In both cases a capillary system was selected as the most promising technique. The recommended configuration for the no-hardware-change restriction (retrofit capability to the existing tankage) is shown in Fig. II-1 with that for the no-hardware-limitation case shown in Fig. II-2. An identical design is used for both the fuel and oxidizer tanks. The propellant properties are such that in general the oxidizer system was the primary sizing consideration. Use of the same design for both propellants then results in a wider performance margin for the fuel tank.

Both designs are functionally similar with the only basic differences being the added support structure for the retrofit design to permit installation of the device through the tank manhole, and the concentric sump around the stillwell to adapt the design to the existing stillwell and gaging system. The evaluation of this configuration rather than other potential capillary configurations such as total liners, collection ducts, or simple lateral barriers is discussed in pages 56 to 67 of the Phase I report (Ref I-1).

The primary variables that influenced the selected design were the operational acceleration environment, as shown on Fig. II-3, and the requirement for 50 restarts independent of the system thrust profile. The restart requirement determines the maximum quantity of trapped propellant required while the acceleration environment is the primary sizing criteria for the capillary barrier retention requirements.

The operating philosophy of both designs is identical and therefore separate discussion and analysis are not required. Basically the propellant management system consists of two compartments located over the tank outlet, as shown schematically in Fig. II-1 and II-2. The compartments are formed by porous conical barriers across the tank diameter. The barriers offer very little resistance to liquid flow, but when in a wetted condition provide a relatively high resistance to gas penetration. Therefore by proper pore size selection the conical barriers form a pressure-stabilized interface that will retain liquid within the compartments during adverse acceleration environments.

Capillary
Barriers

Ring Frame

Tension
Support

Pleated Screen
Liner

A

A

Manhole and Inlet

Center Support
Capillary
Barriers

Dome Flanges
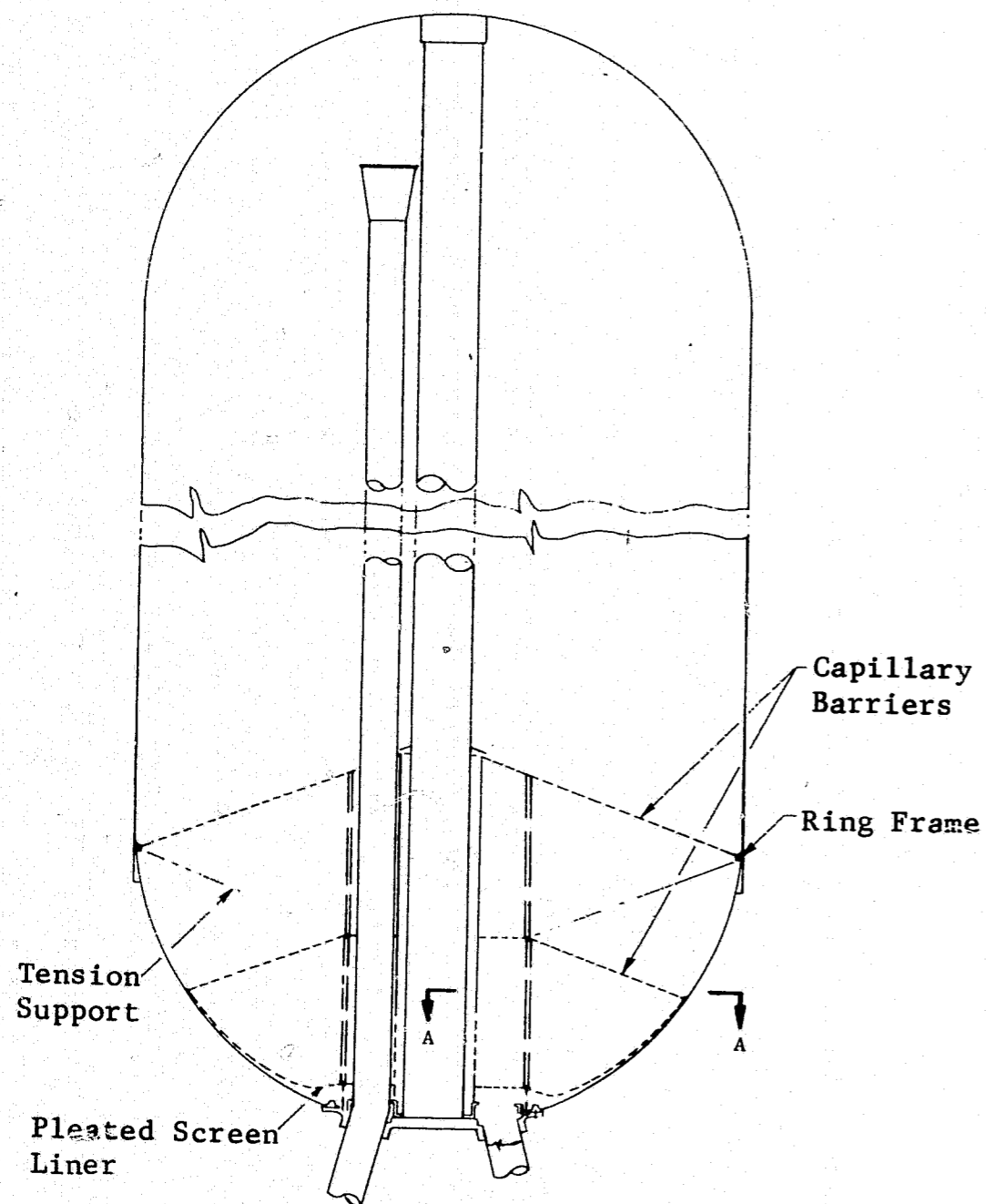
Outlet

Pleated Screen Liner

Fig. II-1 Retrofit Capillary Configuration
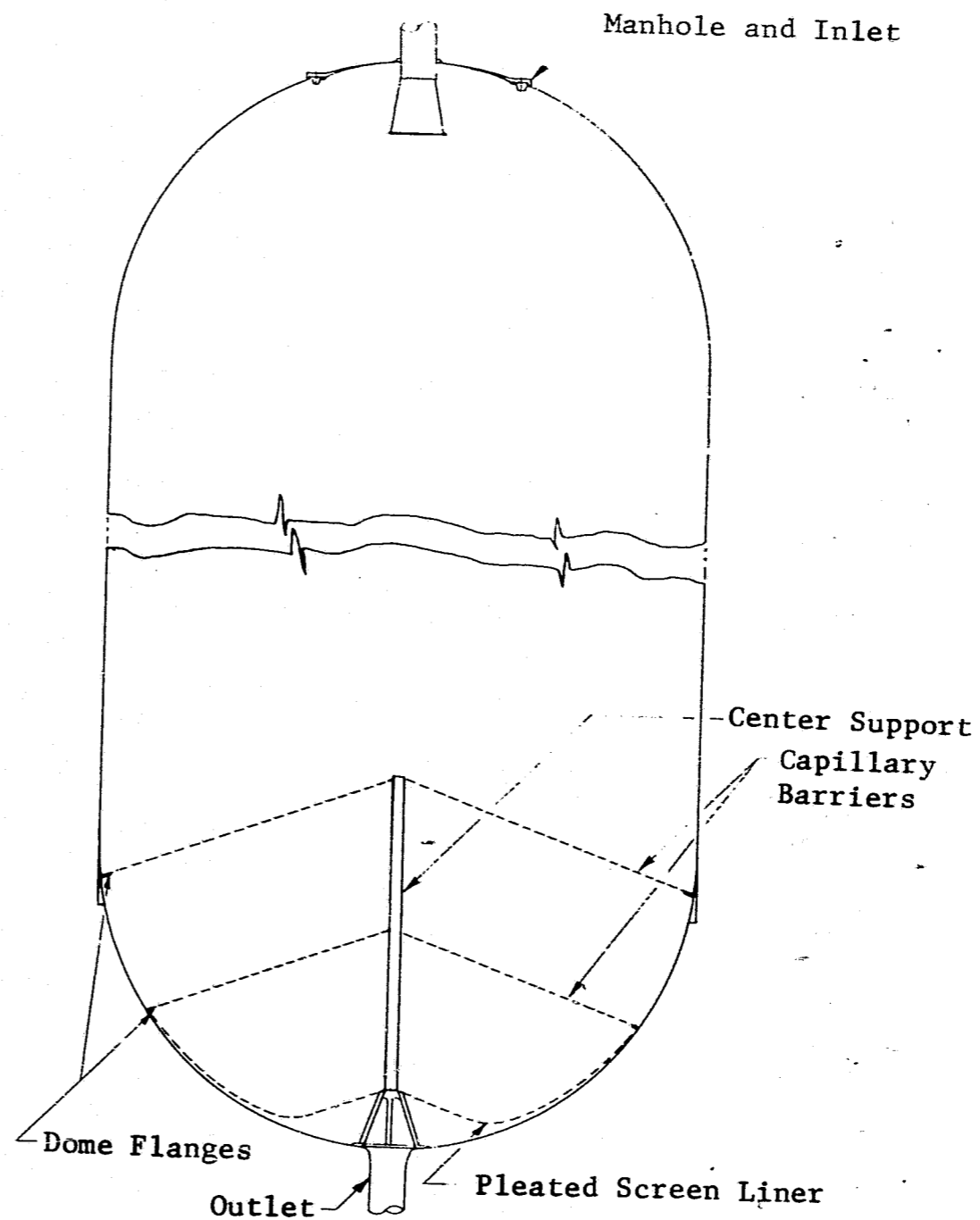
Fig. II-2 No-Hardware-Limitation Capillary Configuration
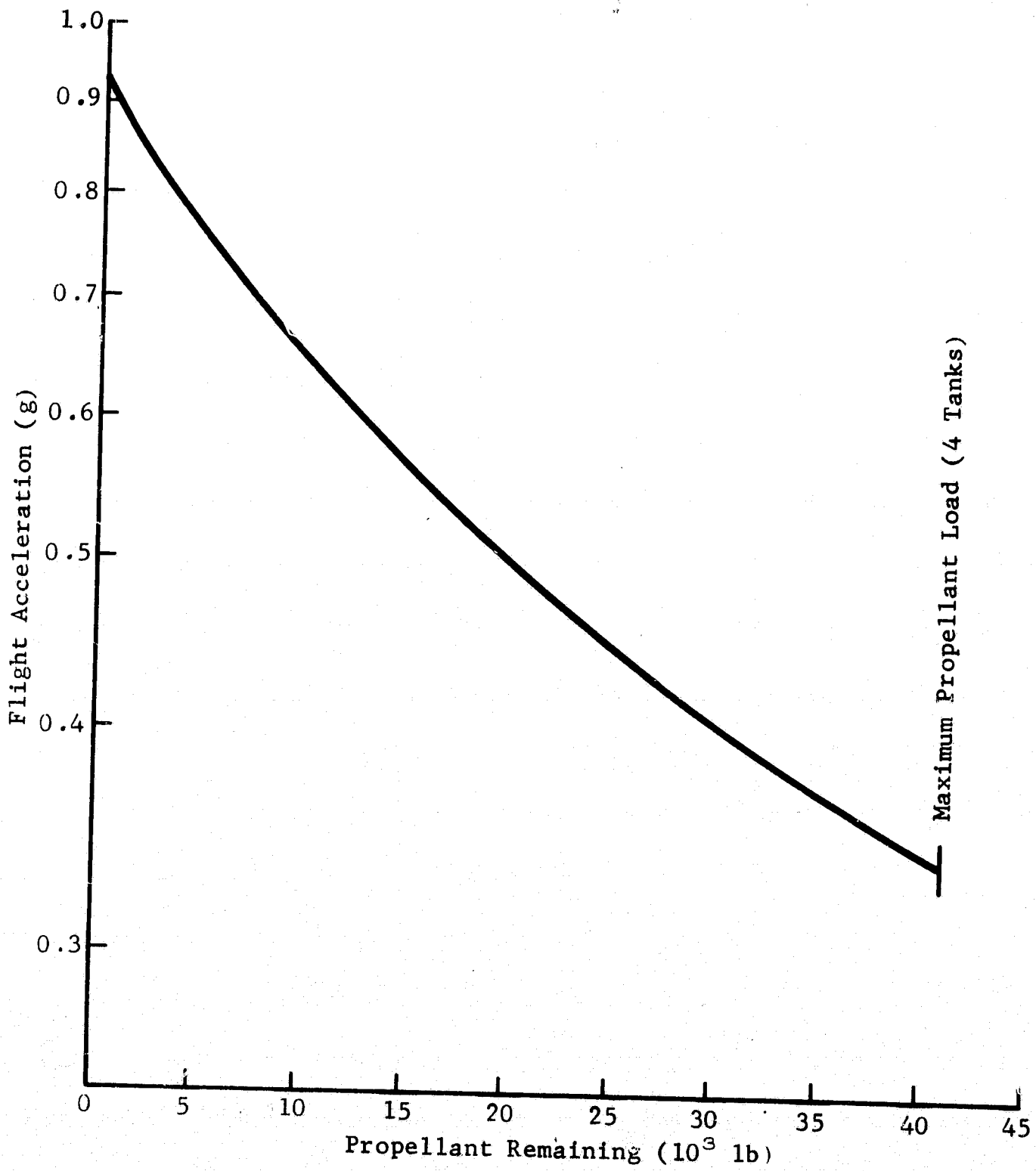
Fig. II-3 Powered Flight Acceleration Profile

The compartment immediately over the outlet contains a capillary barrier adjacent to the tank wall (screen liner) that prevents gas ingestion to the outlet until the liquid in the compartment has been completely expelled. The volume contained within the two compartments is approximately 22 cu ft, which is that required to restart the engine 50 times. The upper compartment contains 17 cu ft with 5 cu ft in the lower compartment. During operation all of the liquid in the tank is drained into the lower compartment before depletion of this compartment. During steady-state thrusting in excess of the propellant resettle time, the compartments will begin to refill with liquid purging any trapped ullage into the main tank ullage area due to the hydrostatic head developed in the liquid. Because refill is not required to meet the mission requirements, this feature makes the compartment capacity highly conservative.

A. DESIGN DESCRIPTION OF NO-HARDWARE-MODIFICATION CONFIGURATION

The SPS propellant retention structure is designed as a modular assembly to be installed through the tank manhole. The design is shown in Fig. II-4. The outer structure assembly (-009) is attached to the inside flange of the tank manhole at the existing attachment holes. The upper support of this assembly is maintained using a preloaded ring. This ring is preloaded in compression to allow the ring to expand with the tank wall when the tank is pressurized.

The four tension spokes connecting the ring to the middle screen inner flange stabilize the ring and tie the upper structure together. The tank deflection during pressurization will allow the upper ring to expand. The expansion holds the middle screen outer seal against the tank by means of the tension spokes. The lower assembly has tension straps across the lower corners to stabilize the structure. All tension members are used to hold the outer flanges in place during negative axial accelerations.

The inner tube of the outer screen assembly (-009) provides a direct load path connecting the screens and the tension spoke hub with the manhole ring. This tube also provides close tolerance seal retainers that are one-piece rings providing both structural continuity of the outer screen assembly and sealing surfaces for the inner-to-outer screen joints.

Section E
No Scale

Connecting Joint for Frame

Brackets
(4 Plcs)

Section F
No Scale

Double Perforated
Plate (.020 Dia)

Dutch Twill Screen
(30 x 250 Mesh) with
Perforated Sheet (.020 Dia)
Backup (Stainless Steel)

Dutch Twill Screen
(30 x 250 Mesh) with
Perforated Sheet (.020 Dia)
Backup (Stainless Steel)

Tension Strap
(13 Plcs)

Pleated
Screen
Liner

Screen
.015

Perforated Plate
.31 x .35 x .015
Each Side

Section D
No Scale

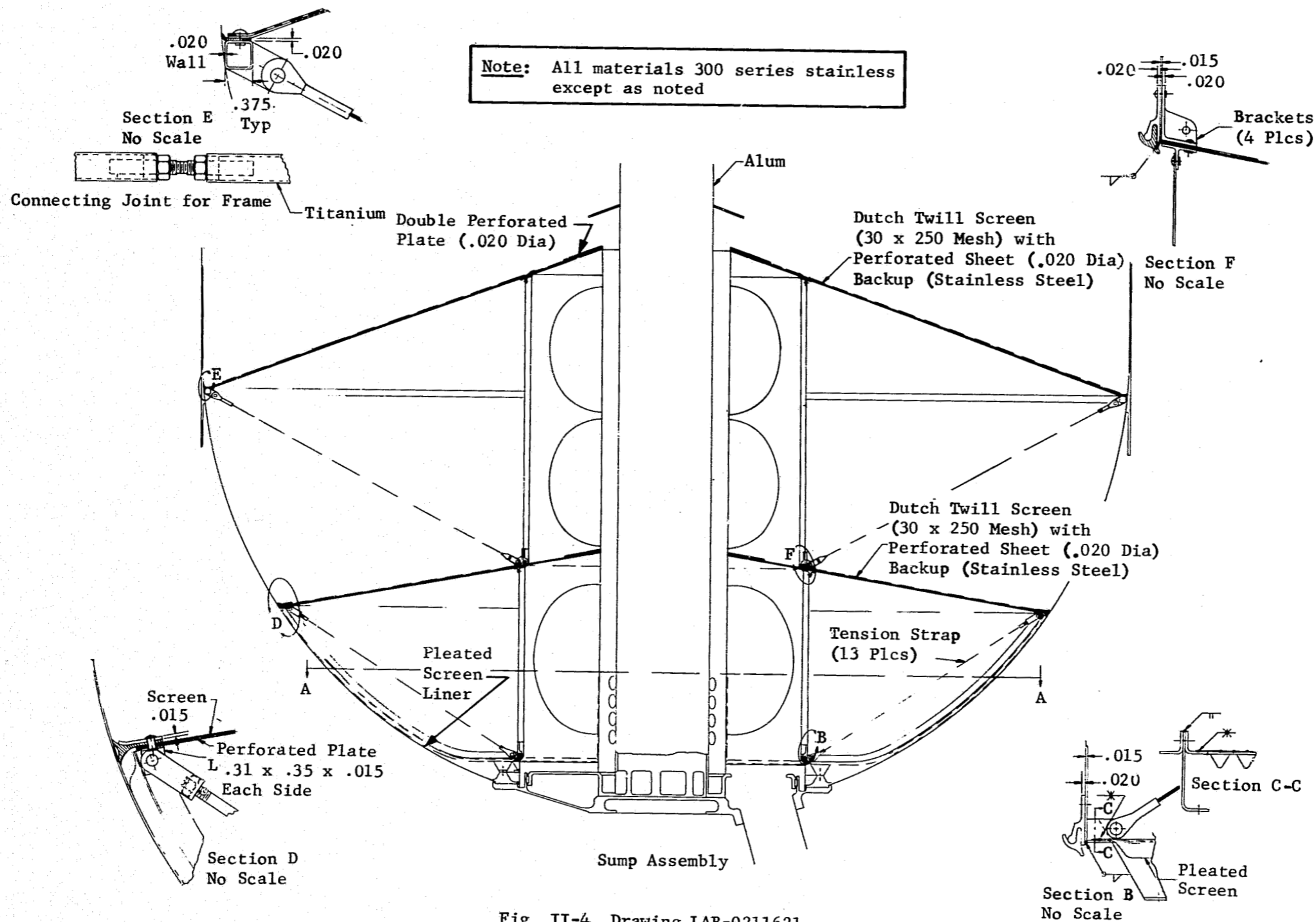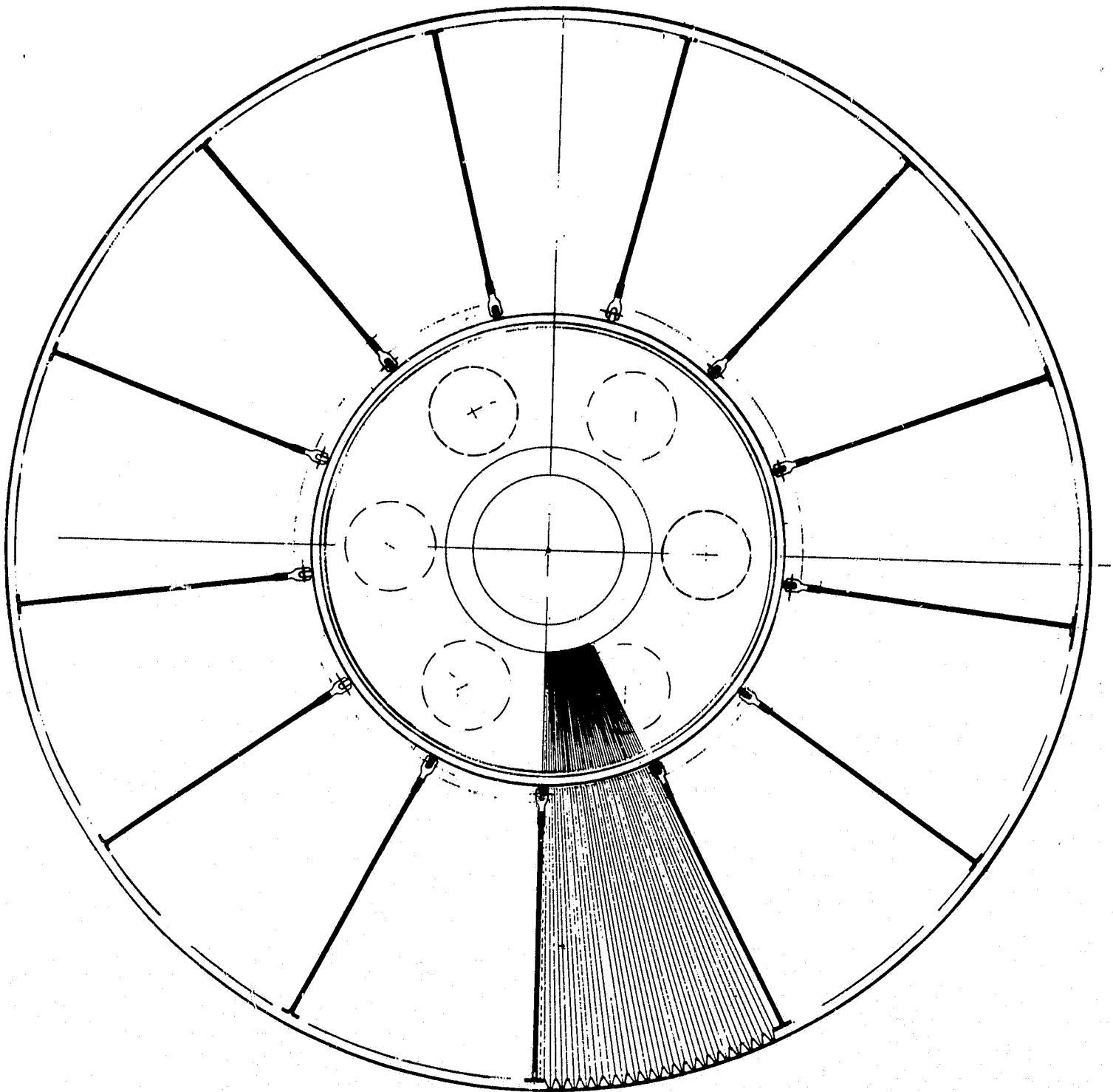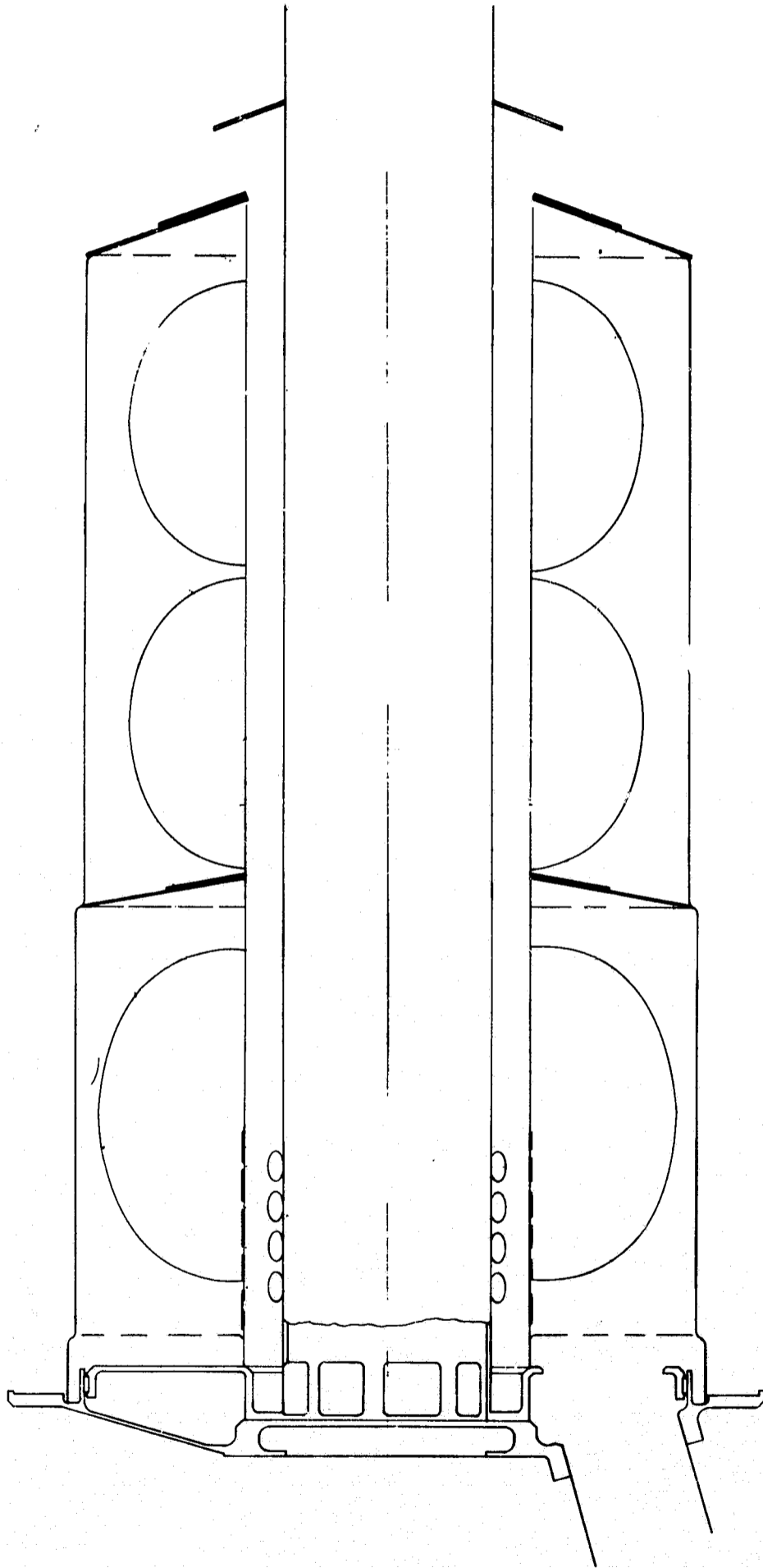Sump Assembly

Section C-C

Pleated
Screen

Section B
No Scale

Fig. II-4   Drawing LAB-0211621

Section A-A

Fig. II-4 (cont)

-019 Assembly

Fig. II-4 (cont)

Note: This assembly must be assembled thru tank stillwell access cover. See installation procedure for steps.
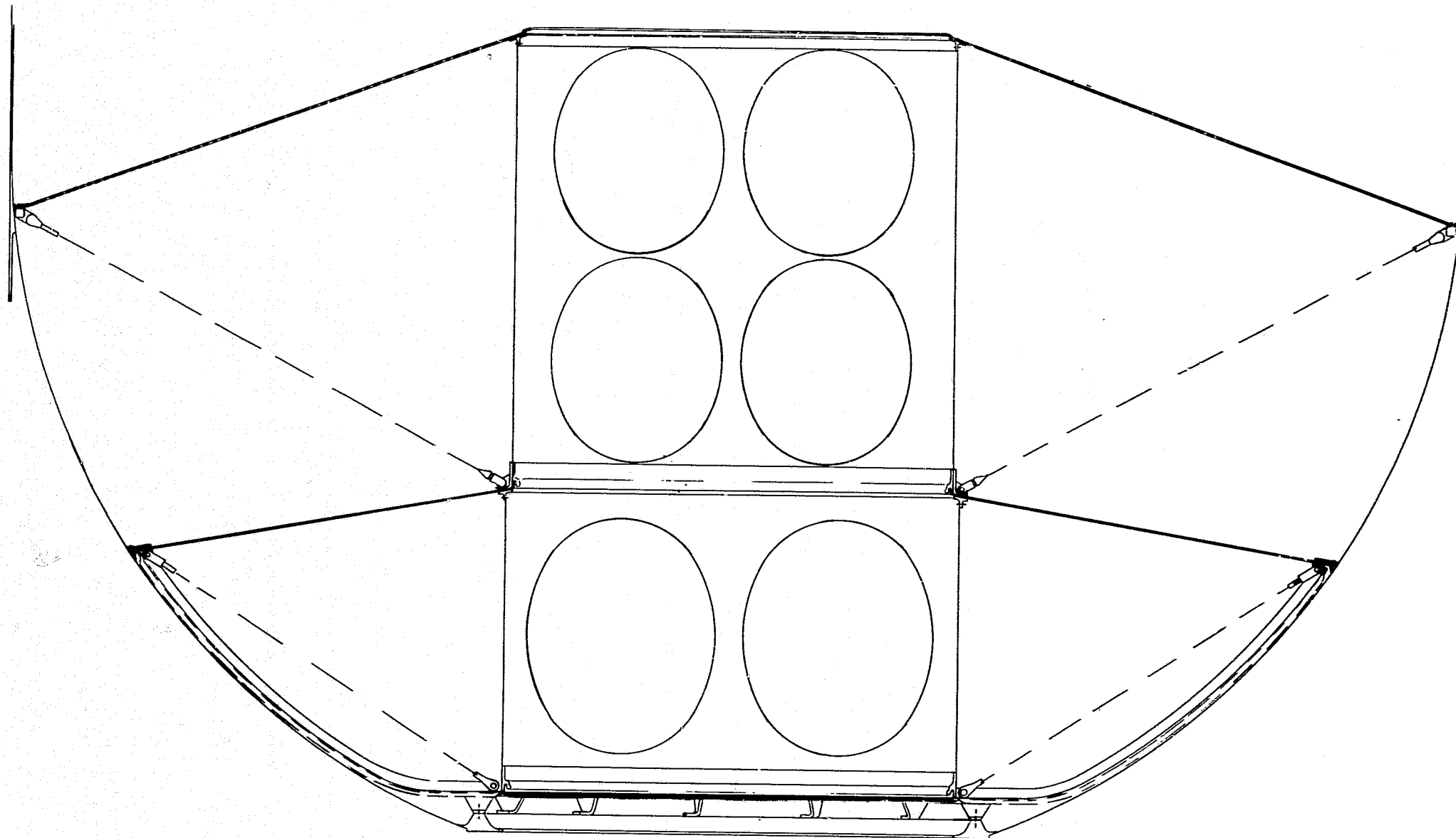
-009 Assembly

Fig. II-4 (concl)

The inner screen assembly (-019) consists of an annular chamber with screens installed within the annulus as shown. This assembly is installed on the manhole door so that when the door is installed, the tube shoulders will mate with the seals of the outer screen assembly (-009). The double tube resulting from assembly and sealing requirements provides additional stabilizing of the screen structure. The tubes are perforated to permit relatively unrestricted liquid flow between the compartments.

The total weight of the SPS propellant retention structure is 19 lb. This design was based on achieving the lightest weight structure compatible with the assembly restrictions. The 19-lb weight of the design should be considered a minimum as derived from approximated steady-state load factors.

Assembly Description (No Hardware Modification) - Procedures for installation of LAB-0211621-009 assembly through the manhole in the tanks V37-343102 NAA for SPS Propellant Retention Assembly are presented below:

1) Each annular screen is preassembled before installation. There are 13 assemblies which include: pleated screen, leg angles, edge angles, flat ring. Figure II-5(a) shows a detail view with the various parts identified;

2) The first part to be placed in the tank through the manhole is the titanium support ring assembly. This assembly includes a titanium tube (square) with threaded ends and brackets in four places. The ring is adjusted in compression to 845 lb [Fig. II-5(b)];

3) The first of the 13 assemblies from step 1) is bolted to the internal flange of the tank. The second of the 13 assemblies is bolted to the flange and bolted with angle brackets and tension support holders to the first screen assembly. This procedure is continued until the 13 screen assemblies are bolted to the flange and the adjoining screen assembly [see Fig. II-5(c)]. A seal weld between edge angles and legs for sealing is completed as each screen assembly is placed in the tank; Fig. II-5(a);

4) Install the external lower tube into the tank and seal weld to the screen sections [Fig. II-5(a)];

5) Rivet the angular tee section to the top of the lower external tube [Fig. II-5(d)];

(a) Screen Details

Pleated Screen

Leg Angles

External Lower Tube

Flat Ring

Pleated Screen

Connecting Joint for Frame

Titanium
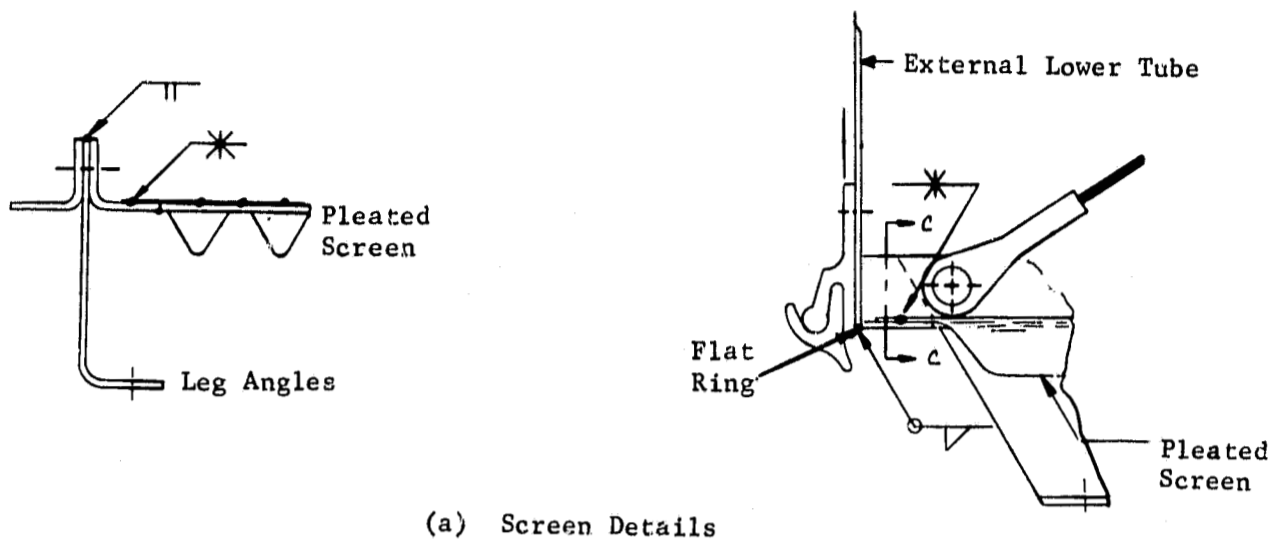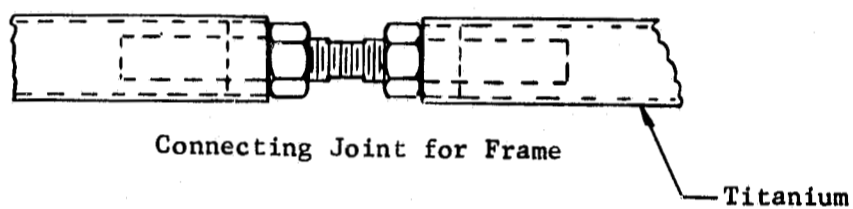
(b) Support Ring Adjustment

Screen

Seal

Perforated Plate

Screen Assembly
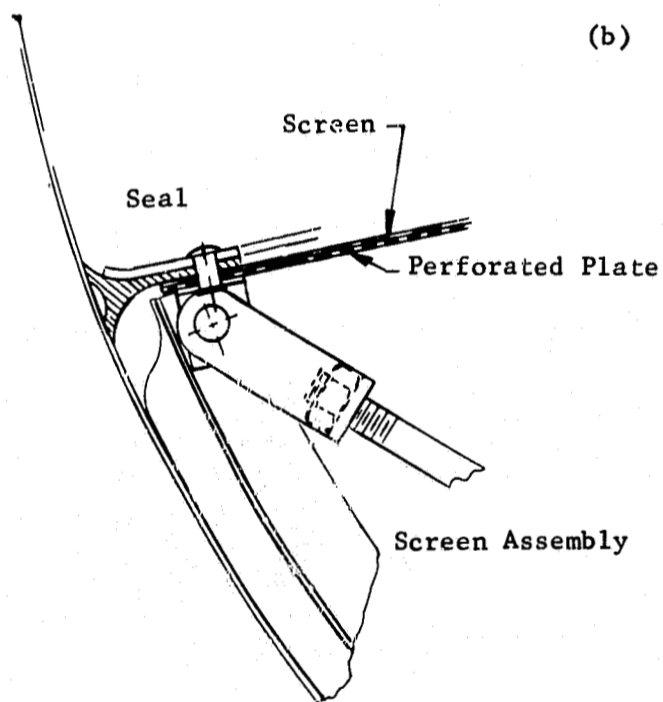
(c) Outer Seal Ring Details

Upper Extension

Seal Holder

Tension Strap Brackets

Tee
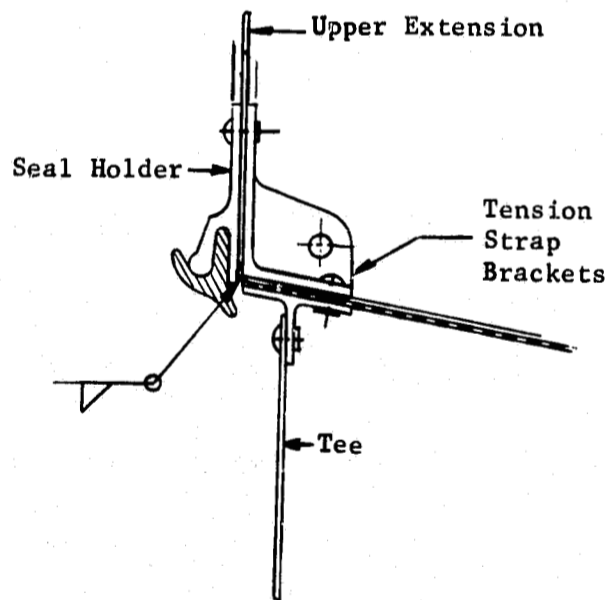
(d) Outer Tube Middle Seal
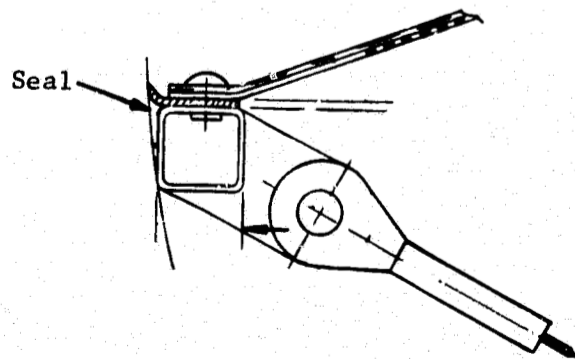
Seal

(e) Top Peripheral Seal

Fig. II-5 Retention Assembly Details

6) Position tension straps and bolt with nuts, lock washers, and safety wire. Adjust the tension of the straps by hand, tightening the nut on the top bracket;

7) Install lower perforated plate and screen barrier sections and resistance weld in place;

8) Rivet in seal and holddown rim to lower screen assemblies [Fig. II-5c];

9) Rivet upper tension strap bracket to the screen, plate, and tee (four places), see Fig. II-5(d);

10) Rivet upper external tube section to seal holder and brackets [Fig. II-5(d)];

11) Rivet seal holder and brackets to upper tube and seal weld as shown in Fig. II-5[d];

12) Install four upper tension straps and adjust tension by hand tightening nuts;

13) Rivet upper tee section to the top of external top tube;

14) Install screen and plate in 11 sections and resistance weld where needed;

15) Rivet seal and upper plate to upper support ring [Fig. II-5e].

Assembly -019 is installed on the coverplate and the system installation completed by bolting the coverplate onto the tank manhole.

B. DESIGN DESCRIPTION OF NO-HARDWARE-LIMITATION CONFIGURATION

The no-hardware-limitation design shown in drawing LAB-0211620 (Fig. II-6), uses integral flanges on the dome to attach the retention system coverplate edges. The screen structure is installed in the dome before tank closure so that a minimum number of parts is used. The screen structure is a double tent arrangement with a center support. The center tube has a quadrapad foot design to allow flow into the centered outlet. The foot is stabilized by a ring that seats on the outlet. The top screen is preloaded at the center pole by the adjustable attachment to hold the center pole firm on the tank bottom. The only attachment to the tank is at the screen-dome junctures. The outlet flange has a seat for the center pole foot ring for lateral load capability and installation location. The upper cone outer edge is firmly attached to the wall flange located at the junction of the cylindrical and spherical sections. The lower cone edge is attached to the flexible convulate ring, which in turn is attached to the tank wall flange (Fig. II-7). The convolute joint permits expansion of the dome during pressurization without structural failure.

Perforated
Plate
Section A-A

Double Perforated Plate
(.020 Dia)

Dutch Twill Screen (30 x 250 Mesh) with
Perforated Sheet (.020 Dia) Backup
(Stainless Steel)

Double Perforated Plate
(.020 Dia)

Dutch Twill Screen (30 x 250 Mesh)
with Perforated Sheet (.020 Dia)
Backup (Stainless Steel)

Pleated Stainless Steel
Dutch Twill Screen
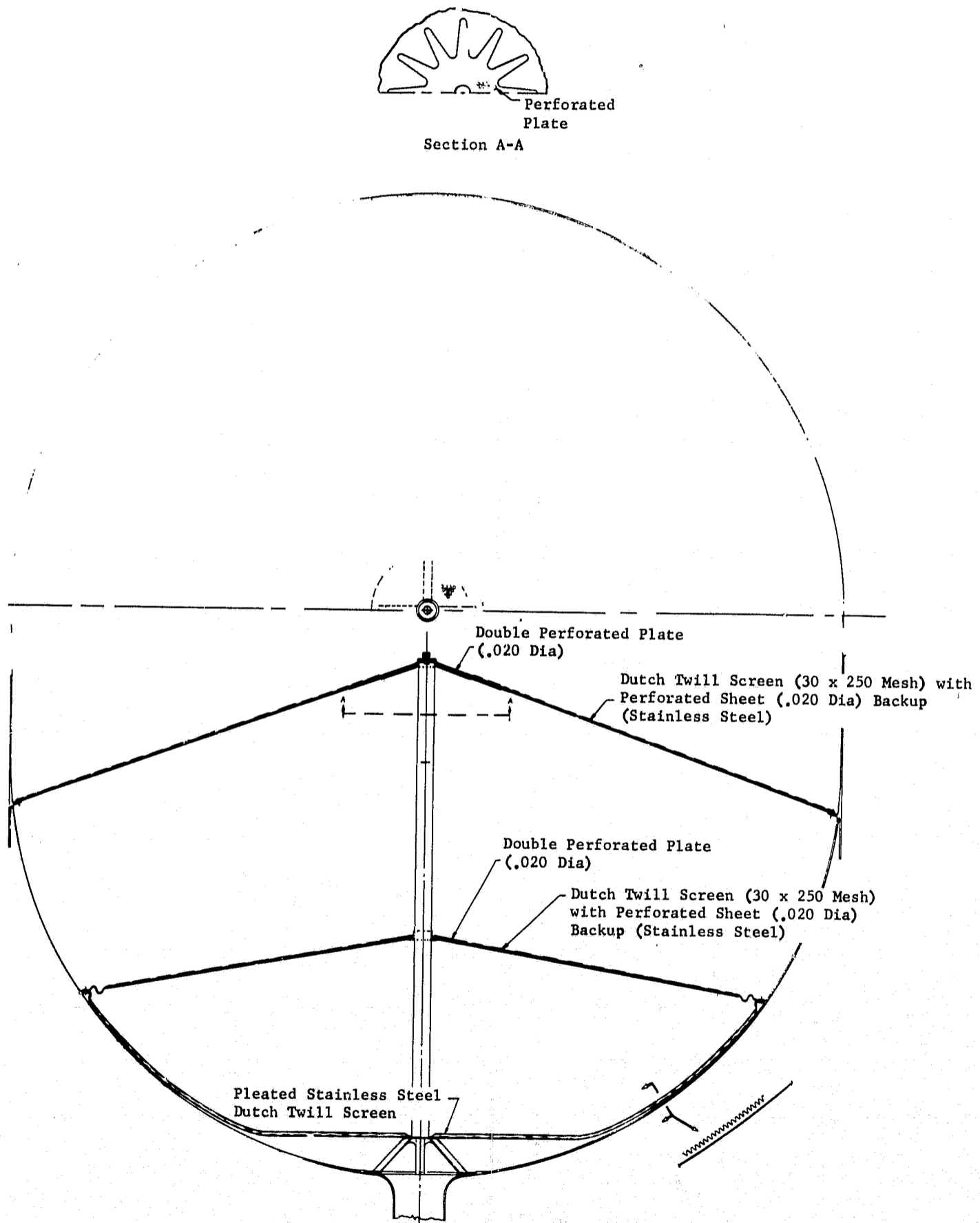
Fig. II-6 Drawing LAB-0211620

Screen/Plate
Barrier

Tank Wall

Convolute
Expansion
Ring
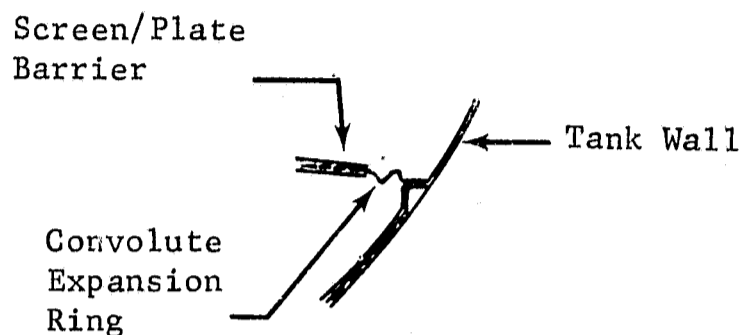
Fig. II-7 Lower Cone Attachment Detail

Dissimilar metals for tank and screen are assumed. Riveted
attachments are used for dissimilar metal joining. Welding would
be more desirable for joining if both screen and tank were of the
same material.

The total weight of the propellant retention structure is 11 lb.

Assembly Description (No Hardware Limitation) - The design
shown in Drawing No. LAB-0211620 (Fig. II-6) is based on instal-
lation of the propellant retention structure in a new tank design.
The -009 subassembly, consisting of center pole, middle screen,
and lower screen, is assembled on a fixture where the screens are
welded to edge members and center pole flanges.

The -009 subassembly is installed in the modified aft dome of
the tank by centering the center pole footing in the seat provided
in the outlet flange, and attaching the outer ring to the tank
dome flange.

The upper screen subassembly (-019) is then placed on the cen-
ter pole and fastened to the dome flange. The adjustable fitting
at the center is then tightened to hold the center pole in the
outlet seat.

C. OPERATIONAL CHARACTERIZATION

The reservoir barriers are designed to retain propellant against the disturbing forces from vehicle maneuvers and to prevent gas penetration into the tank outlet during liquid resettle resulting from system thrust buildup. The specific maneuvers involved are the 0.2-g negative axial and the ±0.009-g transverse accelerations and the loads induced by the pitch and roll rates of 5 deg/sec (see Table I-1).

A sketch of the capillary system under negative axial accelera-tion is shown in Fig. II-8. The conical design of the barrier re-sults in a hydrostatic head pressure gradient across the barrier due to the acceleration environment. This pressure gradient tends to cause the gas to want to enter at the low-pressure region with the liquid draining from the high-pressure area as indicated in the figure. The driving potential for the ullage across the per-forated plate portion of the barrier is caused by the hydrostatic head difference between points 2 and 3; while that for the wire cloth is the difference between points 1 and 3. The hydrostatic retention limits of the coverplate designs are shown on Fig. II-9 for a range of accelerations. As shown the coverplates are stable at the 0.2-g design requirements.
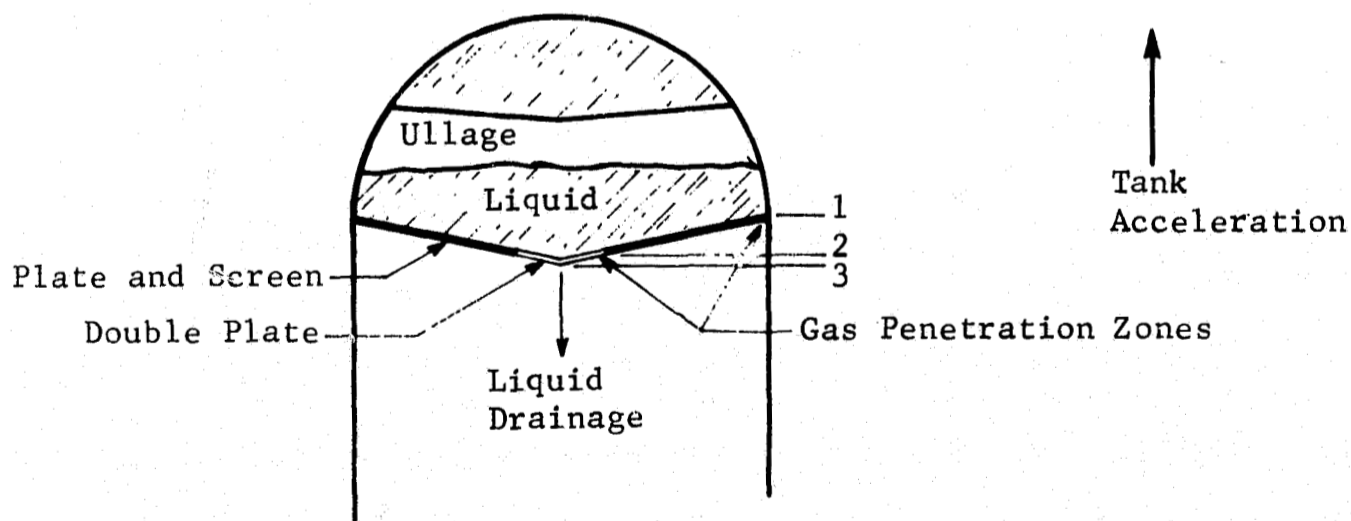
Fig. II-8 Capillary System Schematic for Negative Acceleration Retention
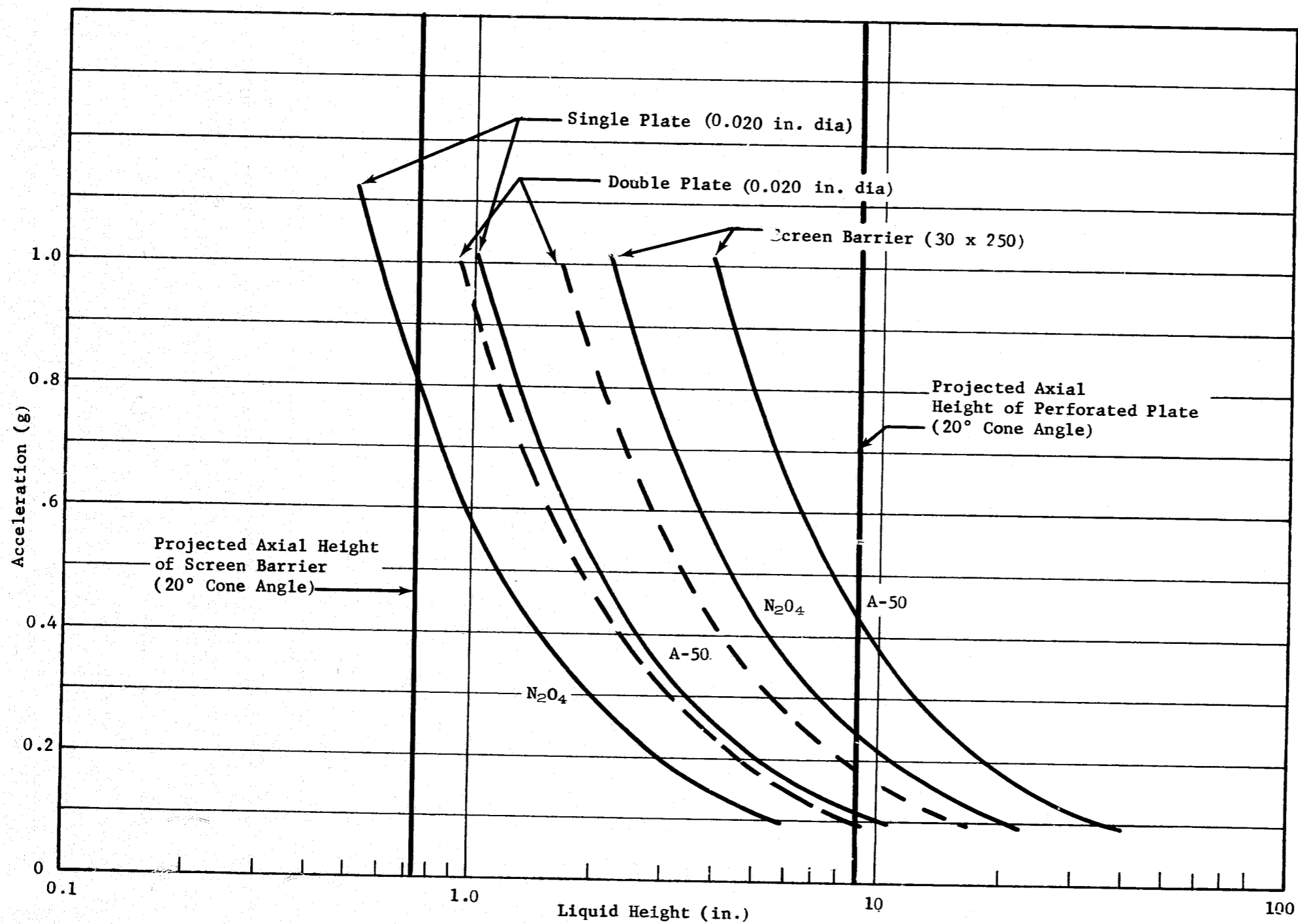
Fig. II-9 Capillary Barrier Liquid Retention Capability

In addition to retention under axial disturbances the barriers must prevent liquid loss under lateral acceleration. The system under lateral acceleration is shown schematically in Fig. II-10 (for simplicity only one compartment is shown). As before the capillary barriers must prevent gas penetration due to the pressure gradient developed along the barrier interface as a result of the different liquid levels in the compartment and the tank (points 1 and 2 on the figure). The pressure difference developed depends on the quantity of liquid in the reservoir and in the rest of the tank. The worst-case situation is with the reservoir 100% full and the remaining tank volume completely empty. A plot of the retention capability as a function of acceleration and the percent of propellant in the tank is shown in Fig. II-11. The system is designed to retain against the 0.009 g lateral acceleration requirement with a safety factor of two for the nitrogen tetroxide tank. The design margin of the barriers in the fuel tank would be even greater due to the higher surface tension value and lower density of the propellant.
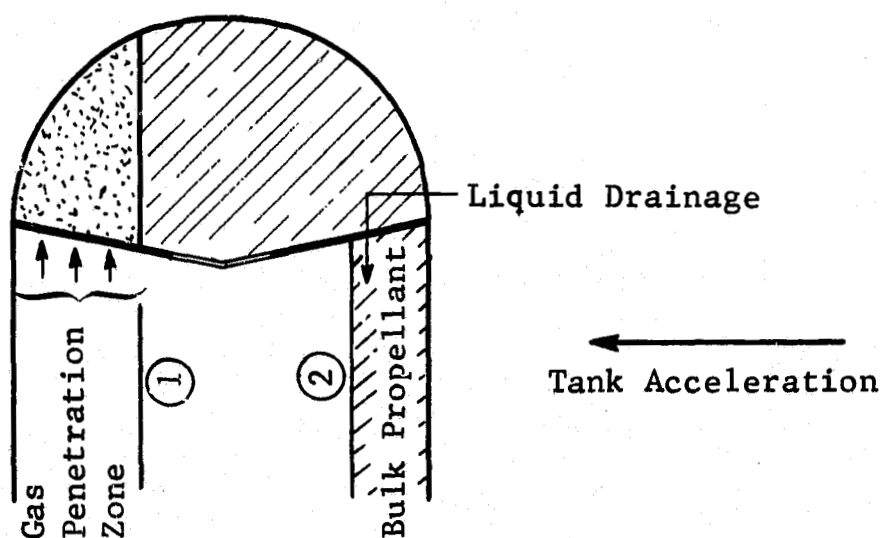
Fig. II-10 Capillary System Schematic for Lateral Acceleration

The hydrodynamic stability of the coverplate designs is much more difficult to establish. For the case where no excess liquid exists above the coverplate, the criteria as presented above for the hydrostatic case has been shown to be valid for both lateral and axial acceleration (Ref II-1). However this condition is extremely unlikely in an actual spacecraft application; rather the liquid level will more probably be above or below the barrier.
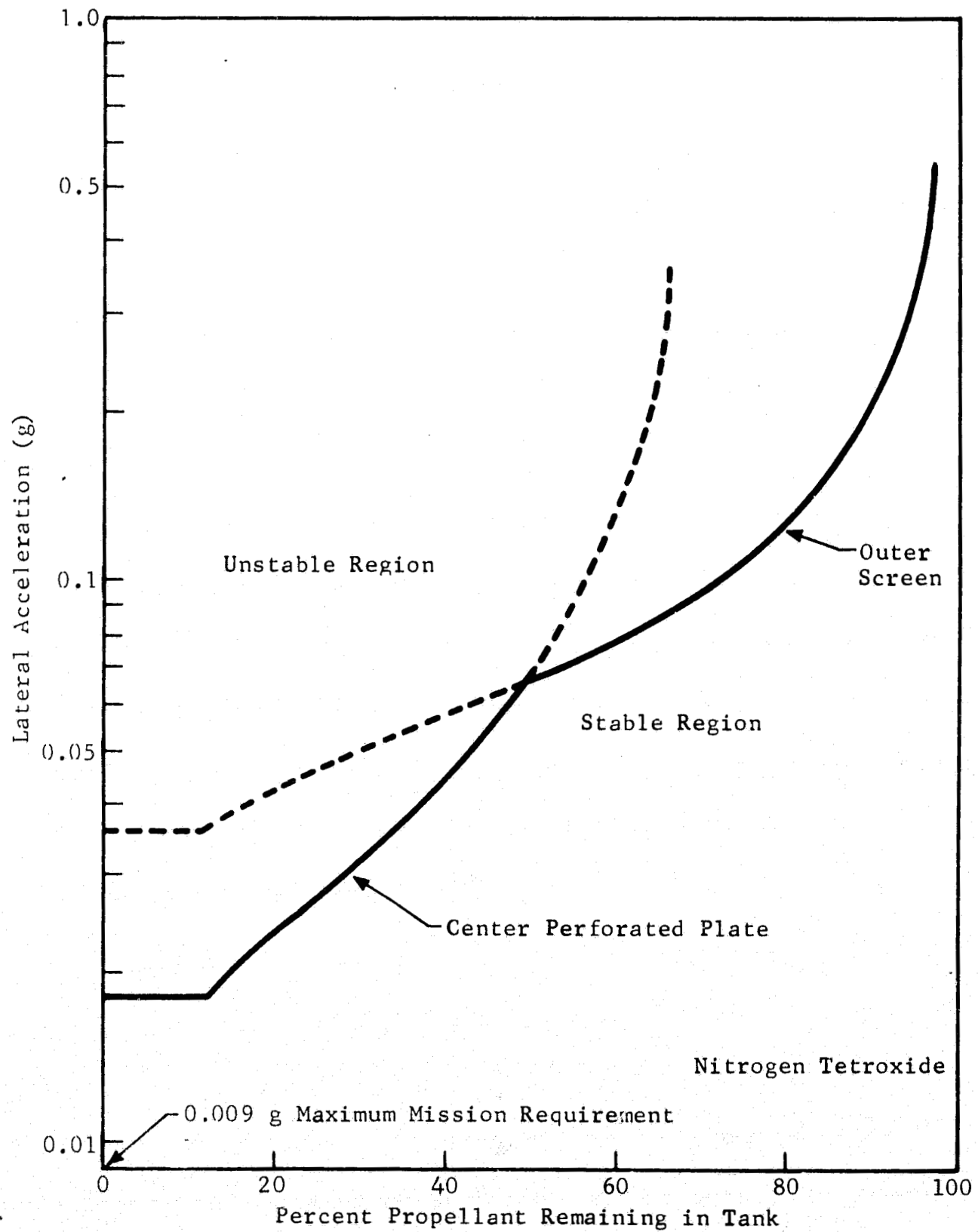
Fig. II-11 Compartment Lateral Acceleration Retention Capability

For the axial negative acceleration, both the case of excess and
no excess of liquid over the barrier at the time of the initiation
of axial acceleration would represent a condition analogous to the
hydrostatic stability case. The excess liquid would migrate to the
opposite end of the tank with a stabilizing gas-liquid interface
formed at the barrier as shown in Fig. II-8. For the case of the
liquid interface below the barrier at initiation of a negative dis-
turbing force, the liquid within the compartment will be displaced
toward the barrier. The barrier must then be capable of damping
the impinging liquid to prevent liquid loss from the compartment.
Barrier performance for this resettle mode has been studied exten-
sively under a Martin Marietta Corporation IR&D program (Ref II-2)
and under NASA Contract NAS8-21259 (Ref II-3 and II-4). This in-
formation indicates no significant liquid loss (Category A through
D damping, see Ref II-3 and Fig. III-13) would be expected for the
barrier design and mission requirements. This degree of damping
is considered satisfactory for the given application.

For lateral or rotational disturbances with the liquid above
the barrier, the inertial effect of the liquid motion relative to
the barrier acts to overcome the surface tension stabilizing ef-
fect. Investigations of rotational disturbances, such as reported
in Ref II-5 thru II-7 have shown that the openness ratio (i.e.,
ratio of open area to total area) is an important parameter since
it is related to the flow blockage through the barrier. The re-
lationship of openness ratio and Weber number, or normalized Weber
number, on the stability of barriers has been demonstrated over a
limited range of barrier pore size and openness ratios. These data
are applicable to single perforated plate barriers. For the pro-
posed design the barriers consist of double perforated plate in the
center region and a plate twilled weave combination in the outer
region. Both of these configurations have essentially no direct
open area for flow. For the flow to travel across the barrier it
must change direction from the no barrier blockage flow stream
lines as illustrated in Fig. II-12. This tortuous flow path
greatly reduces the energy beneath the barrier and dampens the
liquid motion. An analytical treatment of this condition is not
known; however, testing to date indicates a great improvement in
the performance of multiple barriers and Dutch Twill screens over
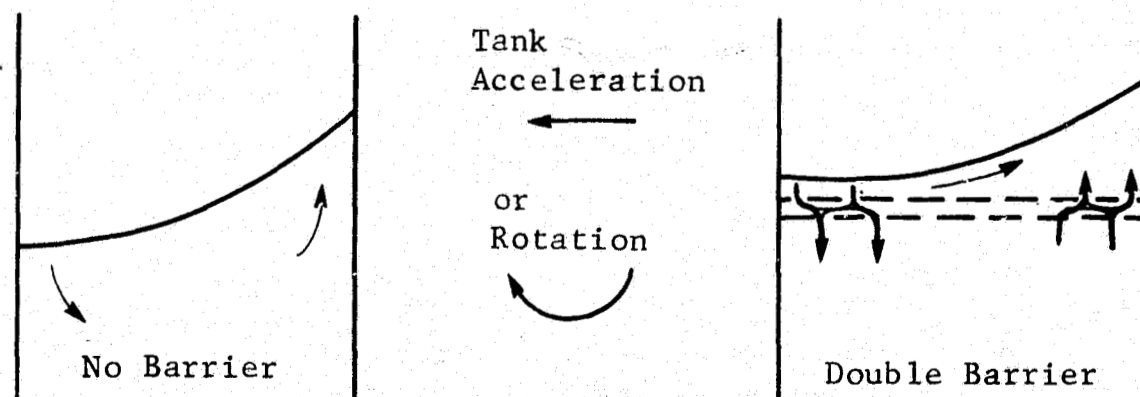single perforated plates (Ref II-3).

Fig. II-12   Lateral Impulse Flow Stream Lines

Tests to verify the stability of the current Apollo umbrella screens during the 5 deg/sec pitch and yaw rate have been conducted (Ref II-6). These tests show that the current single barrier design with 0.020-in. holes of approximately 25% open area are stable. Figure II-13 is a plot of the test results and the existing umbrella screen design point and the proposed design single perforated plate only. As shown, the single plate is between the identified stable and unstable points indicating marginal stability. Since the actual barriers (Fig. II-4 and II-6) contain double layers, it is felt that the system is very conservative relative to the inertial loads.

Hydrodynamic stability of the design during lateral excitation was also demonstrated experimentally during this program. Lateral acceleration tests were conducted in the drop tower with a 1/5-scale model using a barrier pore size essentially identical to the full size system. Weber number scaling based on pore size between the prototype and model was used. Model test results show that the system is stable for the imposed lateral acceleration environment and the pitch, yaw, and roll rates (see Section B.2 of Chapter III for a discussion of the test results).

Barrier performance during the thrust buildup bulk propellant resettle transient was determined experimentally. Subscale resettle tests were conducted to demonstrate the propellant damping effectiveness of the conical barrier design and the "straining" out of entrained gas bubbles from the liquid passing through the barriers. The Froude number, the ratio of inertia to gravity forces, was used as the scaling criteria for the tests. The tests consisted of initiating outflow from the retention compartments, then releasing liquid from a raised reservoir to simulate the resettling bulk propellant. The falling liquid was forced to the tank wall by a conical deflector to more nearly simulate the anticipated resettle flow characteristics. The resettle characteristics were determined from an analysis of the resettle flow field using a modified version of the Marker and Cell computer program (Ref II-8). The resettle Bond number is from an initial interface at a $Bo \leq 2$ to several hundred thousand at the buildup of engine thrust.

A sequence of the resettle and outflow characteristics is shown in Fig. II-14. Figure II-14(a) shows the liquid 0.26 sec after initial impact and 0.85 sec after opening the outflow valve. The fluid above the top cover plate is very frothy, while in the middle compartment only limited surface agitation is present, and in the bottom compartment only single phase liquid is present.

Fig. II-13 Screen Stability
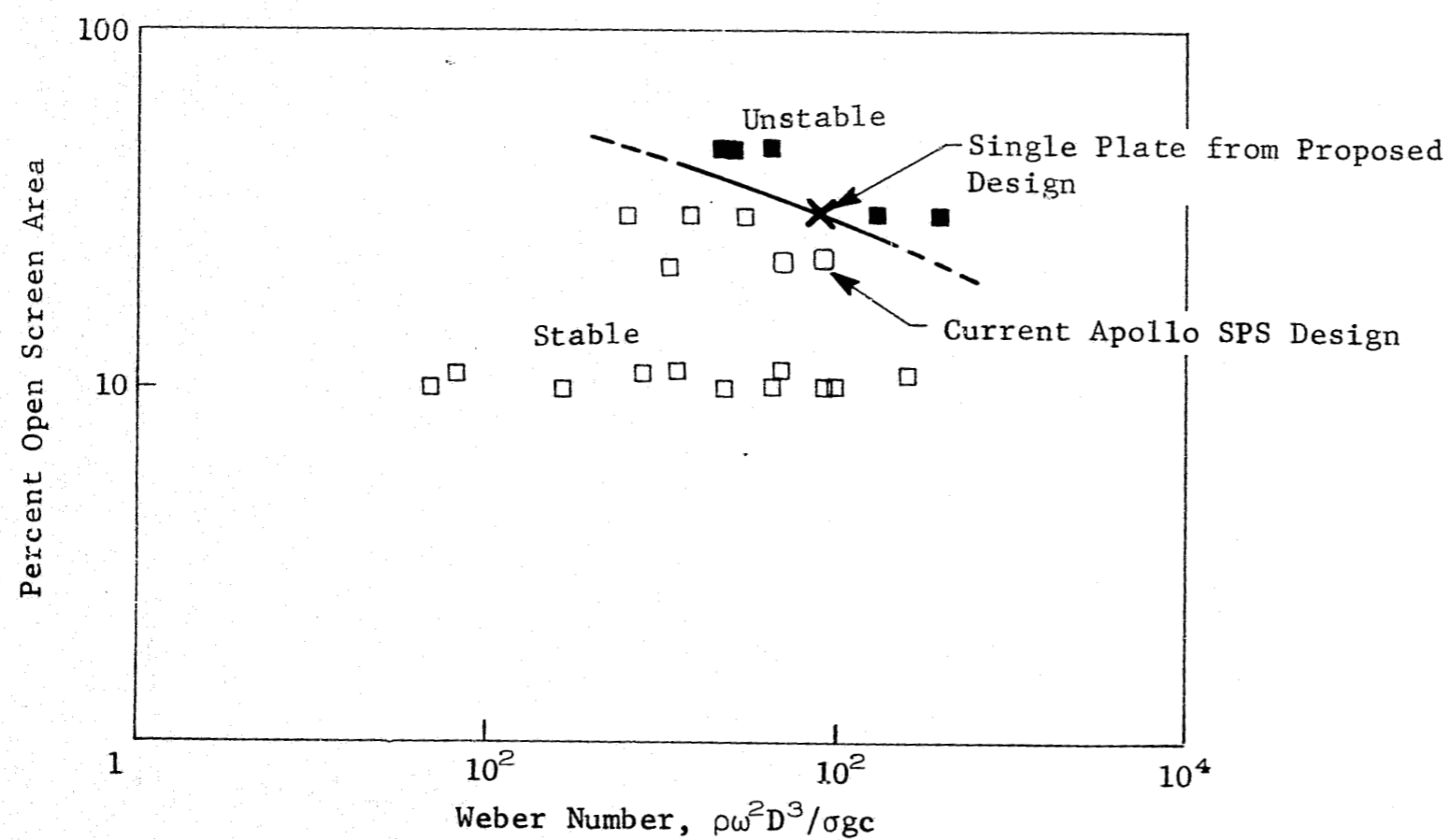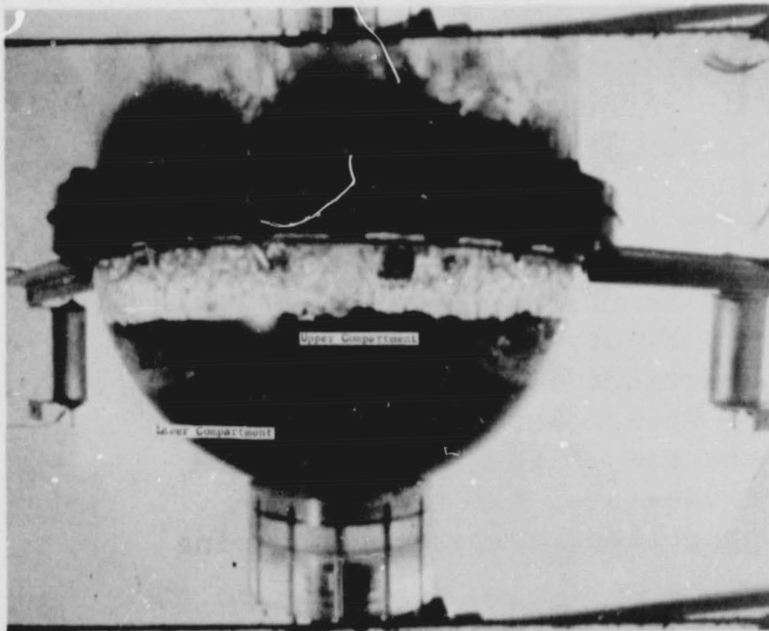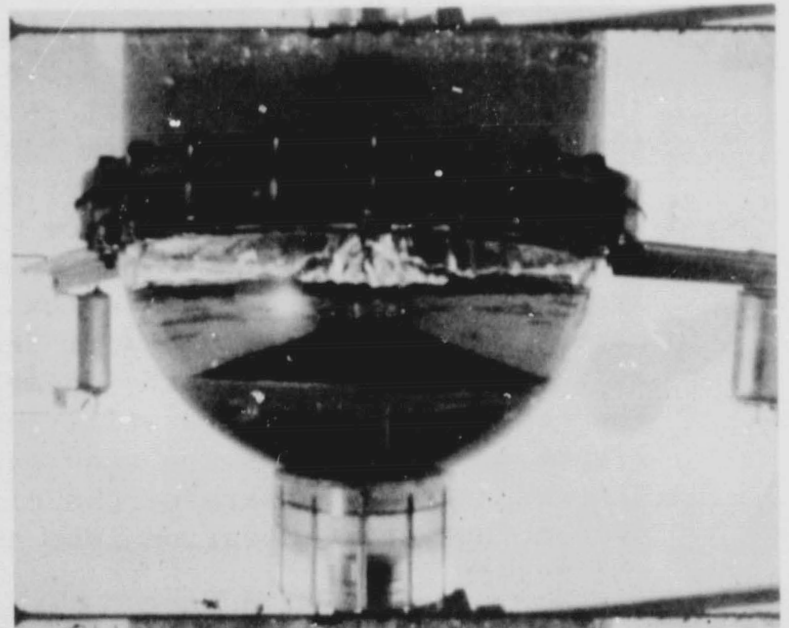
(a)   0.26 sec after Liquid Impact   (b)   2.5 sec after Liquid Impact
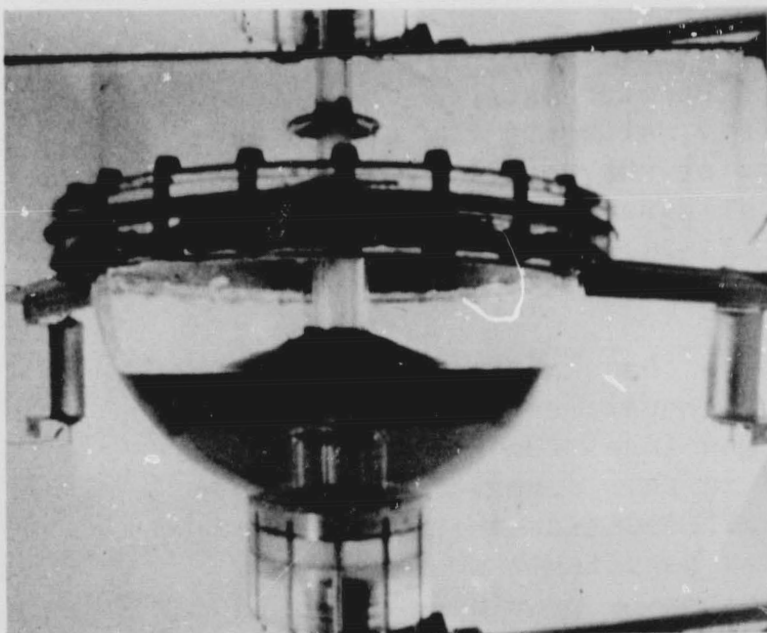
(c)   15 sec after Liquid Impact   (d)   18.5 sec after Liquid Impact

Fig. II-14 System Resettle and Outflow Characteristics

Figure II-14(b) shows that the bubbles have cleared from the bulk of the resettled propellant 2.5 sec after initial resettle liquid impact, No vapor entrainment exists in either compartment at this time. The operational system has a screen liner in the lower compartment that would prevent any gas that happened to penetrate into the lower compartment from entering the feed system. Also the liquid level in the upper compartment at 2.5 sec has increased from its level at 0.26 sec after impact demonstrating the refill aspect of the capillary system design. Figure II-14(c) shows the system at the time when the upper compartment is essentially empty. The lower compartment is still full at this point in the outflow. Figure II-14(d) shows the tank near the end of the terminal drain. This sequence demonstrates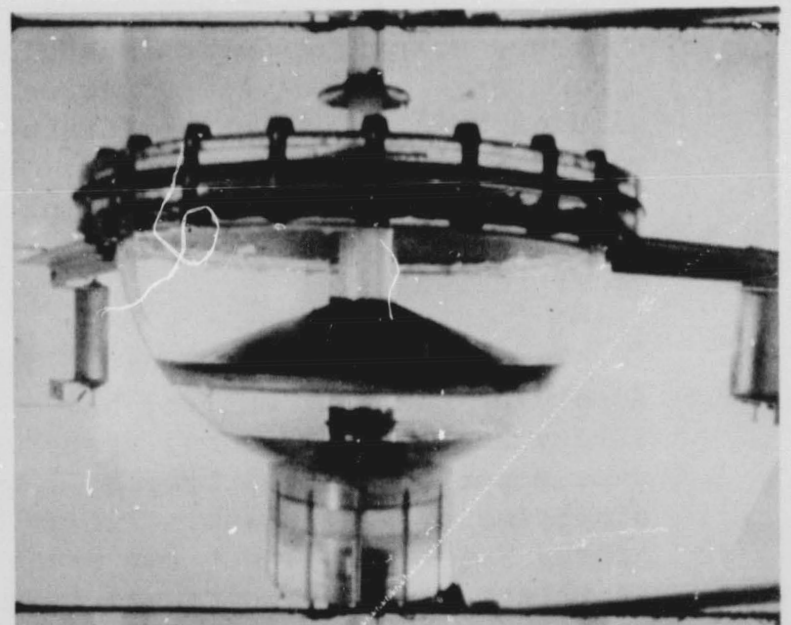 the effectiveness of the barriers in preventing vapor ingestion into the propellant compartments during the resettle mode.

In addition to this experimental program, a mathematical analysis of the terminal drain condition was conducted. The liquid histories during draining are shown in Fig. II-15 for the prototype system with N_2O_4 and A-50.

The conical barrier geometry permits the compartments to be designed to refill during sustained acceleration periods. The hydrostatic head developed across the barrier exceeds the retention capability of the perforated plate, allowing the gas to be purged from below the barrier. Plots of the refill flowrates for the upper compartments for complete ullage exposure on the underside of the plates are shown in Fig. II-16 as a function of the acceleration level.

In addition to the conical barriers that maintain a liquid supply at the tank outlet, the bottom compartment contains a capillary barrier to prevent premature gas ingestion to the feed line once a portion of the trapped liquid in this compartment has been displaced by pressurant. The critical condition is the low-g restarts required without any propellant settling maneuvers. The capillary liner prevents gas ingestion while providing a liquid flowpath to the tank outlet as shown schematically in Fig. II-17. The liner retention capability must be sufficient to prevent gas leakage under the various operating conditions. The critical design conditions occur at restart with an adverse propellant location and during the terminal flight conditions when the positive axial thrust is a maximum.
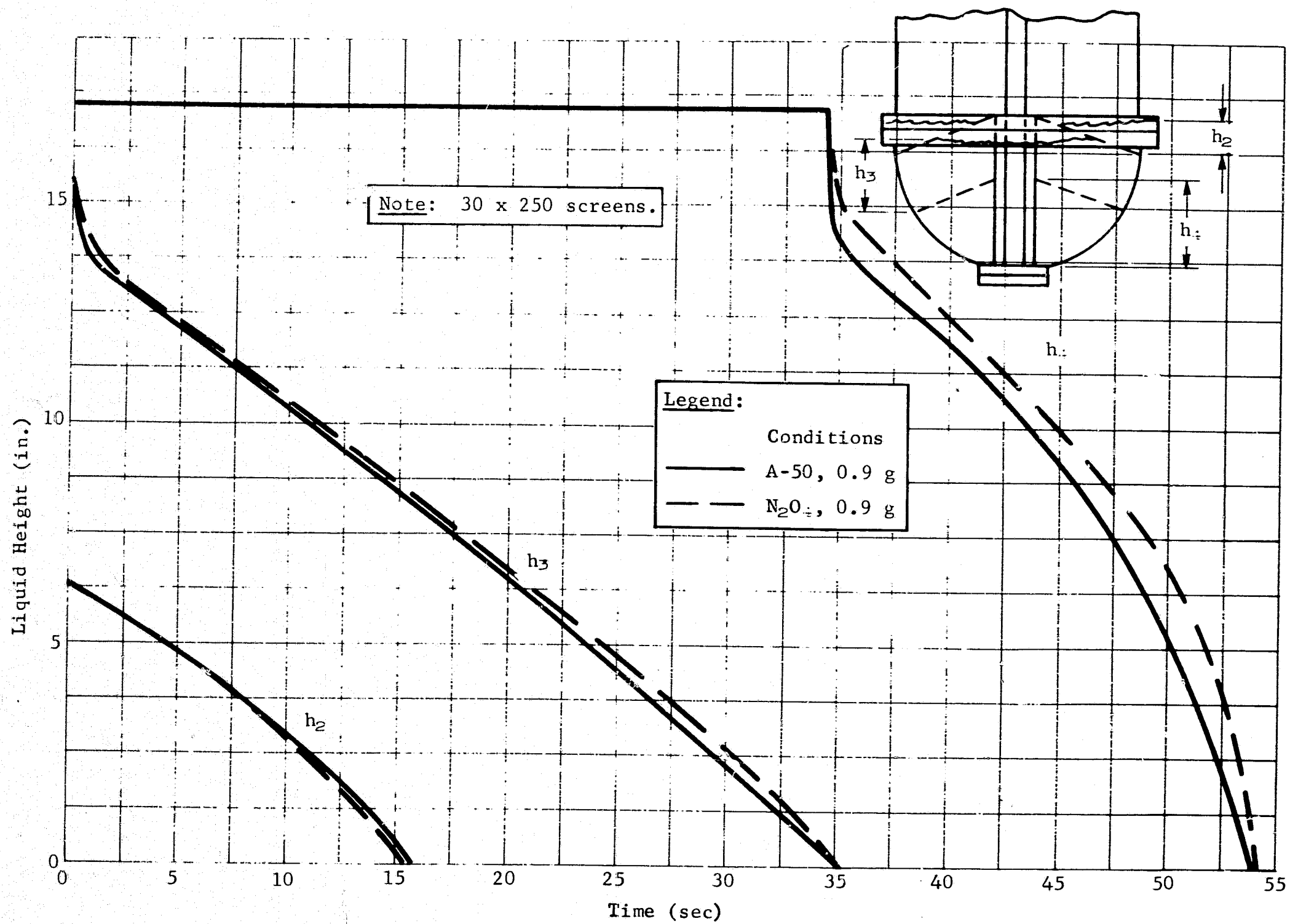
Fig. II-15 Liquid Draining Histories

MCR-69-436

(a) Oxidizer

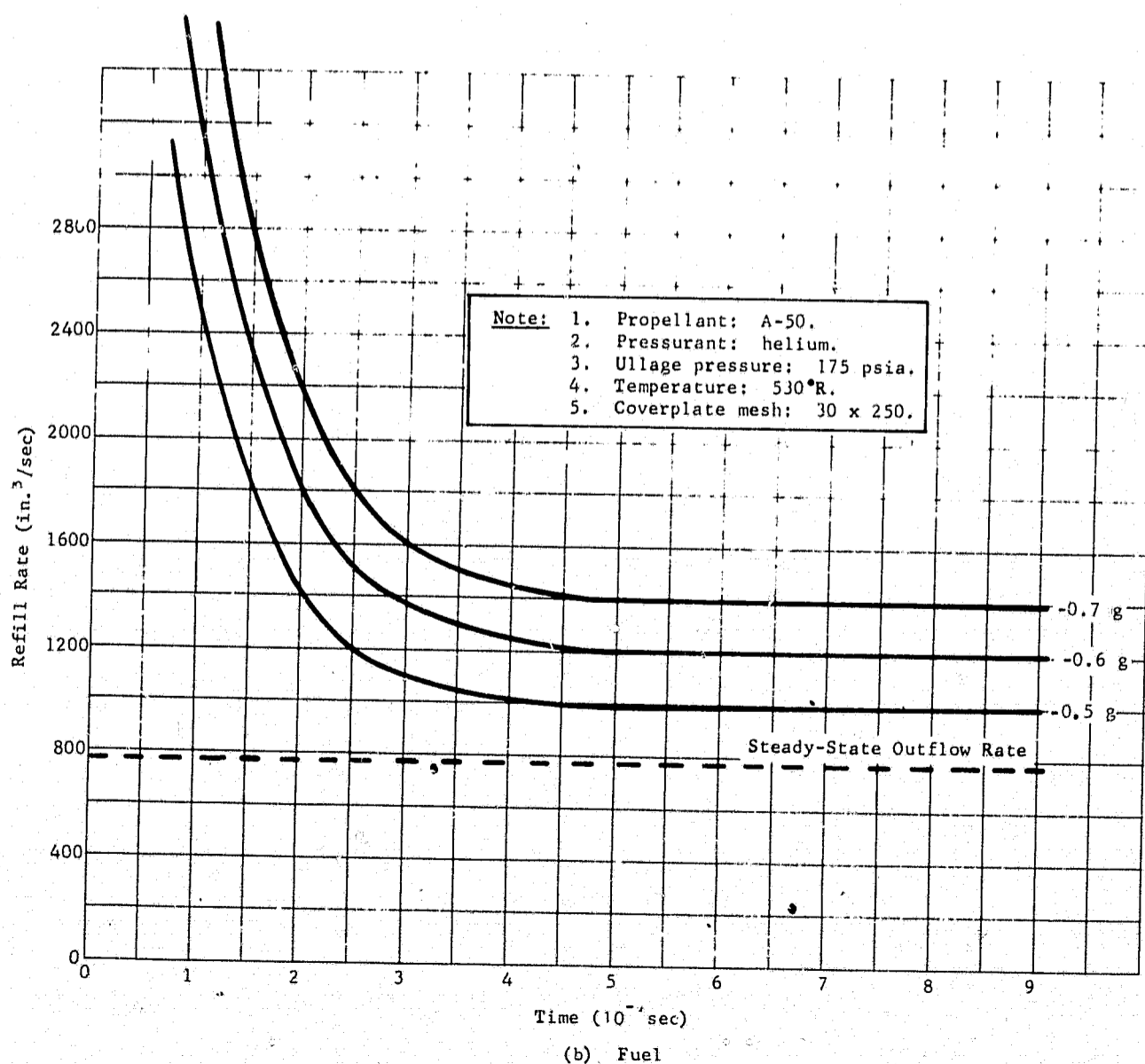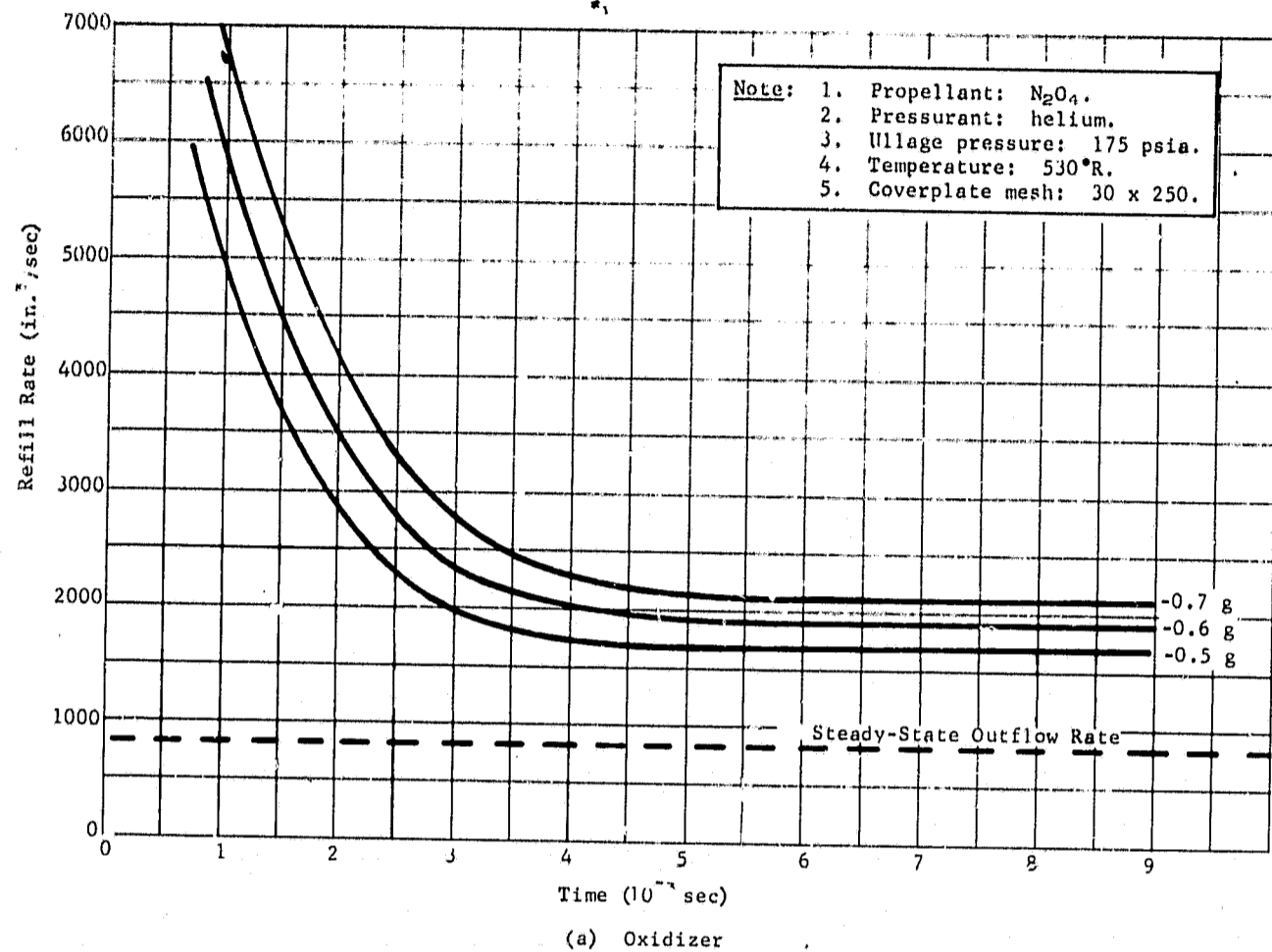(b) Fuel

Fig. II-16 Compartment Refill Flow Rate

Compartment Coverplate

i

Ullage

h

Critical Pore

Capillary Barrier

Flow Annulus

Liquid

Tank Wall

a

Outlet

Tank Acceleration
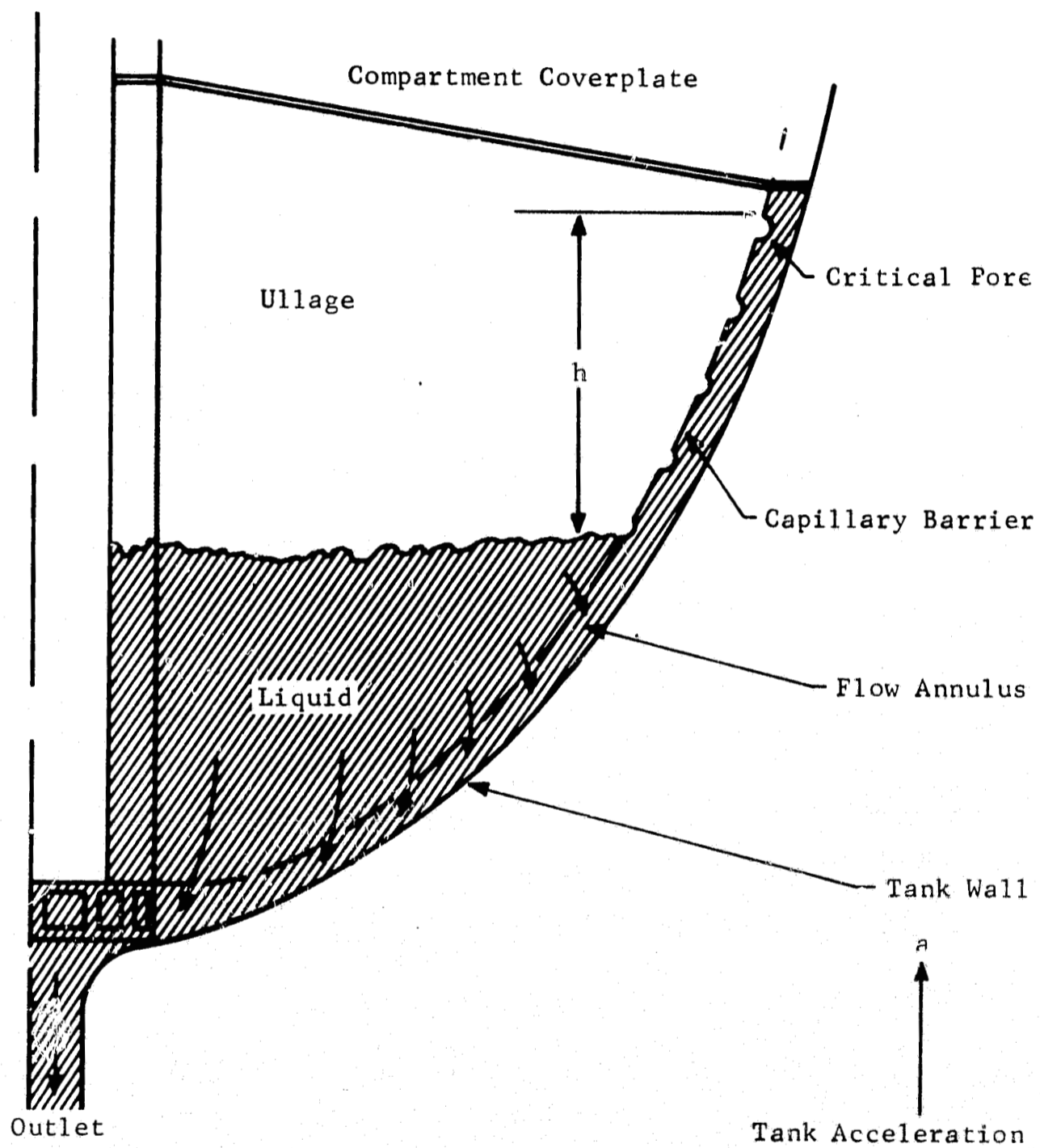
Fig. II-17 Schematic of Screen Liner during Terminal Drain

For the low-g restart condition it is necessary to have sufficient liquid-to-liner contact area to provide the necessary flow area to prevent the viscous losses from exceeding the capillary retention capability of the liner during flow initiation. A test program and analytical study were conducted to define the equilibrium interface condition of the liquid in the compartment in the 10^{-5} g acceleration environment to determine the liquid/liner contact area. The interface position for various percents of liquid fill in the compartment for the low-g environment is presented in Chapter III and Fig. III-25 and II-26. This analysis shows that the liquid/liner contact area is substantial even for low percentages of fluid in the compartments. The calculated contact area as a function of the percent of fluid in the compartment is shown in Fig. II-18. The area required under steady-state outflow to prevent gas ingestion is approximately 1 sq ft. Although a transient analysis of the engine start was not possible because of lack of information about the feed system and valve response characteristics, it appears that sufficient contact is provided to permit successful restart with very little residual propellant.

The compartments are designed to permit gravity fill to a level > 99%. The maximum trapped ullage under both barriers during fill in a 1-g environment is less than 45 cu in. for the N_2O_4 and 160 cu in. for A-50. This only represents about 0.05% of the useable tank volume. This level is conservative and assumes the worst-case condition of barrier wetting prior to filling. The compartments will be subsequently filled further during the boost phase of the flight when the acceleration level reaches a value of 7.35 g. The gas would be purged out because of the hydrostatic head across the trapped ullage pocket.

No special provisions were incorporated into the design to provide liner fill capability. During the test series no difficulties were encountered in filling the liner completely if the screen was dry before introduction of the fluid and the fill rate exceeded the screen wicking rate. The wicking time for the screen liner in 1 g is estimated to be greater than 20 minutes. Therefore, a fill rate of 0.5 cu ft/minute or greater would be adequate to prime the annulus. Figure II-19 shows the results of two fill tests conducted in series. Following the first fill and drain the system was purged for 15 minutes with GN_2 and the second fill was successfully accomplished.

The figure shows a graph with:
- Y-axis: Liquid in Lower Compartment (%)
- X-axis: Surface-Liquid Contact Area (ft²)

● - Point of Discontinuity in Analysis
(approximately 0.5% of Total Tank Volume)
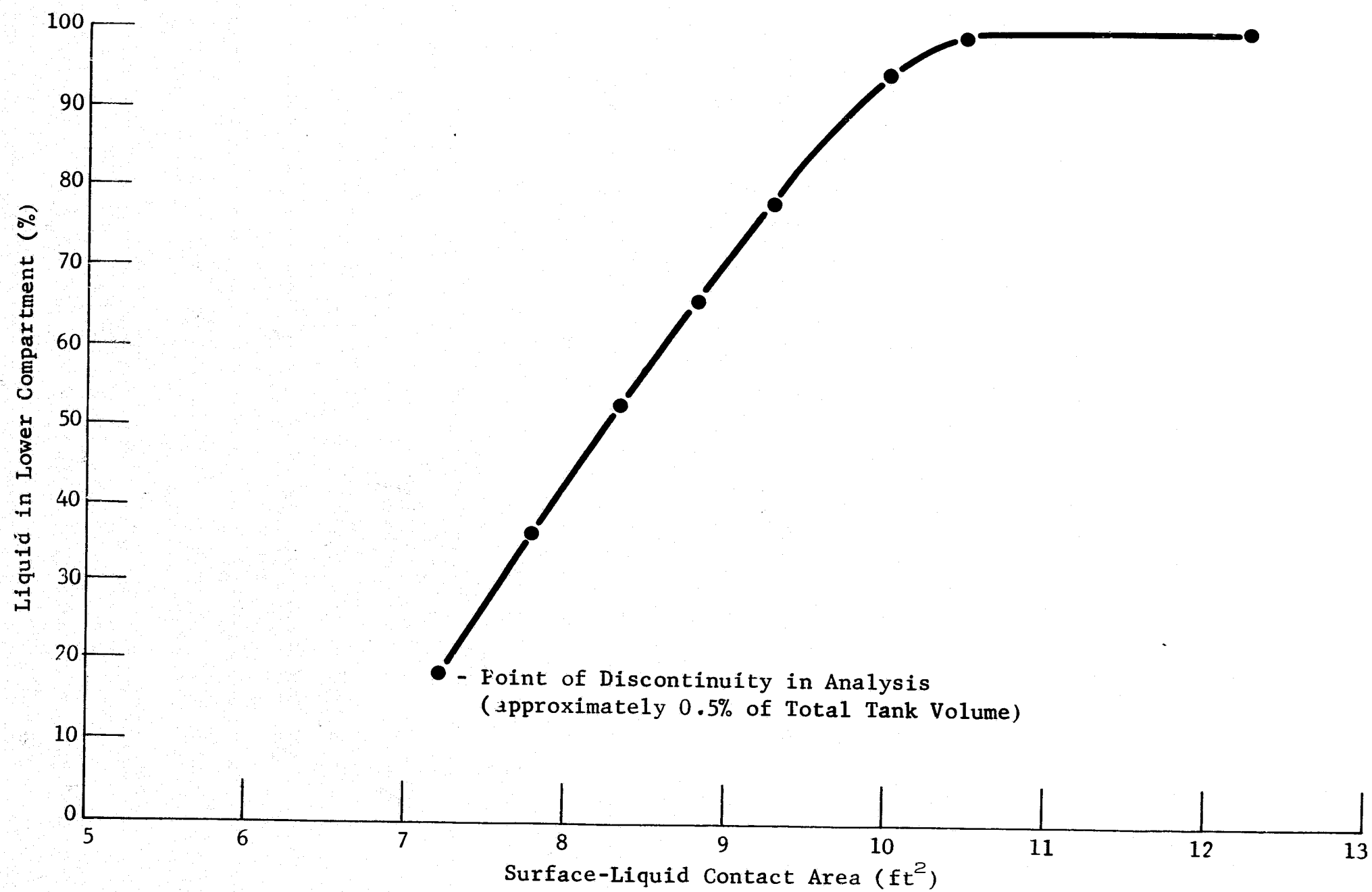
Fig. II-18 Propellant Contact Area on the Screen Liner Surface

MCR-69-436

(a)   First Fill with Dry Screen

(b)   Second Fill Following Draining and GN_2 Purging

Fig. II-19   Liner Fill Test Results

An additional design consideration for the system in the no-
hardware-modification design is to prevent liquid loss from the
compartments due to siphoning through the stillwell during nega-
tive thrust periods. It was not possible to design the barriers
to prevent some siphoning during negative axial acceleration per-
iods and maintain other desirable features as simple 1-g fill ca-
pability and existing stillwell gaging capability. The design
approach selected was to minimize propellant loss due to siphoning
since the probability of experiencing the conditions for siphoning
appear slight, rather than to comprise other factors and prevent
propellant loss due to siphoning. A sketch of the "antisiphon"
aspects of the design are shown in Fig. II-20. The operating
philosophy is that the annulus around the stillwell will be drained
before appreciable propellant is lost from the retention compart-
ments. Once the annulus liquid level recedes past the liquid com-
munication point from the compartments, the siphoning potential is
lost and the compartment is isolated. The screen flow ring is de-
signed to prevent gas passage into the compartment, so the liquid
in the compartments is pressure stabilized and no further loss re-
sults. A plot of the liquid siphoning loss for both propellants
is shown in Fig. II-21 for several different negative axial ac-
celeration levels.
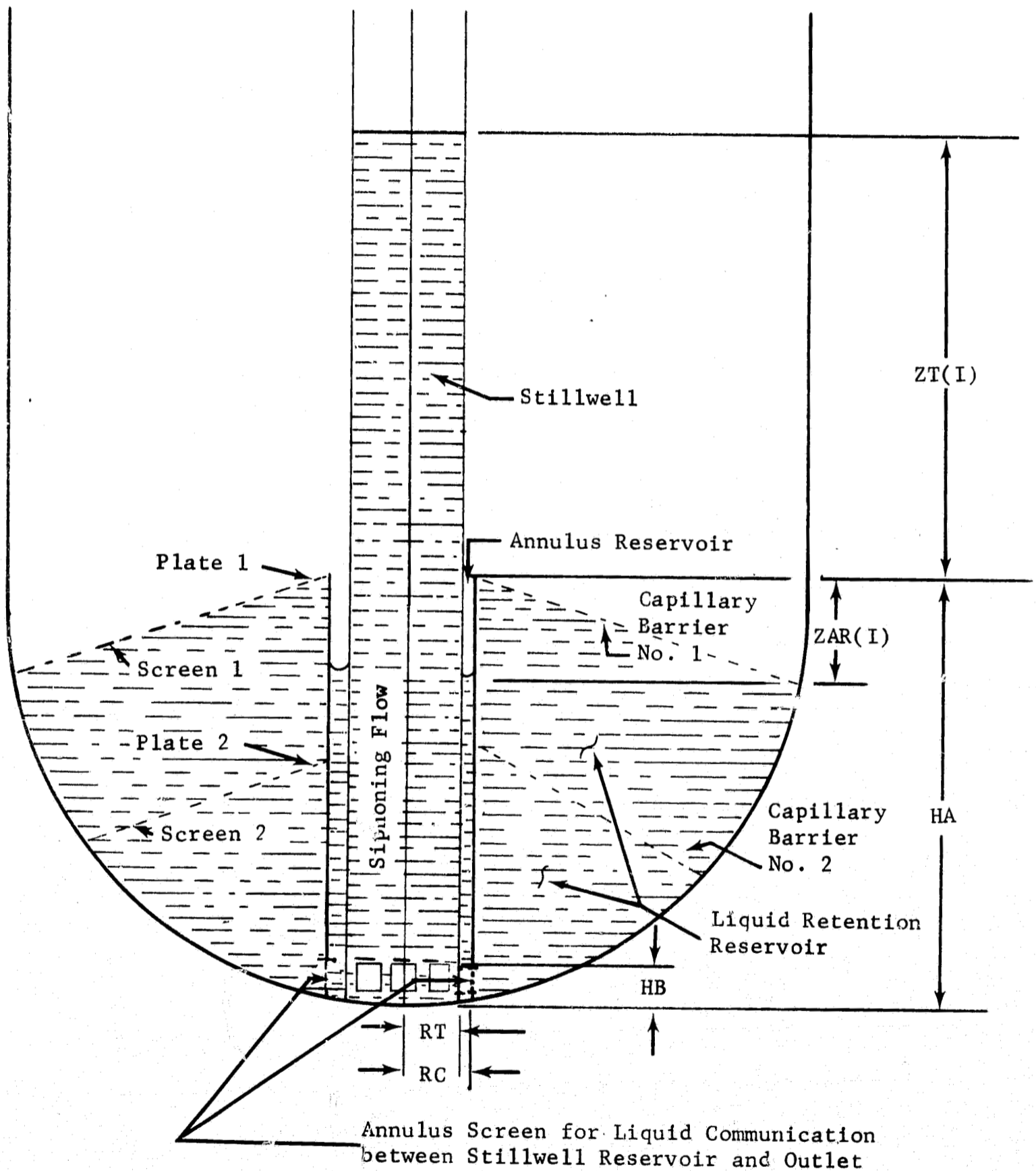
Fig. II-20 Propellant Management System Schematic
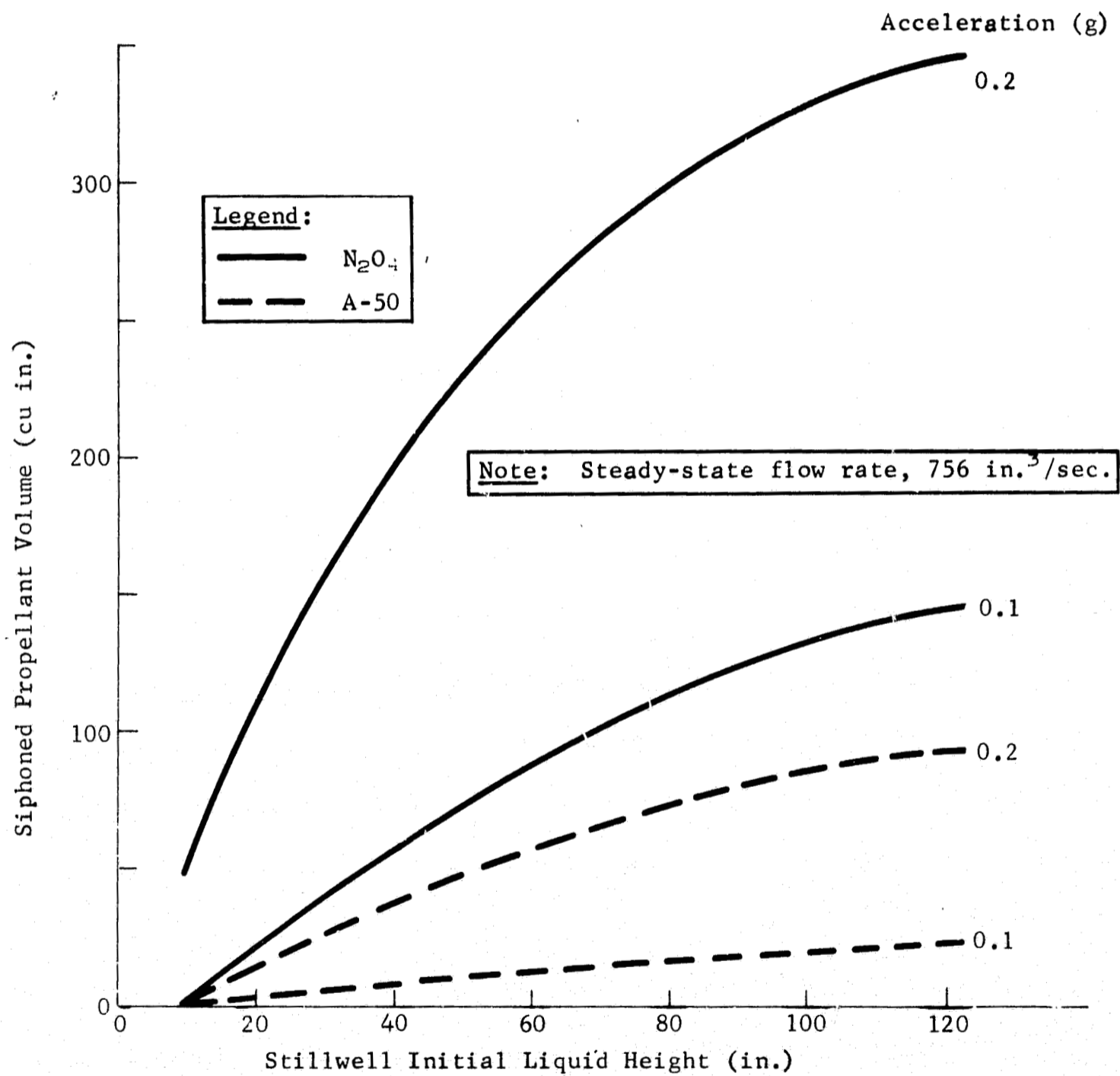
Fig. II-21 Capillary Compartment Propellant Loss from Stillwell Siphoning Action

III. ANALYSIS

The purpose of the Phase II analytical study was to finalize
the selected Phase I capillary system configurations and identify
the operational performance of these systems. The results of
this effort were presented earlier in Section C, Operational Char-
acterization, of Chapter II of this report. This chapter discusses
these various aspects in more detail and presents the results of
the experimental verification testing. The purpose of the experi-
mental program was to verify the analytical predictions in contrast
to developing design criteria. The designs generated are based on
existing criteria, where possible, with those areas lacking suffi-
cient information to yield a high confidence design identified for
further study. It was not within the scope of the program to es-
tablish general basic design criteria.

The analysis of the operational characteristics are quite gen-
eral since detail mission requirements or maneuvers were purposely
not identified. The system is rather designed to be sufficiently
flexible to be able to satisfactorily perform over a wide range of
requirements that would permit general application of the design
to many different missions.

In much of the discussion the liquid solid contact angle, which
appears as a cosine function, is not included in the various dimen-
sionless groups. This was done for simplicity since the contact
angle is zero for both the nitrogen tetroxide and the Aerozine 50
in contact with the 300 series stainless steel capillary barriers
(Ref III-1), which makes the cosine function of the contact angle
equal to one.

Virtually all of the subscale testing was performed with a
one-fifth model of the no-hardware-modification configuration.
The approach used in the model was to maintain geometric simili-
tude and use the identical prototype capillary structure, since
scaling of screen twill meshes is not practical. The subscale
tank was constructed of plexiglass with the capillary system made
from 300 series stainless steel.

Substitute liquids rather than actual propellants were selected
for the experimental program in the interest of safety and material
compatibility. The test liquids simulate the actual propellants in
the pertinent physical properties. Liquid properties are presented
in Table III-1.

Table III-1   Propellant and Test Liquid Physical Properties

Liquid	Density (lb/ft^3)	Surface Tension $(lb/ft \times 10^{-3})$	Viscosity $(lb/ft\text{-}sec \times 10^{-3})$
Ethanol	49.2	1.53	0.806
Methanol	49.4	1.55	0.401
FC-43	117.0	1.09	3.200
N_2O_4	90.6	1.88	0.277
A-50	55.5	2.07	0.550

A.   TEST HARDWARE DESCRIPTION

A plexiglass model of the existing Apollo SPS propellant tanks, approximately one-fifth scale, was used in experiments to demonstrate the performance of the selected acquisition device. A total of 68 tests, including checkout tests, were conducted to demonstrate the performance of the acquisition device. Twenty-four of these tests were conducted in Martin Marietta's Drop Tower, (Ref III-2), under a low-g environment. The remaining tests were conducted at 1 g. Nearly all test results were documented on 16 mm film exposed at 200 or 64 fps. Test procedures and results are included in the analysis section under the specific analytical effort requiring their support.

The model tank, fabricated from cast acrylic plastic, consists of two hemispherical end domes and a 10-in. O.D. barrel section 20 in. long with a 1/4-in. wall (Fig. III-1). Plastic flanges were used between domes and barrel section to provide easy access to the model interior. The gaging standpipe was simulated by a 3/4-in. O.D. plastic tube approximately 30 in. long. The model acquisition device, located in the lower dome (Fig. III-2), consists of two conical coverplates, central tube, and corrugated spherical liner (not shown) which forms an annulus in the compartment below the lower coverplate. The upper coverplate, not clearly visible in (Fig. III-2, is located at the plastic flange on the lower dome. The central tube positioned around the simulated gaging standpipe has a Dutch twill screen band (250 x 1375 mesh) about 1 in. wide around its base to permit draining of the liquid in this cavity into the lower compartment and prevent gas ingestion into the lower compartment during negative g environment. This tube terminates at the top of the upper coverplate forming an open annulus around the gaging standpipe. Screen mesh and perforated plate used in the model was the same as selected for the full-scale tanks. The coverplates (Fig III-3) were fabricated from stainless steel Dutch twill
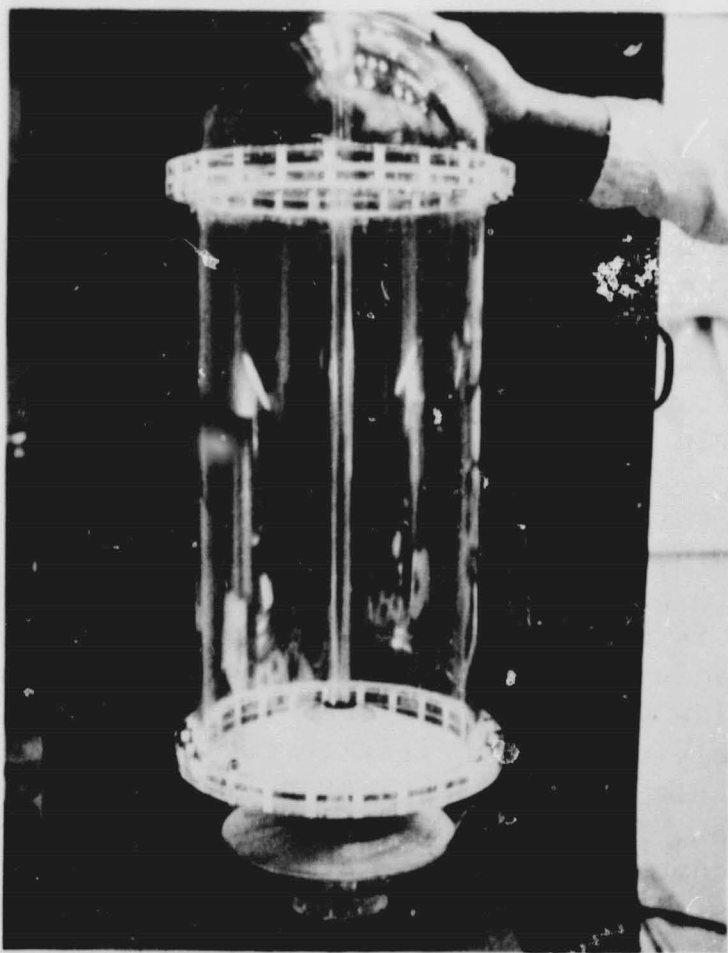
Fig. III-1　Plastic Model with Acquisition Device
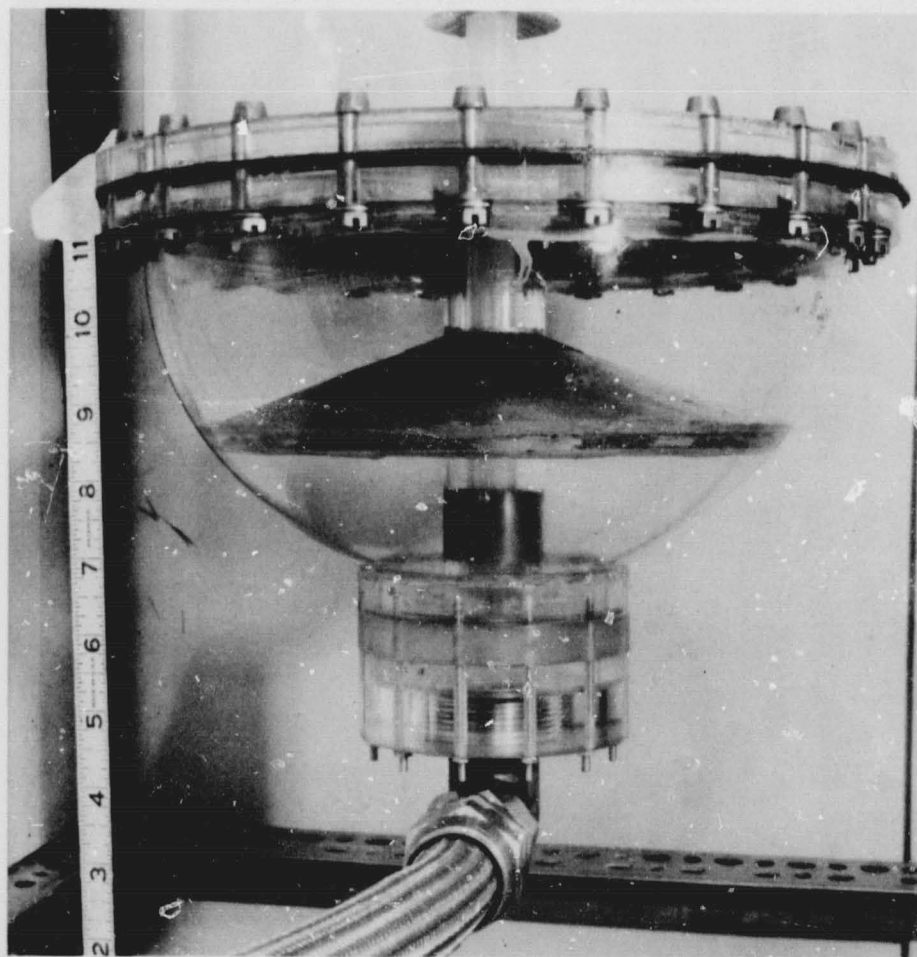
Fig. III-2　Model Acquisition Device

screen and perforated plate. The perforated plate was used to
structurally backup the Dutch twill screen and, in the central
section of the cones, to provide a variation in pressure reten-
tion, permitting refill of the compartments during positive g
environment. Double perforated plate spaced approximately 1/2 a
pore diameter (0.013 in.) apart and extending radially 1/2 in.
from the central tube was used in these areas. Two sets of cover-
plates different in screen mesh size only were fabricated. Both
165 x 800 and 30 x 250 mesh screens were used. The perforated
plate, 0.020 in. thick, contained 0.026-in.-diameter pores in a
60-deg array forming a functional open area of 0.33. An enlarged
view of the double perforated plate area is shown in Fig. III-4.
The second plate is not shown here, however, a 0.013-in.-diameter
wire used for spacing is shown attached to the lower perforated
plate at the inside diameter. Figures III-5 thru III-8 show
sequential assembly of the acquisition device. The corrugated
spherical liner, Fig. III-6, fabricated from 250 x 1370 mesh
Dutch twill screen, forms passageways between the corrugations
and the plastic dome that lead to the tank outlet. As shown, the
passageways are sealed at the junction of the liner and the lower
cone coverplate.
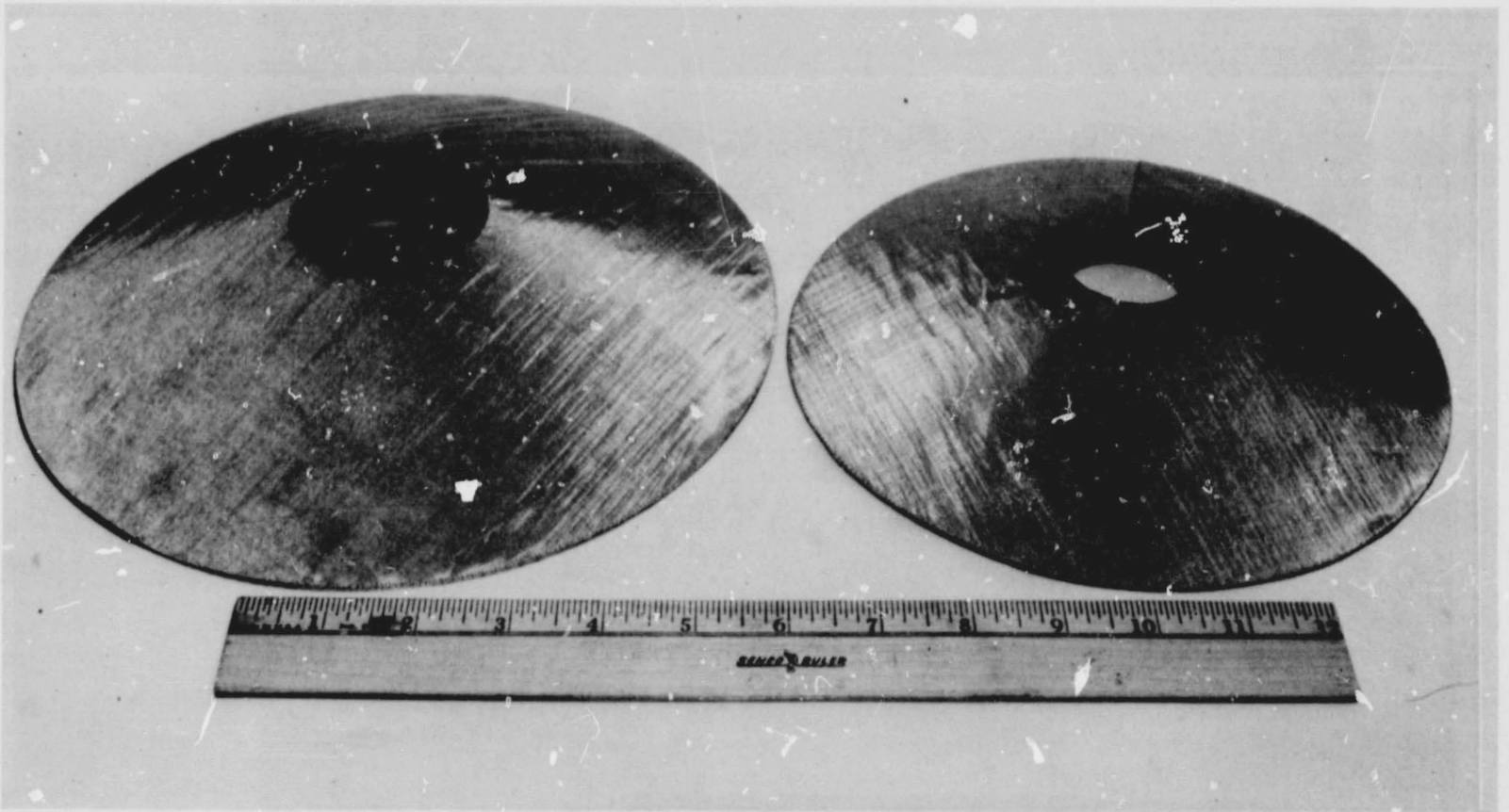
Figure III-3   Conical Coverplates
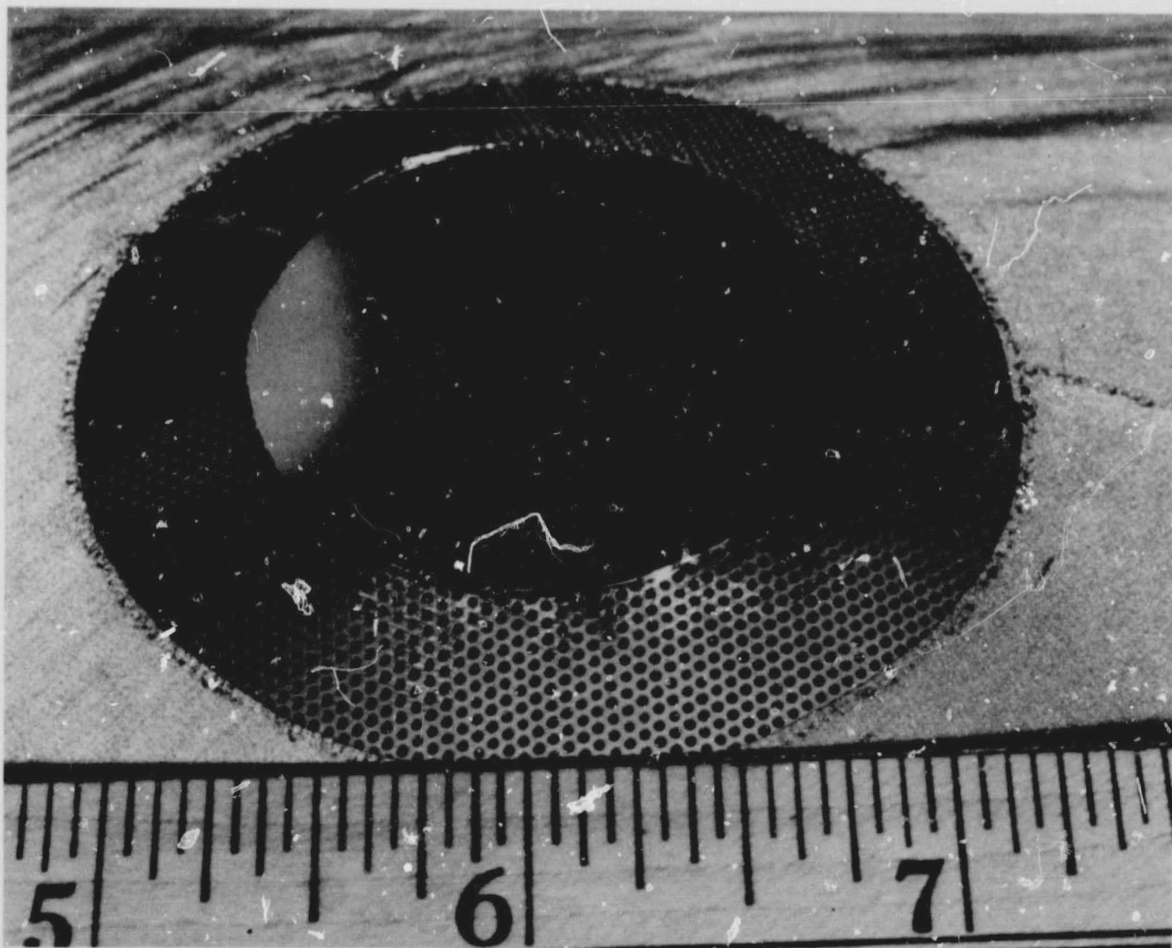
Figure III-4   Double Perforated Plate Area
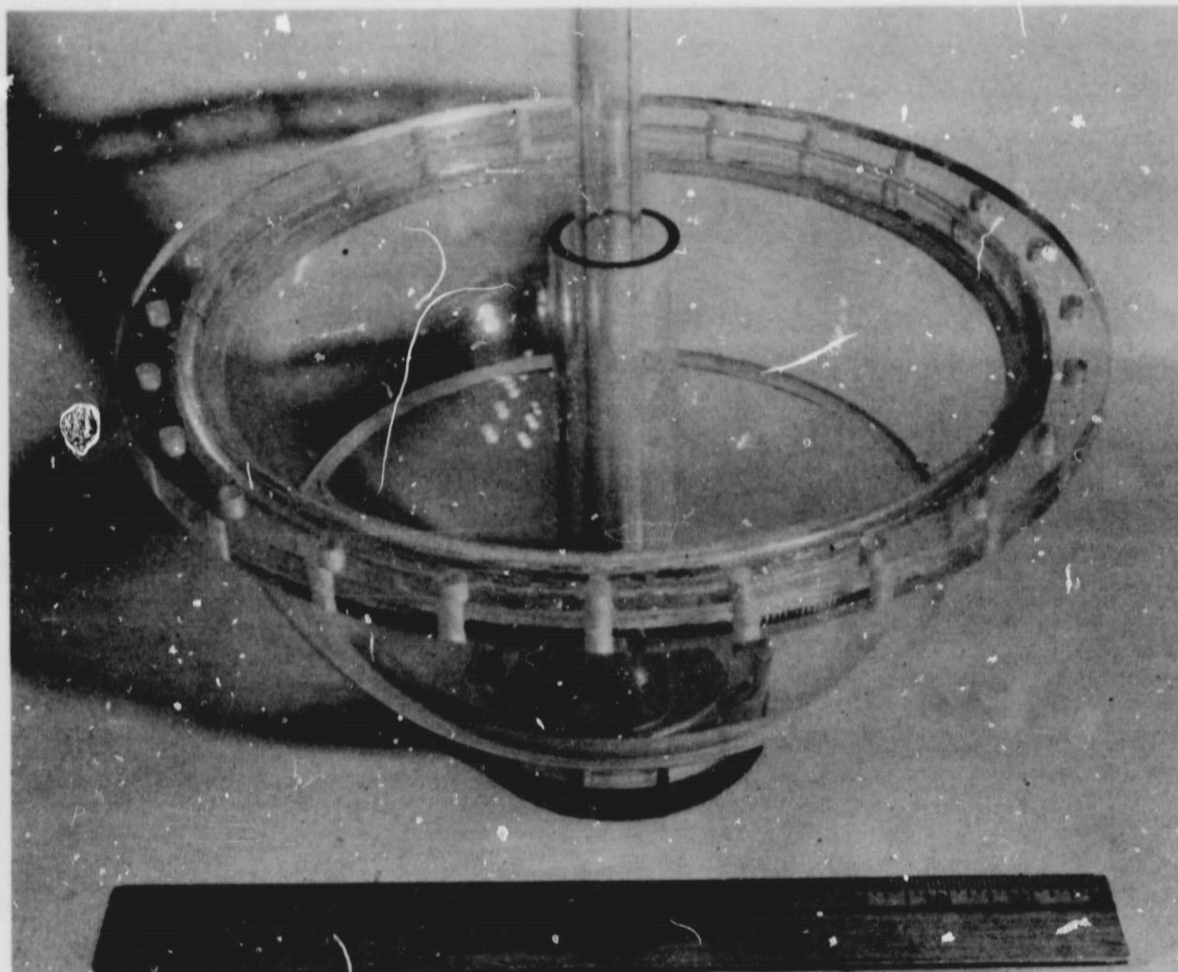
Figure III-5 Model Lower Dome
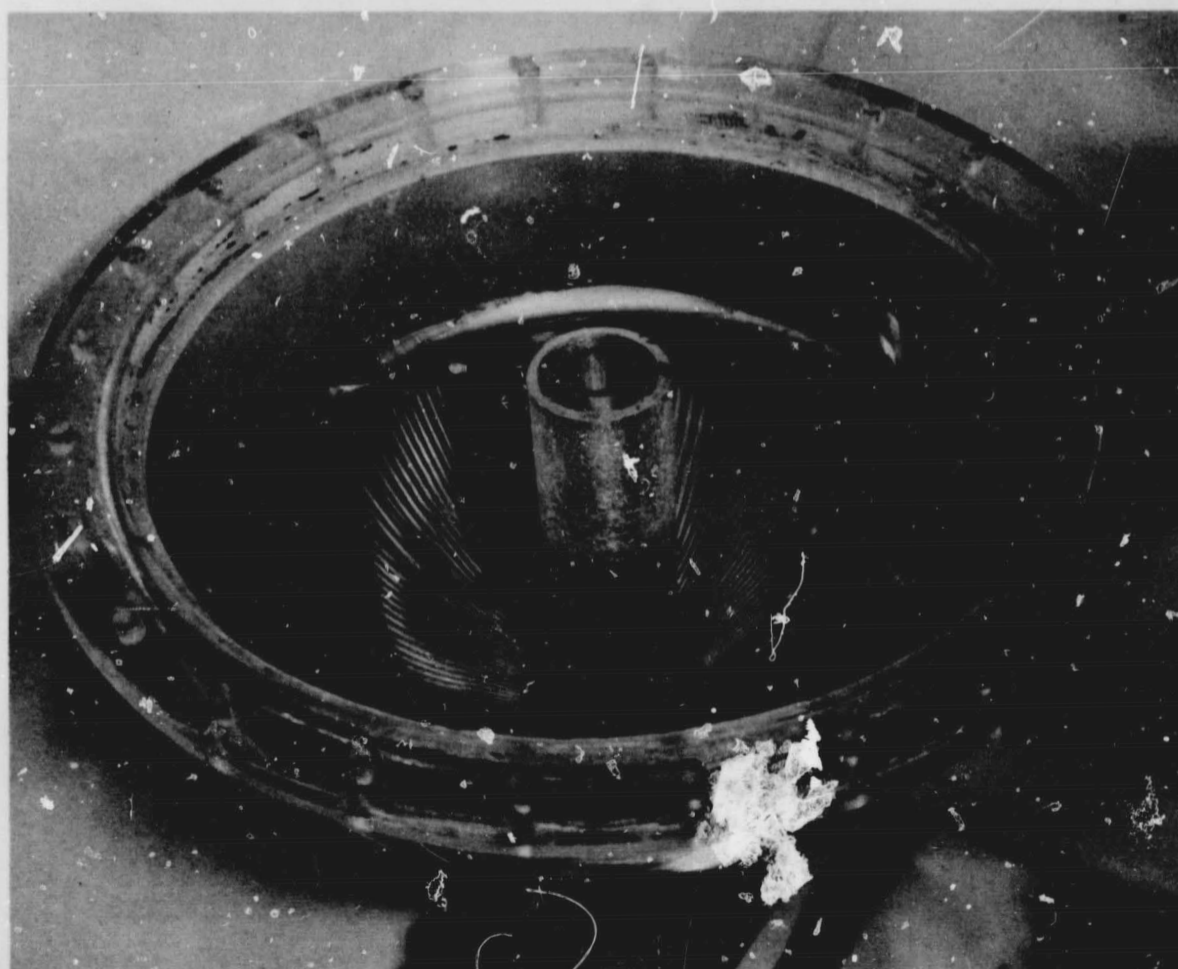
Figure III-6 Corrugated Spherical Liner
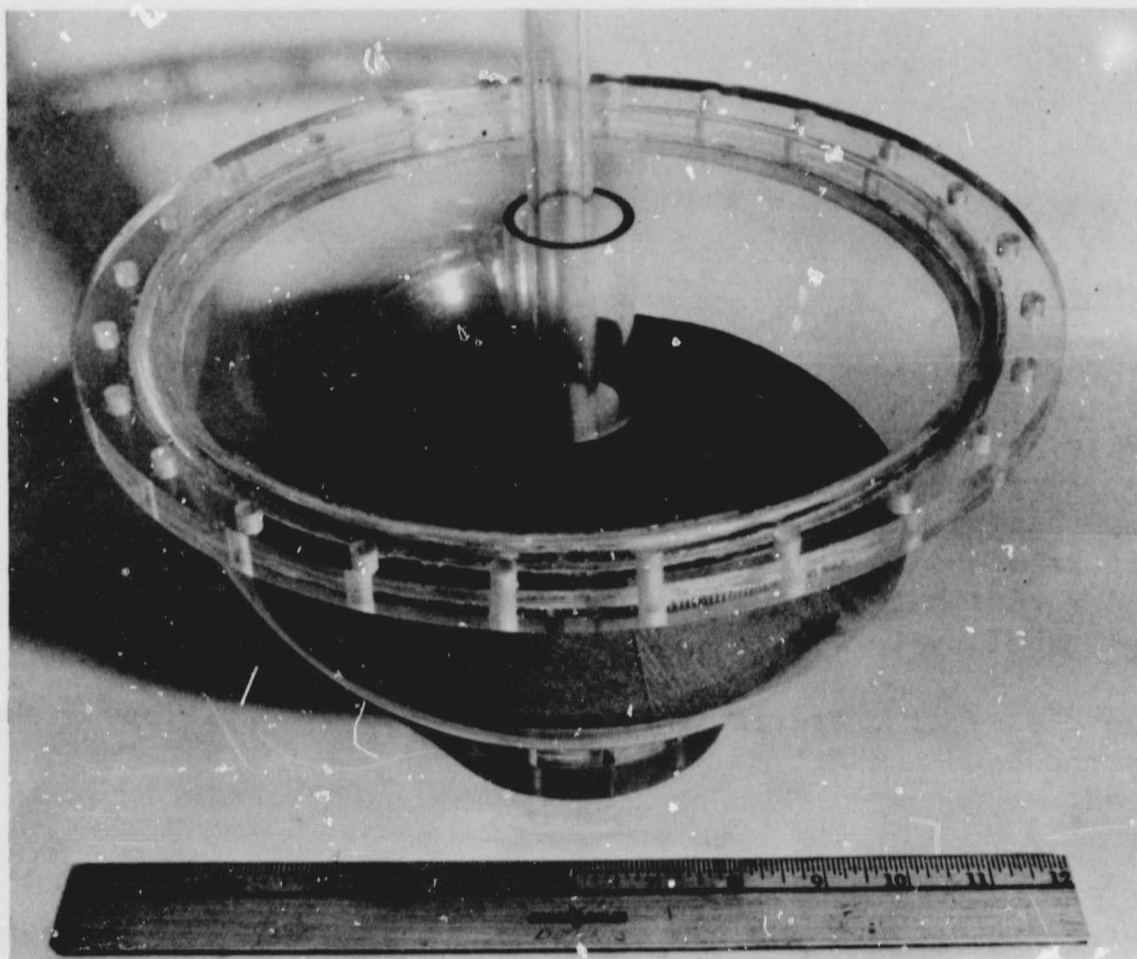
Figure III-7 Lower Coverplate Installed
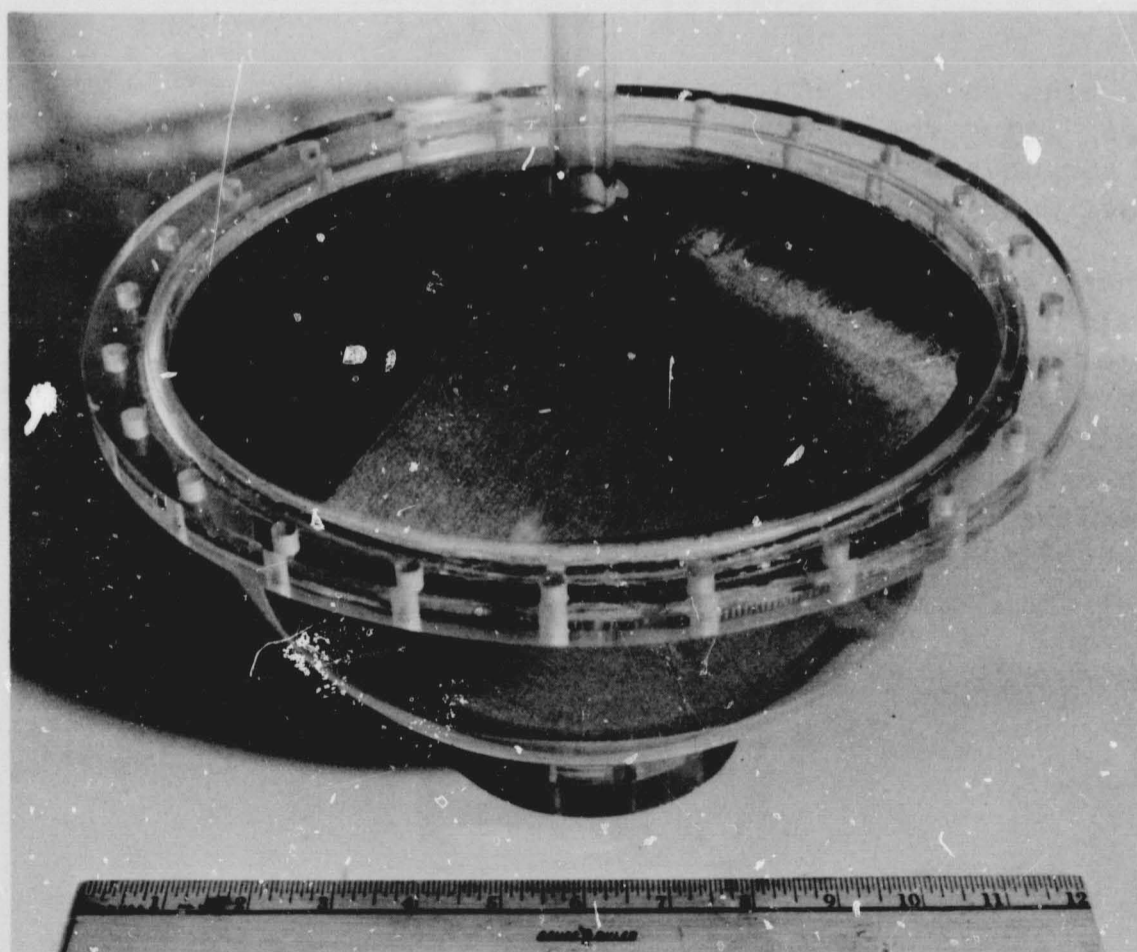
Figure III-8 Upper Coverplated Installed

B. CAPILLARY PROPELLANT RETENTION

1. Hydrostatic

Hydrostatic stability considerations for a capillary system design application were discussed in the Phase I report (pp 51-55 of Ref I-1). Hydrostatic stability can be divided into two categories for purposes of analysis: the case of liquid retention by surface tension forces directly (capillary retention); and the case of pressure forces providing the bulk liquid retention with surface forces acting to stabilize the gas-liquid interface (capillary stability).

The classical criteria for single, interface capillary stability is the Bond number:

$$Bo = \frac{\rho \ a \ L^2}{\sigma}$$

[III-1]

which for design purposes can be rewritten in terms of the critical system dimension:

$$L_{crit} = \left[\frac{Bo_{crit} \ \sigma}{\rho \ a} \right]$$

[III-2]

It has been shown experimentally that for Bond numbers below a critical value the system is stable. Stability data for perforated plate and square weave screen generated by Martin Marietta under Contract NAS3-20837 is shown in Fig. III-9 and III-10.

These results verify that Bo is the criterion for hydrostatic pore stability and substantiate a critical value of approximately 0.84 for circular holes where the characteristic dimension (L) is the pore radius. For square weave screen the results show a critical value of approximately 0.45 where the characteristic dimension is one-half the open width of the screen mesh. The Bond number for various elements in the given propulsion system at various mission acceleration levels are presented in Table III-2.
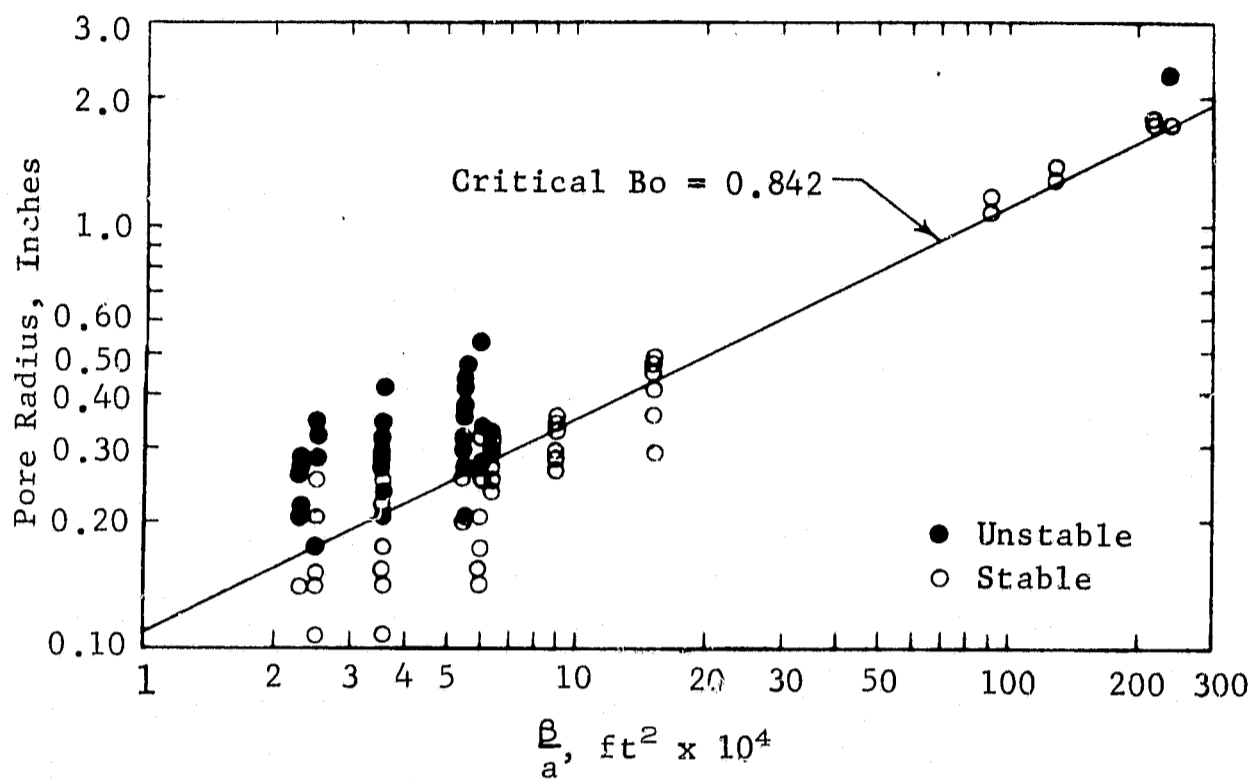
Fig. III-9   Stability Characteristics for Perforated Plate
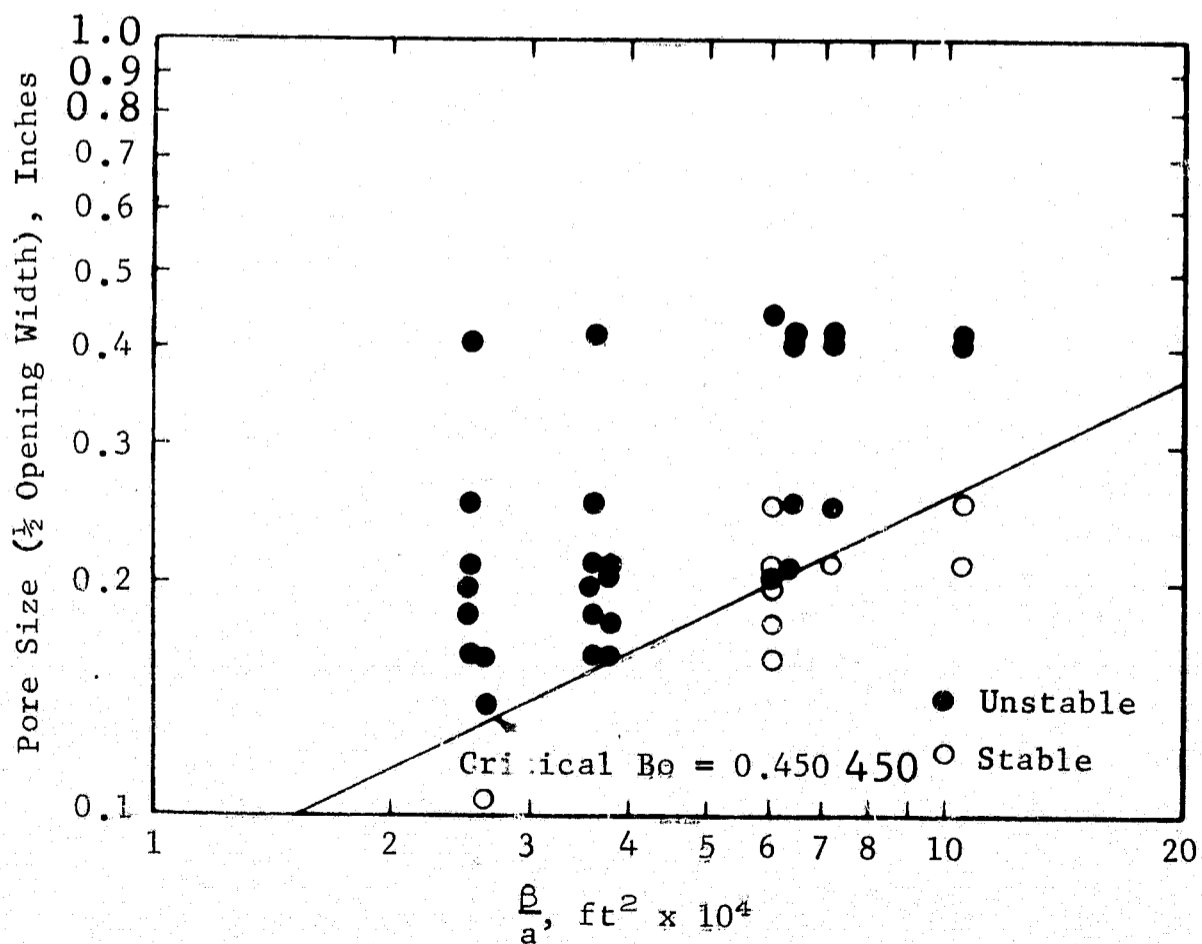
Fig. III-10   Stability Characteristics of Square Weave Screen

Table III-2   Propulsion System Stability Characteristics

Element	Acceleration (g)	Bond Number		Stability
		N_2O_4	A-50	
Coverplate	7.35	0.27	0.15	Yes
Holes	1.0	0.04	0.02	Yes
(0.021 in. D)	0.2	0.007	0.004	Yes
Stillwell	0.2	420	230	No
(5 in. D)	10^{-5}	0.02	0.01	Yes
Tank	0.2	40,000	20,000	No
(51 in. D)	10^{-5}	2.2	1.2	No

The capillary retention condition is associated with a multiple pore barrier as illustrated in Fig. III-11. In this case the system pressure is such that the gas phase is attempting to enter the pores at one extremity while the liquid drains from the opposite end. The capillary force preventing gas entry at each pore can be expressed by the Young-Laplace equation:

$$\Delta P = \sigma \left(\frac{1}{r_1} + \frac{1}{r_2} \right)$$

[III-3]

The critical pore for the system is the one supporting the maximum pressure differential (ρ ah in Fig. III-11). For a circular opening the maximum retention $\left(\Delta P_{max} \right)$ occurs when the interface is hemispherical $\left(r_1 = r_2 = r_p \right)$. For all other interface positions the radius of curvature is greater and therefore the pressure retention capability is less. Equation [III-3] for the maximum retention thus reduces to:

$$\Delta P = \frac{2\sigma}{r_p} = \rho \ ah$$

[III-4]

For a circular pore this can then be used directly to design the system. This equation also suggests a dimensionless group similar to the single pore stability equation:

$$Z = \frac{\rho \ ah \ r_p}{\sigma}$$

[III-5]

For complex geometry pores, such as Dutch twill cloth, the value
of the pore radius cannot be calculated. Even circular holes can
exhibit a considerably different retention capability depending
on how they are manufactured (e.g., punched, drilled, and reamed
holes of essentially the same diameter have exhibited different
retention characteristics during testing at Martin Marietta).
One way to account for this variation is to modify the retention
equation with a factor (φ) which would be a function of the pore
geometry, material surface condition, and liquid-solid contact
angle. Rearranging Eq [III-4] and solving for the required pore
size to support the hydrostatic pressure yields:

$$r_p = \frac{2\sigma\,\varphi}{\sigma\;ah}\left(\frac{1}{s}\right)$$ [III-6]

where s is the design safety factor for the system. Use of this
equation requires establishing a φ factor for the various types of
materials. This can be done empirically by use of a technique such
as the bubble point test using a control fluid of known properties.

The retention capability of the various elements of the sub-
scale system hardware is presented in Table III-3. The values
were obtained by determination of the bubble point using methanol
as the liquid medium. Since the screens used in the subscale sys-
tem are the same mesh as for the full-size design, the values
presented also apply to the prototype. The prototype 0.020-in.
double perforated plate retention capability as calculated from
the φ value for the 0.026-in. plate is 0.040 psi in methanol.
This is equivalent to 0.048 psi in N_2O_4 or 0.053 psi in A-50.
These retention values were used for all of the subsequent analysis
and modeling.
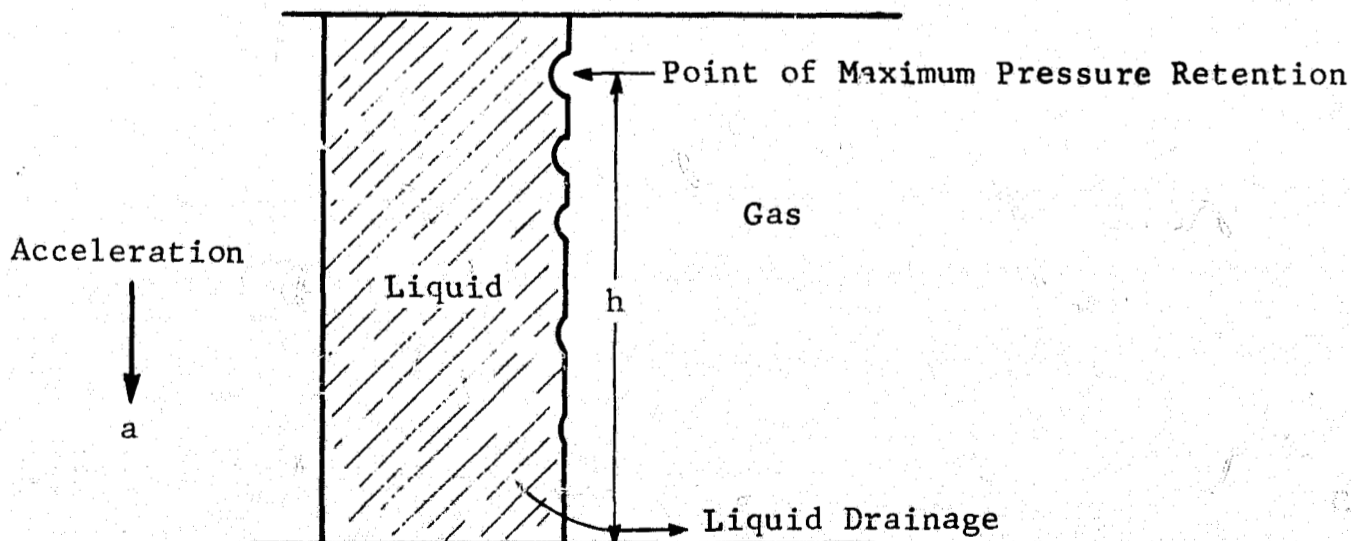
Fig. III-11 Multiple Pore Capillary Retention

Table III-3 Capillary System Retention Values

Element	Bubble Pressure (Methanol Test Fluid)	φ
Coverplate Single Layer (0.026 in. D)	0.021 psi	1.0
Double Layer (0.026 in. D holes 0.019 in. gap)	0.032 psi*	1.47 (based on single pore surface
30 x 250 mesh	0.094 psi*	0.728 (based on 100µ equivalent pore size)
250 x 1370 mesh	0.505 psi*	0.701 (based on 18µ equivalent pore size)
*Tested after fabrication into test model hardware.		

2. Hydrodynamic Stability

In addition to retaining liquid under steady-state acceleration the retention system must be able to damp liquid motion to prevent fluid loss from the retention compartment. Fluid motion induced by both axial and lateral acceleration must be considered. In looking at fluid damping, three initial liquid conditions with respect to the barrier must be considered: full compartment with liquid above the barrier; liquid exactly even with the barrier; and liquid below the barrier with an ullage pocket between the barrier and liquid interface. For axial perturbations the case of the liquid covering the barrier and exactly even with the barrier are analogous to the static Bond number condition. Following a disturbing acceleration that tends to locate the propellant away from the compartment, the liquid will reorient away from the barrier leaving the interface in the pores in the static "stuck" interface position. No velocity or inertia is induced into the trapped liquid in the compartment. The conventional Bond number stability criteria for these fill conditions was verified under Contract NAS8-21259 (Ref II-4).

For the condition where an ullage pocket exists between the liquid and the compartment coverplate, a negative disturbance will cause the liquid to impact the barrier at a velocity dependent on the distance traveled and magnitude of the disturbing acceleration. The nature of the liquid impacting configuration depends on the initial liquid configuration and the disturbing acceleration Bond

number. A categorization of liquid resettle modes over a range of resettle Bond numbers starting with a flat interface was conducted by Martin Marietta Contract NAS8-11328. The results are shown in Fig. III-12.

The retention compartments must damp out the liquid inertia to prevent flow loss from the barrier. The capillary barrier damping capability has been shown to be a function of the Weber number; the ratio of inertial to capillary effects:

$$We = \frac{Lv^2}{\sigma g_c} \qquad\qquad [III-7]$$

The damping category Weber number relationships established for double layer perforated plate and Dutch twill barriers under Contract NAS8-21259 (Ref II-4), are presented in Fig. III-13. Damping categories A through D represent virtually complete contaminent with no liquid flow through the barrier other than a few drops from coalescing liquid on the barrier surface.

For the prototype system, the lower compartment perforated plate impacting Weber number under the most severe negative acceleration (0.2 g) and liquid fill condition (near empty with flat interface) is in the range of 7 to 13 depending on the impacting liquid velocity assumptions. Although this value is slightly higher than the test range shown in Fig. III-13, it should be representative of D category or better damping. Lower negative accelerations and larger quantities of liquid would decrease the Weber number. At 0.02 g and the same fill condition the Weber number is only 2.8 and at the maximum 0.2 g condition with the compartment half full the Weber number is 6. These values are based on an impact velocity using a free-fall calculation. This velocity assumption is conservative, yielding Weber numbers considerably higher than what would be expected under actual conditions.

FLOW REGIMES

1. No flow.

2. Flow along the walls only.

3. Dome of liquid forms in the center, then recedes.

4. Dome forms in the center, grows to a certain size, then stops growing and remains virtually stationary until the liquid below is depleted due to flow along the walls.

5. Dome or cylinder forms in the center, continues to grow until it hits the top or joins the flow along one wall.
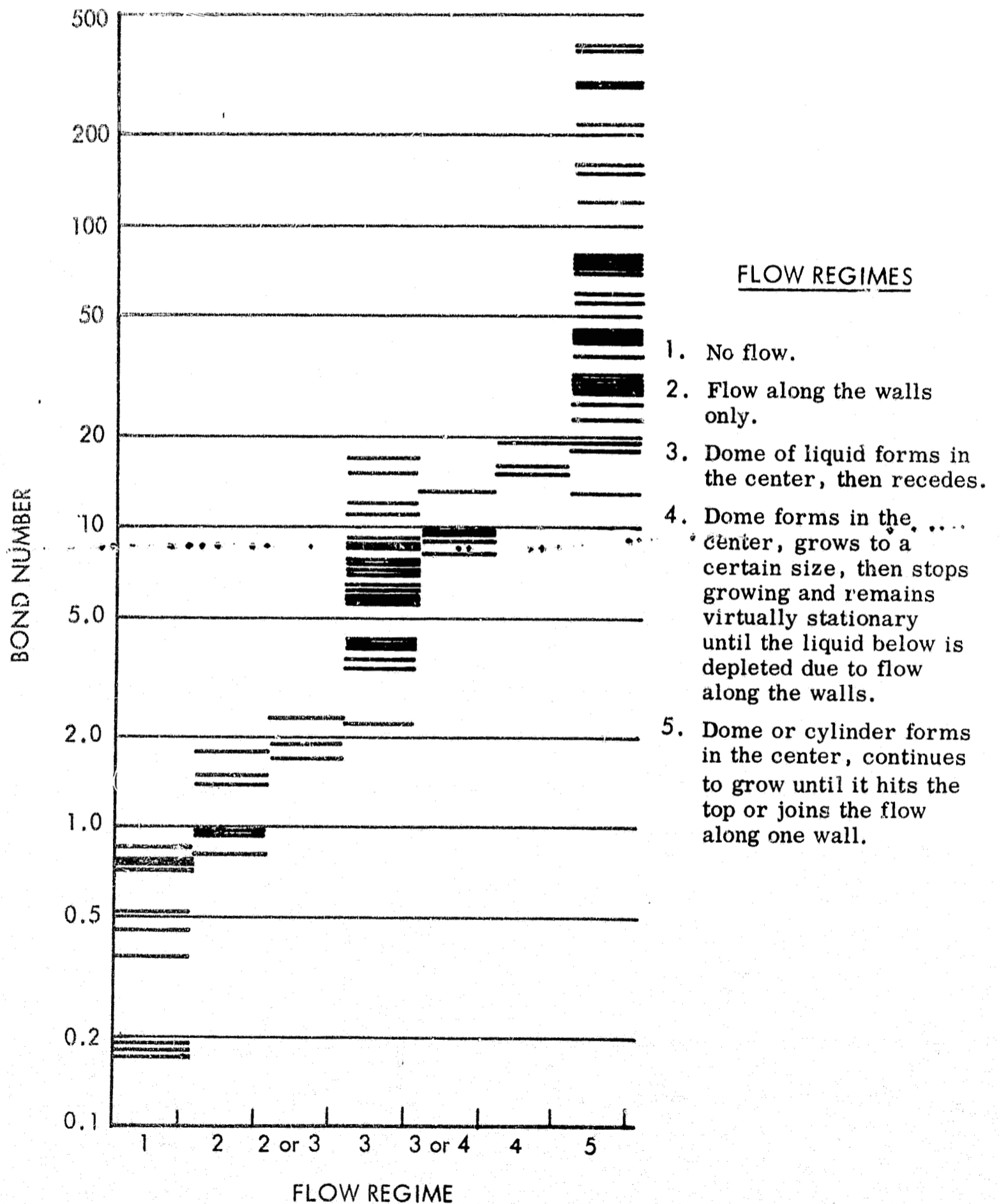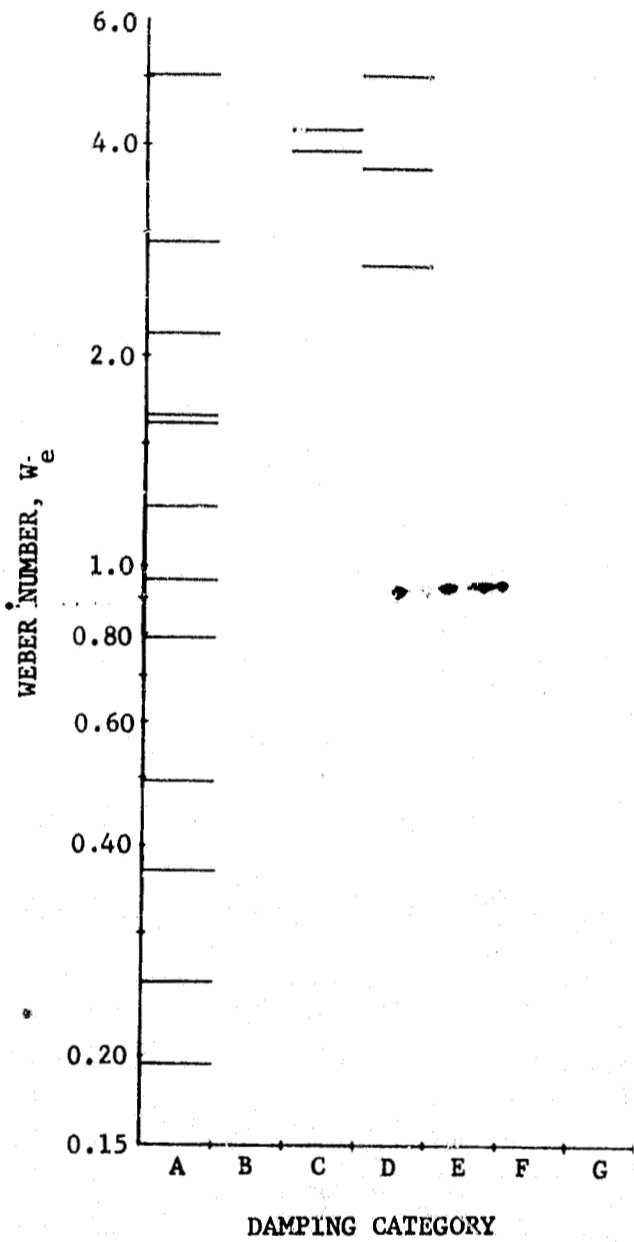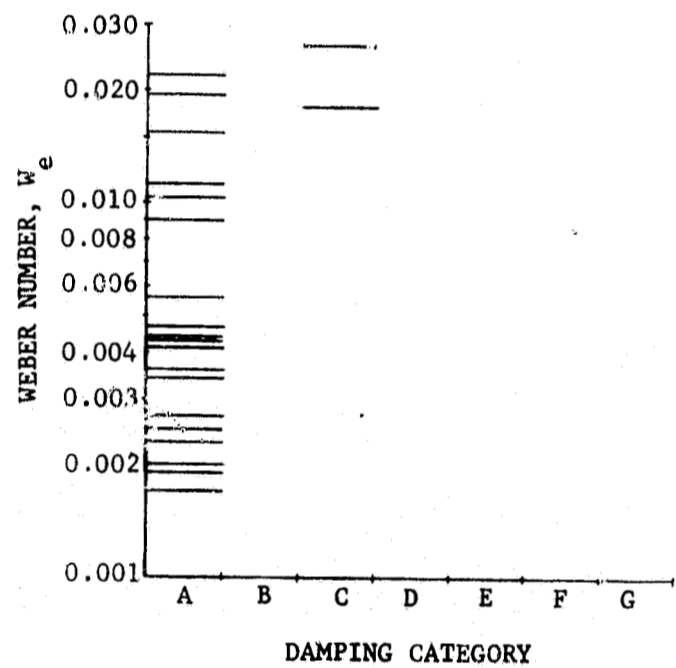
Fig. III-12   Categorization of Flow Regimes During Settling (Contract NAS8-11328)

(a) Double-Layer Perforated Plate
     Barriers

(b) Single-Layer Dutch-Twill Barriers

Fig. III-13 Double- and Single-Layer Barriers Damping
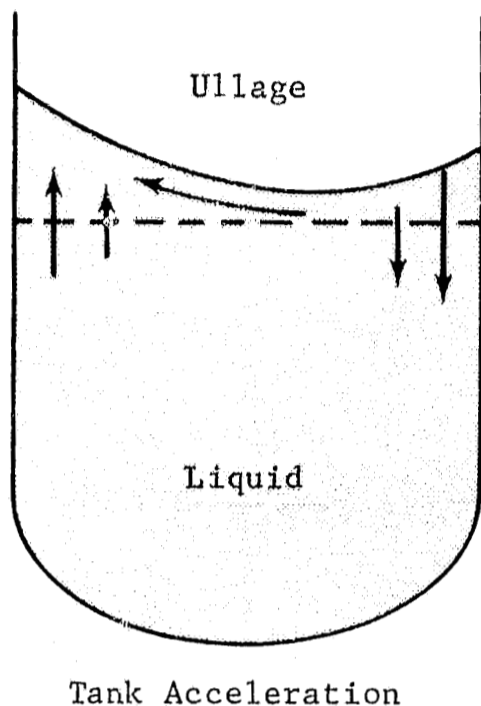
Tank Acceleration

Fig. III-14 Induced Liquid Motion
from Lateral Acceleration

In addition to axial disturb-
ances, the system must prevent li-
quid loss due to lateral perturba-
tions. The induced liquid motion
is shown in Fig. III-14. The bar-
rier must damp out the relative
momentum between the liquid and
the capillary barrier to avoid in-
gestion of gas at the outer holes
along the leading edge of the bar-
rier. This type of stability was
investigated extensively by Gille
(Ref II-1) for suddenly applied
accelerations. It was shown that
the conventional static stability
criteria applied equally well to
the dynamic case when no excess
liquid was located above the bar-
rier. For the condition of a
slight excess of liquid, the test
results indicated a decrease in
barrier stability. No analytical
or experimental treatment of this stability regime is known. An
experimental study is currently in progress by Martin Marietta
under Contract NAS8-21259 to investigate this phenomena and estab-
lish design criteria. The results from this study will not be
available for several months.

Rotational maneuvers of the spacecraft create a propellant
retention requirement that is similar to the transverse impulse.
The rotation of the spacecraft induces a relative inertia between
the liquid and the coverplate. The momentum of the liquid must
be damped out by the barrier to prevent gas ingestion into the
reservoir as liquid attempts to flow out as shown in Fig. III-14.
This phenomena was investigated for the Apollo SPS propellant ori-
entation device (Ref II-6 and II-7). The dimensionless parameter
used to describe this stability criteria was a modified form of
the Weber number:

$$We^* = \frac{\rho \, \omega^2 \, D^3}{\sigma \, g_c}$$

[III-8]

In this program the stability of the capillary barriers was defined in terms of the rotational Weber number and the barrier open area. Analyses (Ref III-5 and III-7) verify that this rotational Weber number is the proper descriptive parameter. However, the analysis does not include the effect of viscosity, which is expected to offer a significant damping effect in the proposed design with the tortuous flow path created by the Dutch twill screens and double-plate barriers. No known rotational stability analysis of the multiple-plate barrier or Dutch twill barrier has been conducted. However, test results have shown considerable performance improvement with multiple barriers.

To verify adequate stability of the design to either the lateral translation or the rotational maneuvers scale model testing was conducted.

3. Lateral Stability Tests

A total of five drop tests were made to demonstrate the retention capability of the coverplate screen assembly under a lateral acceleration environment. The lower dome of the 1/5-scale model with the lower coverplate was used. The model was mounted in an attitude with the centerline 10° from vertical so a portion of the screen cone would be parallel with the liquid surface. This was the leading portion in the lateral translation. The specimen was attached to a platform that moved along rails on low friction bearings. Coverplate liquid retention was observed through film coverage (200 fps) during the drop. Space limitation on the drop platform made it necessary to use a mirror arrangement for complete coverage (Fig. III-15). The test setup, assembled specifically for this effort, was mounted on the trailing end of the drag shield barrel section. Ordinarily, the test package is encased in a capsule that is contained in the evacuated drag shield to achieve zero g. This test package was too large for that procedure, so a zero-g condition in the vertical direction was not achieved. The drag force on the capsule causes an approximate 10^{-5} g positive acceleration on the test package. This acceleration is not large enough to affect the test results. The lateral accelerating force is provided by a compression spring that acts over a short distance (0.25 in.) imparting an impulse and subsequent coast period to the test article. The acceleration was initiated after a 1-sec delay during the 2.1-sec drop period to permit low-g liquid vapor interface formation before lateral impulse.
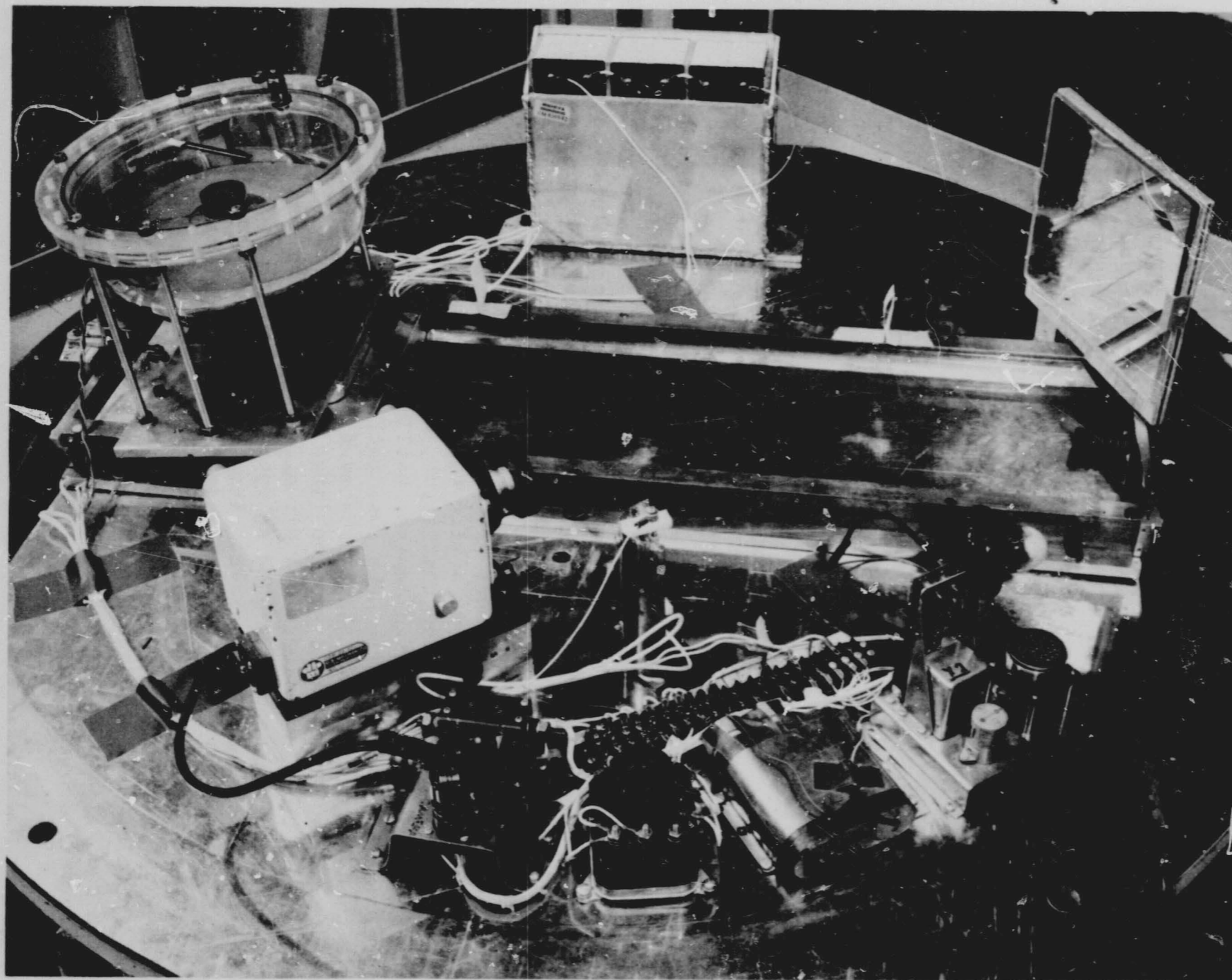
Fig. III-15 Lateral Acceleration Test Setup

The variables selected for the tests resulted from a scaling
exercise that considered the forces generated by impulsive pitch
and yaw maneuvers. These maneuvers, resulting from a force couple
provided by the RCS engines, cause a rotation of the vehicle about
its center of gravity. Relative motion between propellant and tank
results from vehicle angular acceleration during RCS firing. The
inertia of the moving liquid will tend to pull gas into the com-
partments below the coverplate barriers (Fig. III-16).

(a) Angular Acceleration   (b) Inertia Effects Continue
     with RCS Firing   after Firing
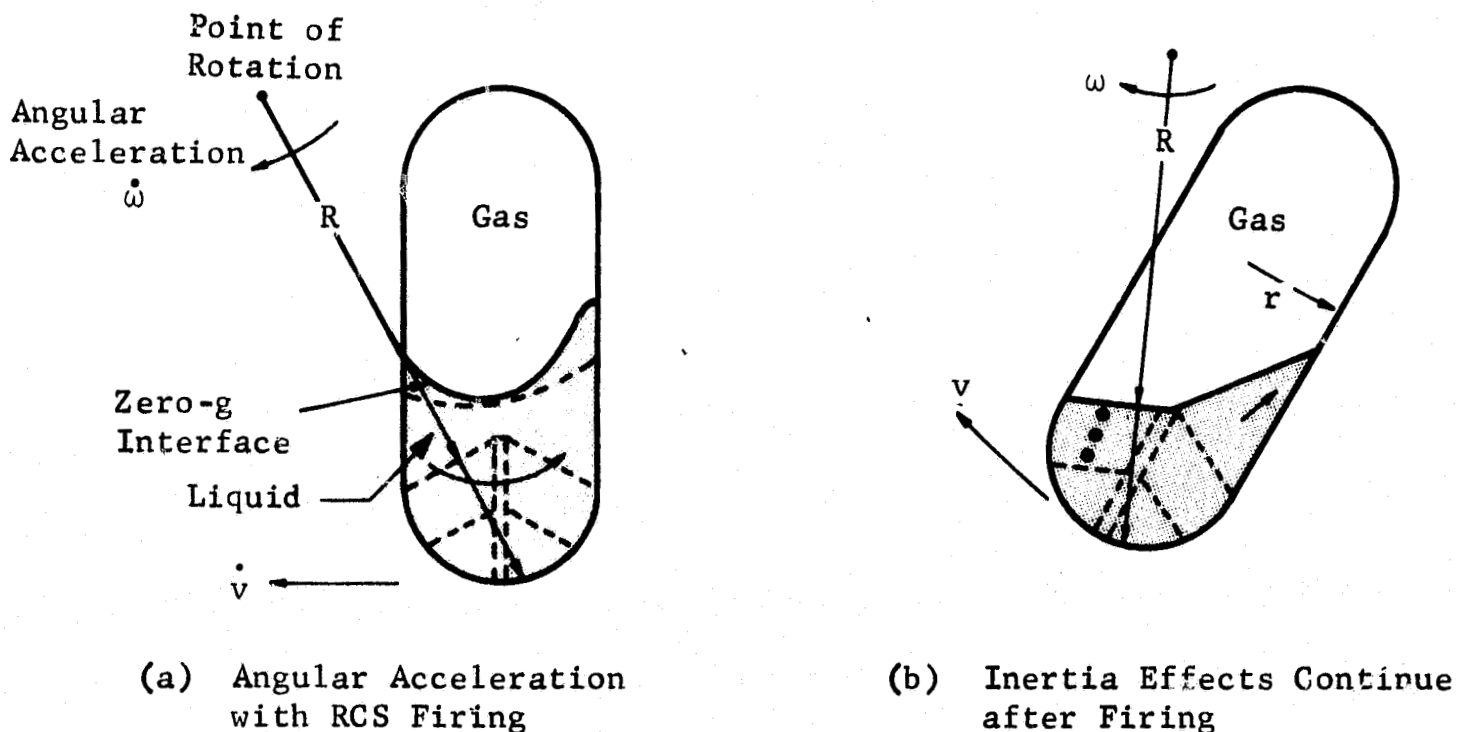
Fig. III-16 Liquid Movement During Pitch and Yaw
            Maneuvers

The critical scaling parameter between model and prototype is
the Weber number, the ratio of inertia to capillary forces.

$$We = \frac{v^2 L}{\sigma g_c}$$

[III-9]

In the prototype it is more convenient to express the velocity in
terms of the angular velocity, ω, and turning radius, R (see Fig.
III-16).

$$v^2 = R^2\omega^2 \qquad\qquad\qquad [\text{III-10}]$$

The We then becomes:

$$We = \frac{R^2\omega^2 L}{g_c\ \sigma} \qquad\qquad\qquad [\text{III-11}]$$

where R is the propellant tank radius. The conditions of interest occur during the steady-state rotation after impulse termination. The inertia of the moving liquid under constant ω depends on the magnitude of the accelerating torque as well as the time it acts. A most severe condition would result with an instantaneous impulse of sufficient magnitude to cause the maximum angular velocity of 5 deg/sec. Short-duration impulses were used to accelerate the model to the scaled velocity required to conserve We. Lateral translation rather than **rotational motion was selected for model** tests because it simplifies the test hardware required for the low-g tests without seriously affecting test results. The $R^2\omega^2$ variables in the prototype will be represented in the model by constant lateral velocity resulting from the short-duration impulse. Then to conserve We;

$$\left(\frac{R^2\omega^2 L}{g_c\ \sigma}\right)_p = \left(\frac{v^2 L}{g_c\ \sigma}\right)_m \qquad\qquad [\text{III-12}]$$

where subscripts p and m refer to prototype and model, respectively. The We to be conserved in the model tests is based on the oxidizer tank, which is the most critical,

φ = 90.6 lb/ft^3 (NTO),

R = 90 in. = 7.5 ft,

ω = 5 deg/sec = .0925 rad/sec,

g_c = 32.2 ft/sec^2,

L = 25.5 in. = 2.12 ft,

σ = 1.88 x 10^{-3} lb/ft,

$(We)_p$ = $(We)_m$ = 1,515 based on the above variables.

The variables for the model We, based on a 1/5-scale test model
and ethanol as the test fluid, are,

$$\phi = 49.2 \text{ lb/ft}^3,$$

$$L = 4.75 \text{ in.} = 0.395 \text{ ft,}$$

$$\sigma = 1.53 \times 10^{-3} \text{ lb/ft,}$$

$$g_c = 32.2 \text{ ft/sec}^2,$$

$$R\omega = v = 1.96 \text{ ft/sec.}$$

The lateral velocity selected for the model tests was 1.96 ft/sec
after impulse. The impulse force and action time was adjusted to
accelerate the test specimen and translating platform to this ve-
locity within a 1/2-in. displacement.

Two test conditions were used to demonstrate the retention
capability of the coverplates. The liquid level was maintained
at the screen surface in one case and slightly above in the sec-
ond case. Both methanol and ethanol were used as test liquids.
In all of the tests a small vapor bubble was observed below the
coverplate during the low-g period prior to lateral impulse ini-
tiation due to incomplete trap volume filling. There is no evi-
dence of gas ingestion during the lateral translation period as
observed from the filmed results for either liquid level. The
retention potential of the coverplates exceeds that imposed by
the tests. A series of photographs taken from the filmed results
of the tests are presented in Figure III-17.
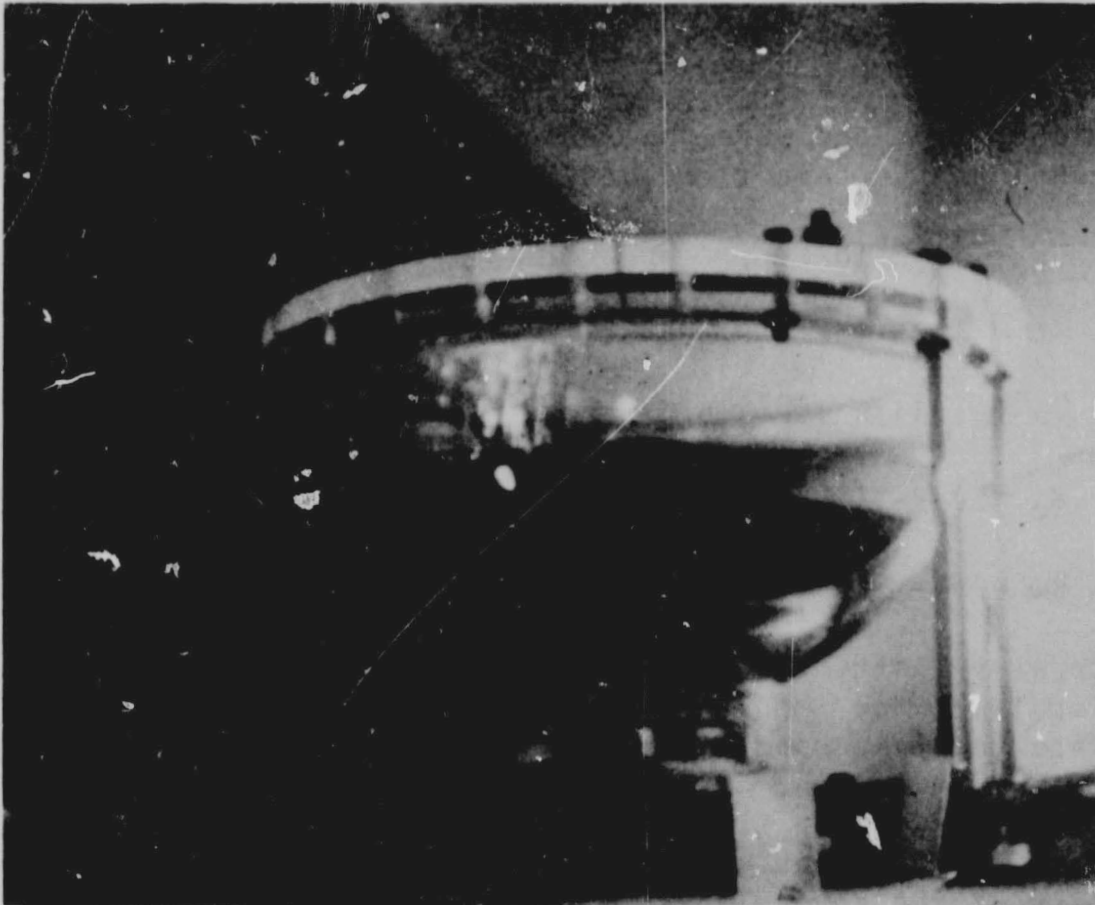
(a)   Test 23, 0.65 sec after Zero g before Lateral
       Impulse
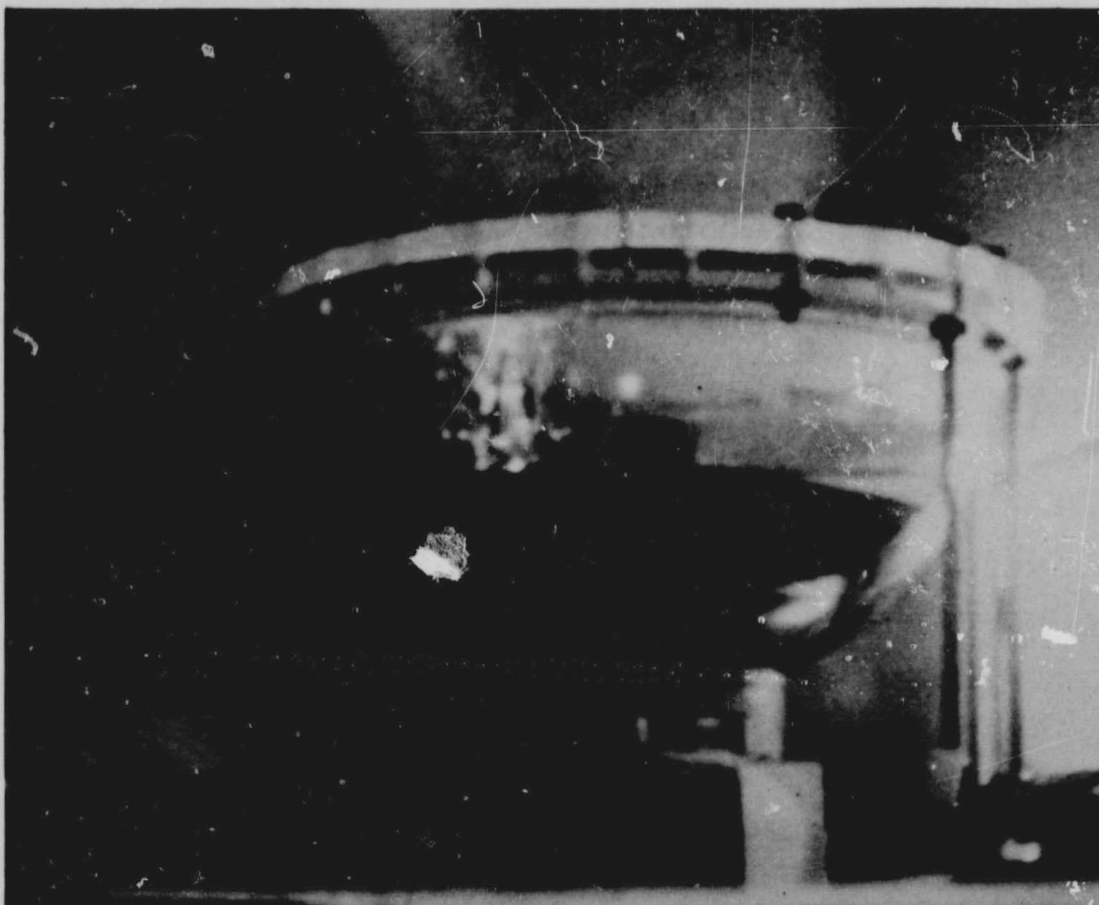
(b)   Test 23, 0.75 sec after Zero g Initiation,
       Leading Edge of Barrier Uncovered as a Re-
       sult of Translation without Gas Ingestion

Fig. III-17   Lateral Acceleration Test Results

(c) Test 24, 0.646 sec after Zero g before Lateral
    Impulse

(d) Test 24, 0.74 sec after Zero g Initiation,
    Leading Edge of Barrier Uncovered with No Gas
    Ingestion due to Liquid Inertia

Fig. III-17 (concl)

C. PROPELLANT REORIENTATION

Reorientation of the propellants from the forward ends of
their tanks back toward the outlets by accelerating the vehicle
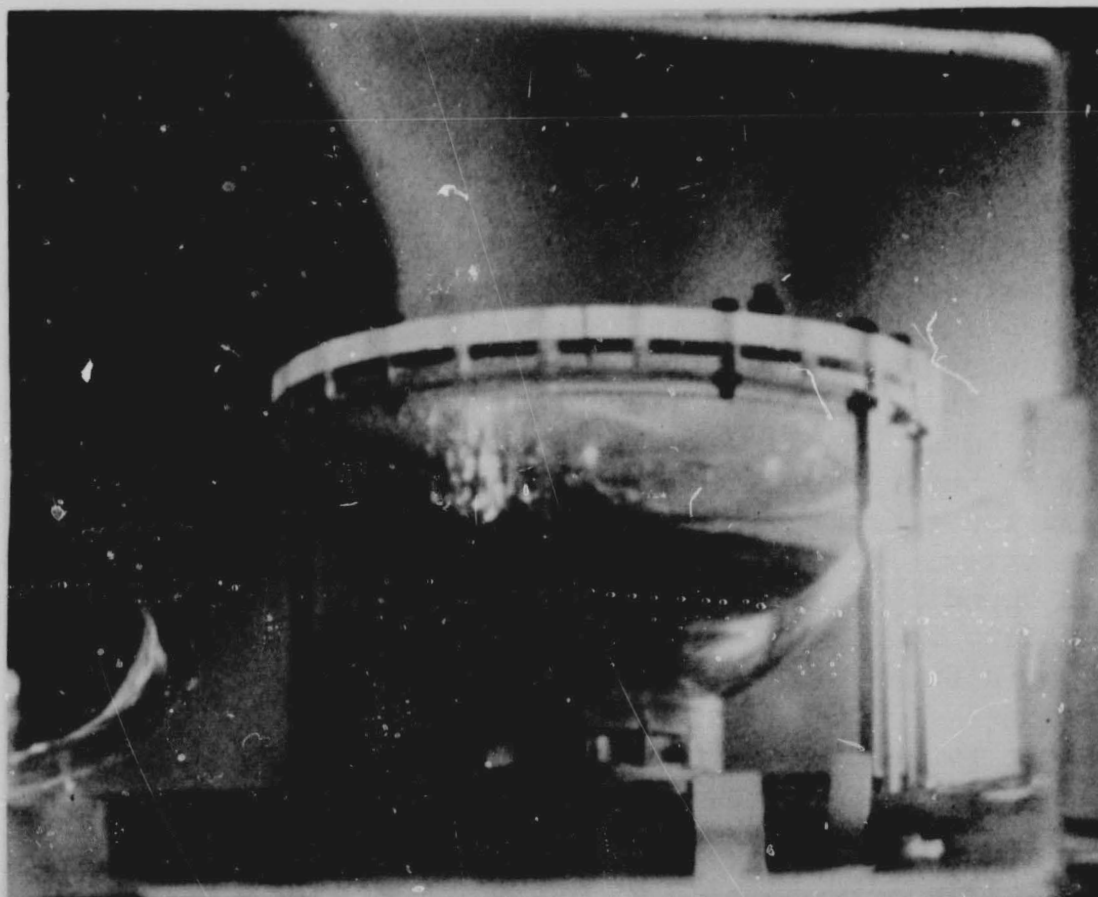was analyzed using the Marker and Cell (MAC) computer program
mentioned earlier in this report. The following paragraphs de-
scribe the Marker and Cell computational scheme at greater length.

The basic MAC technique was developed by Dr. Francis Harlow
and co-workers at Los Alamos Scientific Laboratory, and has been
reported in detail in a series of papers and reports (Ref II-8
and III-3 thru III-5). A correction to the free-surface viscous
stress conditions has been reported by Hirt and Shannon (Ref
III-6). Some of the stability considerations essential to proper
application of the technique have been elucidated by Hirt (Ref
III-7). Incorporation of surface tension effects were first dis-
cussed by Daly and Pracht (Ref III-8), and have since been treated
at much greater length by Daly (Ref III-9 and III-10).

The MAC technique is based on a formulation of the full non-
linear, viscous, time-dependent equations of motion in terms of
primary variables (pressure and velocity), with a finite-differ-
ence solution using an Eularian grid mesh. The liquid configura-
tion (and hence, indirectly, the free boundary) is indicated by a
Lagrangian set of marker particles located in the liquid and mov-
ing with it. Pressures are calculated at cell centers, horizontal
velocities along vertical cell boundaries, and vertical velocities
along horizontal cell boundaries.

The actual calculations are based on three equations. Poisson's
equation is derived by combining the full Navier-Stokes equations
with the incompressible continuity equation; written in finite-dif-
ference form, this equation allows the pressure field to be calcu-
lated on the basis of the velocities calculated at the preceding
time step. Boundary conditions specify the pressure on the free
surface and the normal components of the pressure gradients at
fixed boundaries. (The normal component of the pressure gradient
at a fixed boundary must be equal to the normal component of grav-
ity or boundary acceleration.) Solution, in the basic MAC tech-
nique, is by a Gauss-Seidel iterative process.

The other two equations used are Navier-Stokes equations, which
are used to solve for the two velocity components on the basis of
the pressure field just calculated, and the velocity field calcu-
lated in the preceding time step. Boundary conditions are the van-
ishing of normal velocity components at fixed boundaries, and the

vanishing of liquid shear at a free surface. (The latter is not
really a proper free-surface boundary condition, as pointed out
by Hirt and Shannon. For cases in which viscosity is not of great
importance near the free surface, however, it should not adversely
affect the accuracy of the method.)

There are two primary differences between the MAC program writ-
ten at Martin Marietta and the basic MAC program described in Ref
II-8 and III-3 thru III-5. Most significant is the fact that the
Martin Marietta program uses a successive overrelaxation iterative
procedure for the pressure calculations in place of the more ele-
mentary Gauss-Seidel procedure normally used, thereby significantly
reducing the computation time required per time step for a given
number of computational cells. In addition, the Martin Marietta
program was written in terms of two concentric cylindrical bound-
aries (with plane perpendicular end boundaries). The inside bound-
ary can, of course, be removed to allow more standard cylindrical
geometries to be investigated.

The initial stationary liquid configuration was set up in ac-
cordance with a low Bond number equilibrium surface generated by a
computer program based on the following method of analysis:
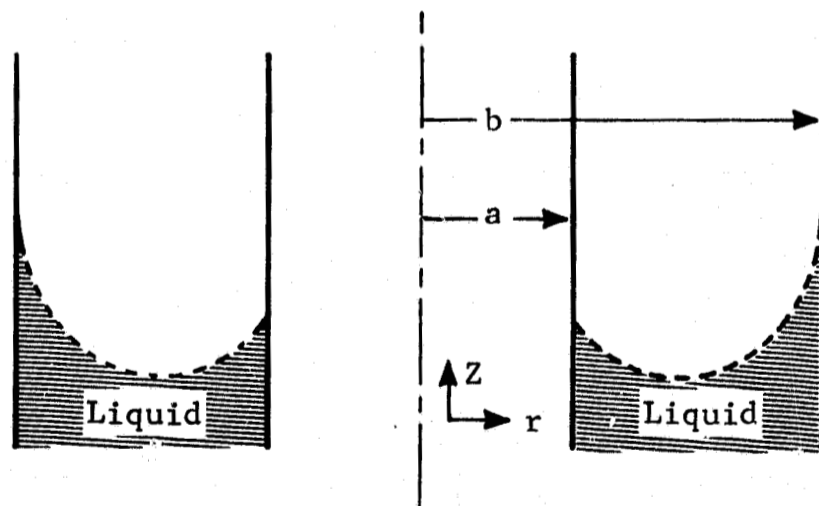
The Young-Laplace equation governs the free-surface shape.
Using the coordinate system marked on the diagram, the Bashforth-
Adams form of the equation is a parametric set for $Z_L(\varphi)$ and $r_L(\varphi)$
(the coordinates of the free-surface position.)

$$dr_L = \cos \varphi \ d\varphi \Bigg/ \left[C + \left(\frac{\rho g}{\sigma}\right)\left(Z_L\right) - \sin \varphi \Big/ r_L \right] \qquad [III-13]$$

$$dZ_L = \sin \varphi \ d\varphi \Bigg/ \left[C + \left(\frac{\rho g}{\sigma}\right)\left(Z_L\right) - \frac{\sin \varphi}{r_L} \right] \qquad [III-14]$$

φ is the surface slope,

$$\frac{dZ_L}{dr_L} = \tan \varphi \qquad [III-15]$$

The constant C is the free surface curvature at $r_L = a$; it is an unknown to be determined from the boundary conditions.

The conditions at the inner wall are

$$r_L = a \qquad [III-16]$$

$$Z_L = 0 \qquad [III-17]$$

$$\varphi = \frac{\pi}{2} + \alpha \qquad [III-18]$$

where α is the contact angle, a physical property. The conditions at the outer wall are

$$r_L = b \qquad [III-19]$$

$$\varphi = \frac{\pi}{2} - \alpha \qquad [III-20]$$

To perform the integration of this nonlinear problem from the inner to the outer wall, some initial estimate of the curvature C must be found. A useful linear form of the Young Laplace equation is

$$\frac{1}{r_L} \frac{d}{dr_L} \left(r_L \frac{dZ_L}{dr_L} \right) = C + \left(\frac{\rho g}{\sigma}\right) Z_L \qquad [III-21]$$

The solution of this equation with the correct boundary condition is

$$z_L = \frac{-b \cot \alpha}{\sqrt{B}} \left\{ \frac{K_1\left(\sqrt{B}\right) + K_1\left(\sqrt{B}\,\frac{a}{b}\right)}{I_1\left(\sqrt{B}\right) - I_1\left(\sqrt{B}\,\frac{a}{b}\right)} \left[I_0\left(\sqrt{B}\,\frac{r_L}{b}\right) - I_0\left(\sqrt{B}\right) \right] \right.$$

$$\left. + \frac{I_1\left(\sqrt{B}\right) + I_1\left(\sqrt{B}\,\frac{a}{b}\right)}{K_1\left(\sqrt{B}\,\frac{a}{b}\right) - K_1\left(\sqrt{B}\right)} \left[K_0\left(\sqrt{B}\,\frac{r_L}{b}\right) - K_0\left(\sqrt{B}\right) \right] \right\}$$

[III-22]

where the Bond number is

$$Bo = \frac{\rho g b^2}{\sigma}$$

[III-23]

Thus the linear theory yields an estimate of C (replacing $\cot \alpha$ with $\cos \alpha$)

$$C \approx \frac{b \cos \alpha}{\sqrt{B}} \left[\frac{K_1\left(\sqrt{B}\right) + K_1\left(\sqrt{B}\,\frac{a}{b}\right)}{I_1\left(\sqrt{B}\right) - I_1\left(\sqrt{B}\,\frac{a}{b}\right)} I_0 \sqrt{B} + \frac{I_1\left(\sqrt{B}\right) + \left(I_1\sqrt{B}\,\frac{a}{b}\right)}{K_1\left(\sqrt{B}\,\frac{a}{b}\right) - K_1\left(\sqrt{B}\right)} K_0\left(\sqrt{B}\right) \right]$$

[III-24]

Performing the integration of the Bashforth-Adams equations from

$$\varphi = \frac{\pi}{2} + d, \quad r_L = a \quad \text{to} \quad \varphi = \frac{\pi}{2} - \alpha$$

yields

$$r_\varphi \left(\frac{\pi}{2} - \alpha \right) \neq b$$

[III-25]

since the value of C is only an estimate. Repeating the integration with new values C based on a second convergence method leads to the correct value of C and thus an accurate numerical solution for the axisymmetric static-free surface shape. This solution is represented by a mesh of $\left(z_L, r_L\right)$ coordinates.

Surface tension was included only for the purpose of calculating the initial configuration; no attempt was made to incorporate surface tension into the MAC technique. In addition, the actual propellant tanks were approximated by a plane-ended circular

cylinder, 51 in. in diameter, with a 5-in. diameter concentric
cylinder forming the inside boundary.

Liquid configurations, as generated by the computer, are shown
in Fig. III-18 for a few of the calculated time steps. Vehicle
acceleration was taken to be 0.6 g. Computational cells were just
under 2 in. square.

Calculations were not carried much beyond 0.16 sec because of
prohibitive expense. At 0.16 sec, 31.6 minutes of CDC 6500 central
processor time had already been expended. Much more serious, the
size of the time step had already been reduced from 0.008 sec to
0.000125 sec in accordance with stability requirements based on the
liquid velocities.

Because of the extreme expense involved in applying the MAC
program to obtain the desired propellant reorientation description,
a new program being developed at Martin Marietta, SMASHIN (Surface
Markers Added to Some Hydrodynamic Iterative Nefariousness), was
applied to the problem. This program is quite similar to the basic
MAC program except for the method of bookkeeping used (that is, the
way of keeping track of the location of the liquid) and the way the
boundary conditions are applied at the free surface in the pressure
and velocity calculations.

This matter of free-surface boundary conditions is perhaps the
primary weakness of the basic MAC technique when applied to prob-
lems of the sort we are interested in. Serious difficulties arise
twice during the computational scheme because of the inability to
precisely define the surface. The first time is in the computation
of the pressure field; the computation, no matter how accurate, can
never actually be accurate in the critical region near the free sur-
face since the free surface pressure condition is not applied on the
free surface, but rather at the nearest cell centers. Hence the
pressure computation "sees" a free surface that is always somewhat
displaced from the actual free surface, and grossly different in
shape. The second difficulty occurs when velocities are calculated
near the free surface. Because of the lack of definition of the
surface, the basic MAC method cannot generate surface cell veloci-
ties that properly reflect the flow of liquid into or out of the
surface cell from the previous time step. The normal procedure has
consequently been to neglect changes in the quantity of liquid in
any surface cell from one time step to the next. Errors introduced
in this manner will naturally propagate into the interior of the
liquid in succeeding time steps, hence affecting the more exact
velocity calculations that can be made in cells completely sur-
rounded by liquid.
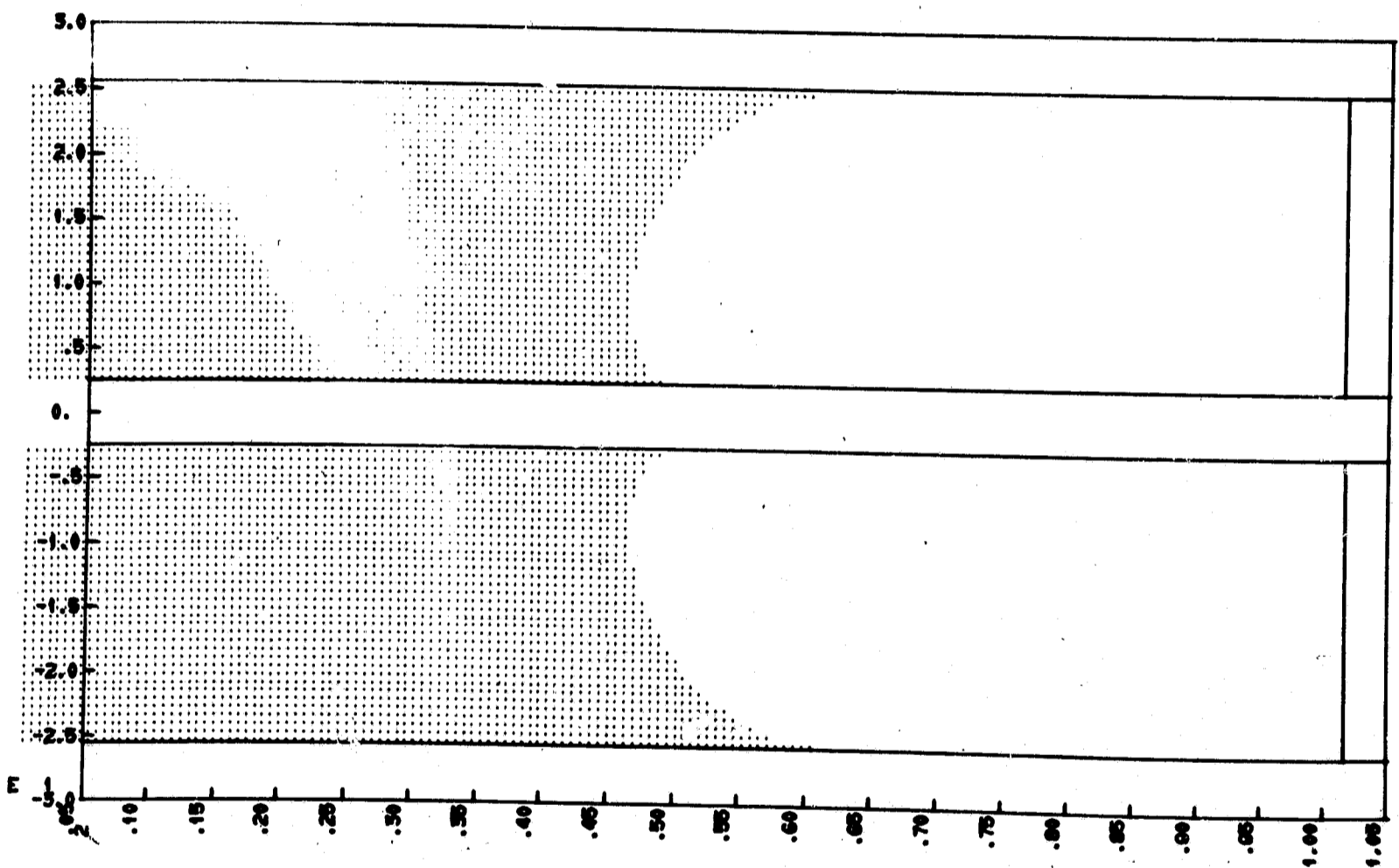
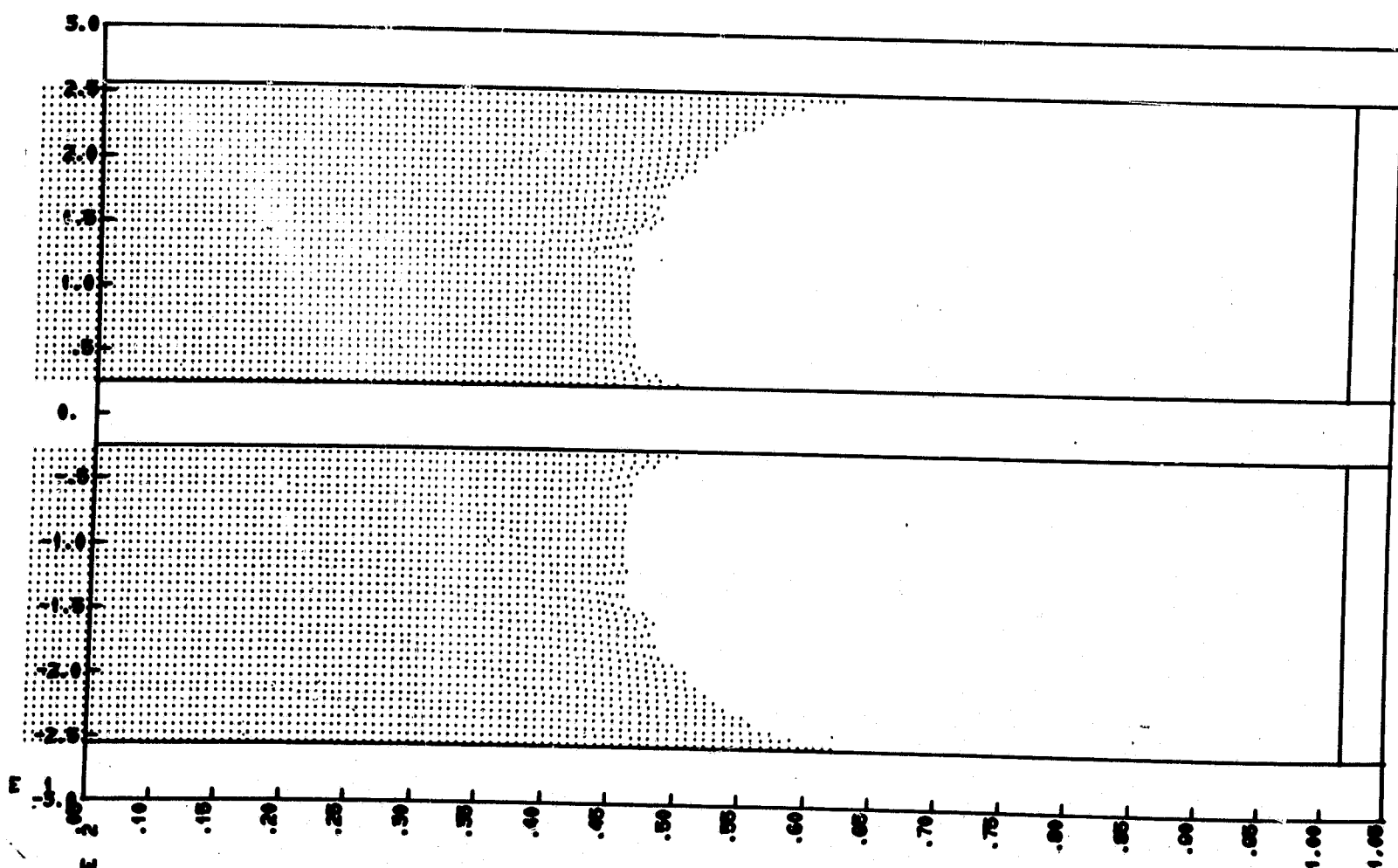.0080 SECONDS

(a) CP = 0.4 min

Fig. III-18 Propellant Reorientation Profile
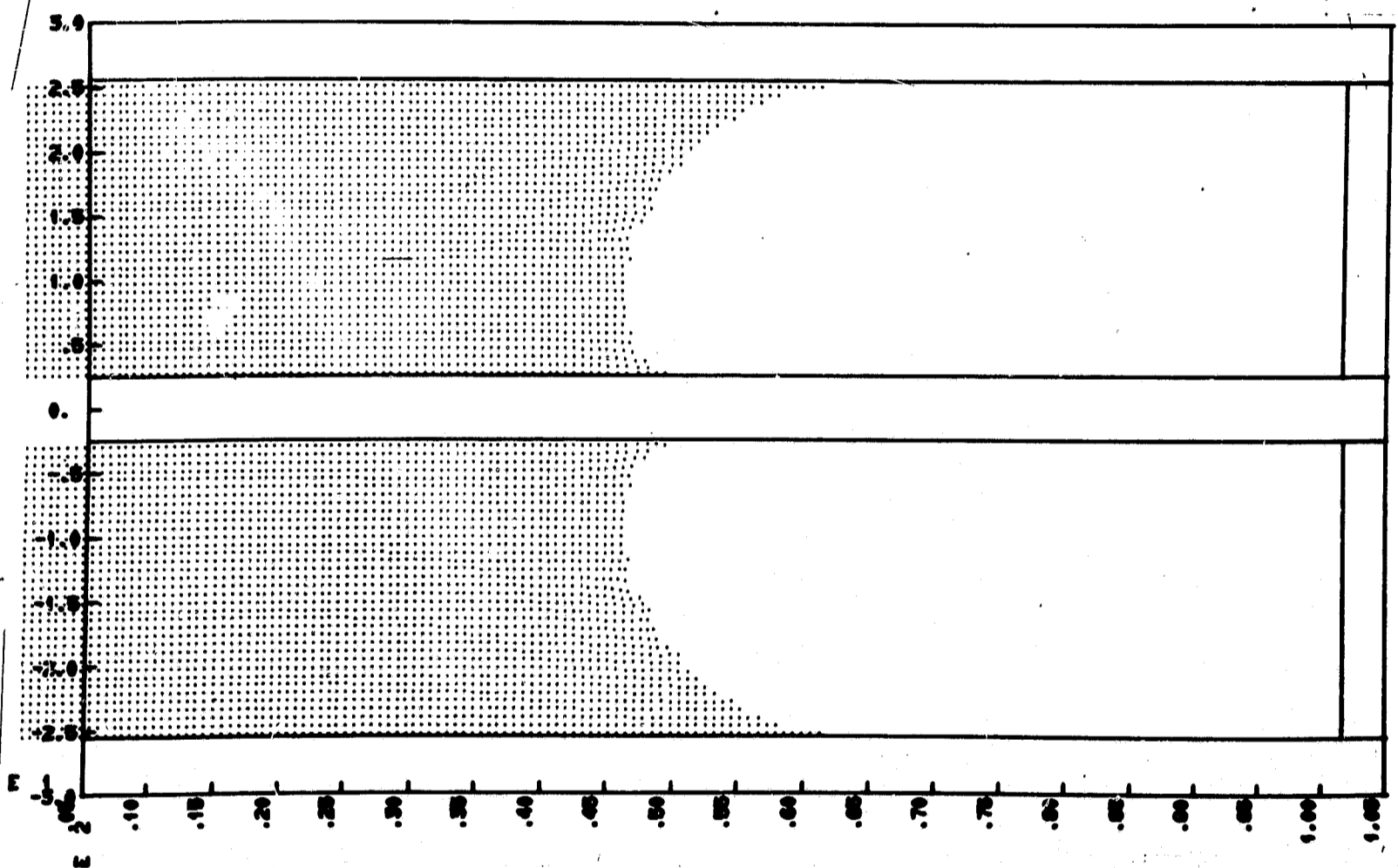
.0810 SECONDS
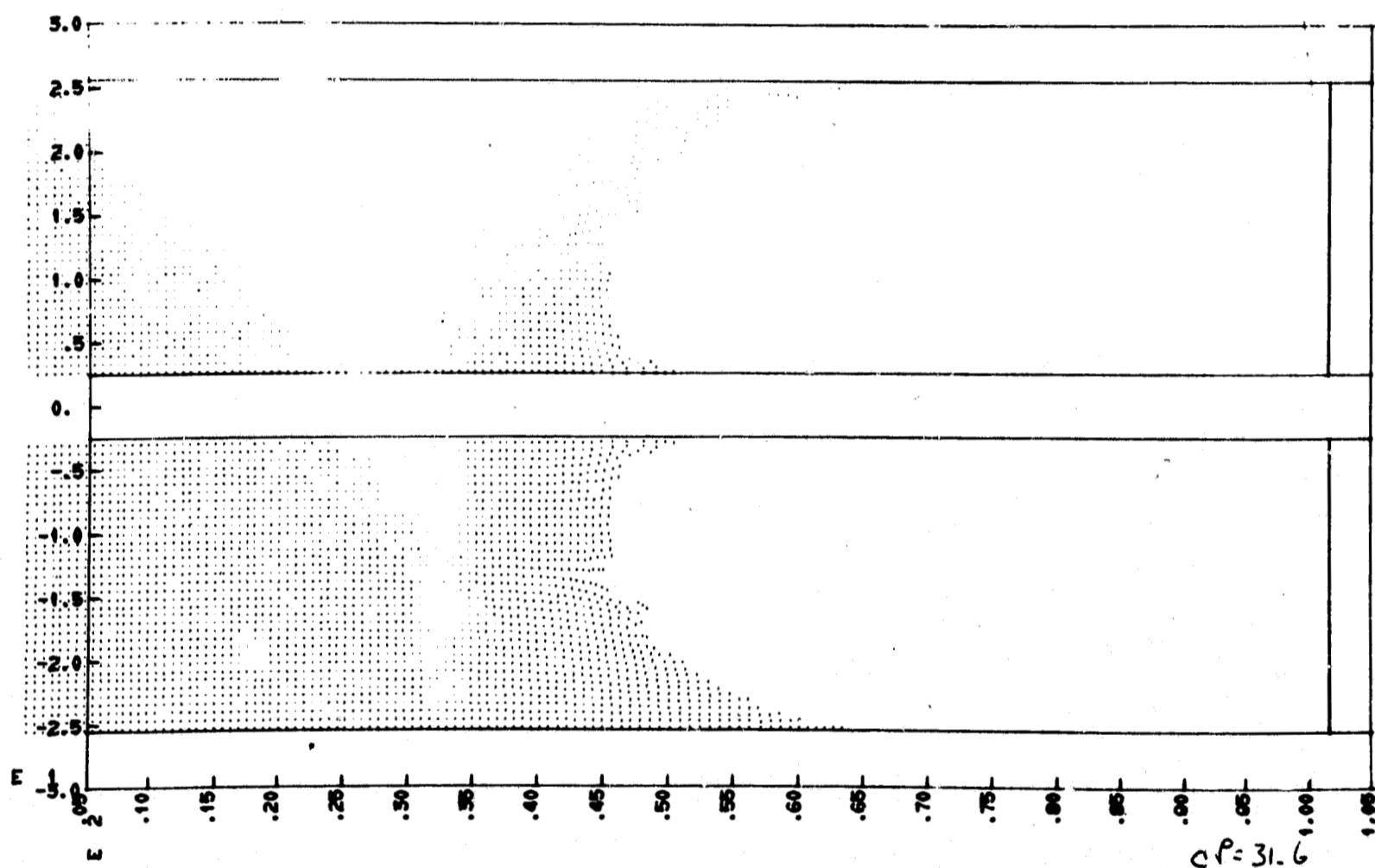
(b) CP = 5.8 min

Fig. III-18 (cont)

.1200 SECONDS

(c) CP = 16.1 min

Fig. III-18 (cont)

.1600 SECONDS

(d)   CP = 31.6 min

Fig. III-18   (concl)

The primary objective of SMASHIN was to remove these difficul-
ties by introducing an additional set of marker particles, initi-
ally lying on the surface and hence always moving with the surface,
to define the surface. At present a fairly large number of such
markers are used, and the surface is simply approximated by the
straight line segments connecting these markers. (A more sophis-
ticated curve fit would allow surface tension to be incorporated
without too much difficulty.) With the surface as defined, the
pressure boundary condition is applied virtually on the free sur-
face, and an unequal-arm Poisson's equation derived for the pres-
sure calculation near the free surface. Incorporating these changes
into the overall pressure iteration matrix should result in a con-
siderably more accurate calculated pressure field. In addition, by
knowing where the surface actually is, the volume of liquid in each
surface cell can be calculated, the change from one time step to
the next recorded, and this change fed back into the velocity cal-
culations in the form of a non-zero divergence for each of the
surface cells.

The primary benefit to be expected from these improvements in
computational accuracy is a savings in machine time required for a
given set of results. More accurate treatment allows larger (and
hence fewer) cells to be used, and consequently the time step can
start out larger, and not be reduced as drastically. An additional
time saving has been introduced by basing all of the "bookkeeping"
operations on the surface markers themselves, hence allowing the
normal MAC fluid markers to be eliminated. This step considerably
streamlines the computational procedure since it removes the neces-
sity of calculating velocities and, on the basis of the velocities,
new positions, for what normally was a very large number of fluid
markers.

This program was used to investigate the propellant reorienta-
tion problem for the same conditions as before, but with the com-
putational cell size increased to 2.3 in. on a side. Some of the
results are presented in Fig. III-19.
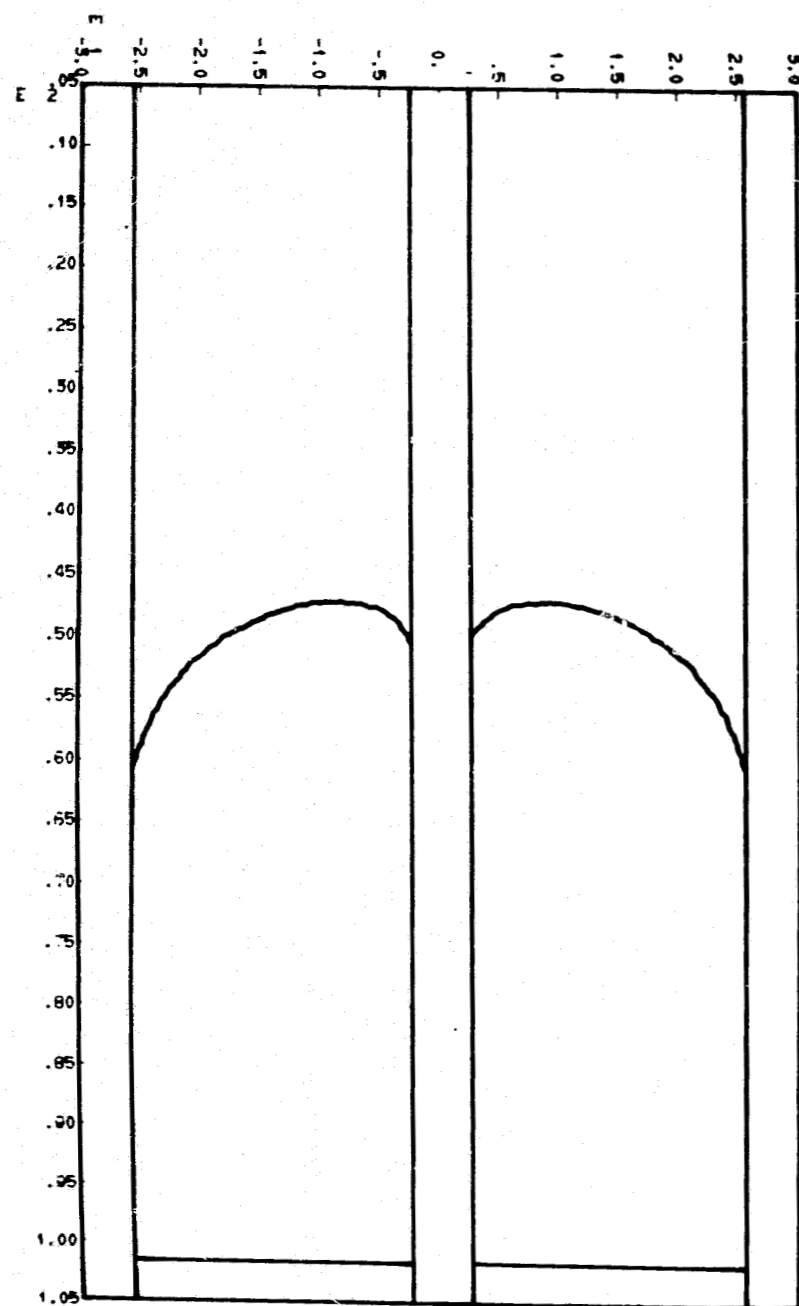
(a) Initial Interface in 10^{-5} g Environment
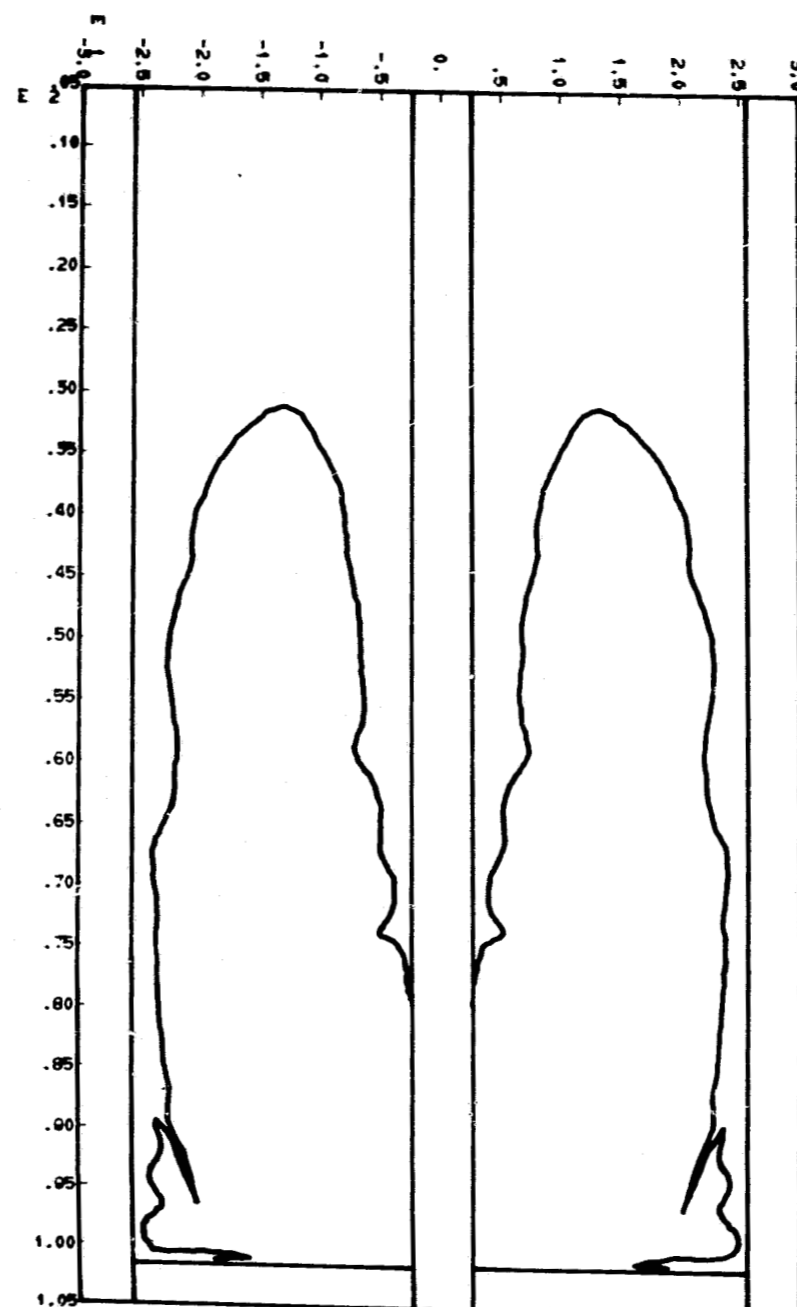
(b) Interface 0.75 sec after Initiation of
0.6-g Resettle Acceleration

Fig. III-19 Propellant Resettle Characteristics

D. BARRIER PROPELLANT RESETTLE CHARACTERISTICS

Two basic considerations were investigated relative to propel-
lant resettle in the SPS tank with a capillary barrier. The first
was to investigate the liquid impact on the coverplate to determine
the resettle fluid behavior and the liquid accumulation rates. The
second was to determine the ability of the capillary barrier to
prevent large gas accumulations from being forced into the compart-
ments, i.e., prevent the gas bubbles entrained in the liquid due
to resettle from passing through the coverplates.

Since one of the primary design goals for the propellant man-
agement system was to be capable of engine restart without any re-
quirement for propellant settling maneuvers, the propellant collec-
tion rate at the capillary control system is extremely important
to the proper sizing of the retained propellant compartment. If
propellant is in contact with the compartment, little or no pro-
pellant is consumed from the compartment during engine restart and
operation. However, if the propellant has migrated to the opposite
end of the tank, the propellant feed will be supplied from the com-
partment being replaced by ullage gas until sufficient liquid flow
is established from the bulk liquid resettling to supply the pro-
pellant being displaced. The liquid collection rate is a function
of the propellant flow to the containment device due to the accel-
eration from engine thrust buildup minus the amount lost due to
propellant geysering or rebound from the containment area. The
acceleration environment before engine thrust buildup is on the
order of 10^{-5} g (typical value for spacecraft of this size class),
which results in a Bond number of approximately two for the N_2O_4
tank. The tank interface associated with this acceleration level
is shown in Fig. III-19 for the tank containing a stillwell. The
resettle acceleration level varies from about 0.6 to 0.85 g. This
results in a resettle Bond number of approximately 100,000 for the
oxidizer tank and 75,000 for the fuel tank, based on tank radius.

The subject of liquid reorientation has been discussed both
analytically and experimentally at considerable length (Ref II-6
and III-11 thru III-13). However, in most of these cases the
discussion has been confined to a case for a clean cylindrical
tank with a spherical bottom and sufficient propellant to elimi-
nate the tank top end effects.

For a cylindrical tank with a curved interface it has been
experimentally shown that the nature of the reorientation is for
liquid to flow along the wall with the liquid gas interface moving

up in the center as shown in Fig. III-20. When the leading edge
of the liquid reaches the bottom, momentum of the liquid results
in a tendency for the liquid to rebound or geyser. An experimen-
tal study of geyser formation was conducted (Ref III-12), which
established a Weber number criterion for geyser formation for both
convex and concave bottom tanks. For the configurations tested
geysering always occurred at a Weber number greater than 4. While
these data were generated for a reorientation Bond number range of
3 to 70 [much lower than the resettle Bond numbers for the SPS
(Bo $\gg$ 1000)], additional data (Ref III-13), has shown geysering
to occur for Bo of 2900 and We > 19,000, which is nearer the range
for this system. Therefore propellant geysering following impinge-
ment of the leading liquid edge on the capillary coverplates would
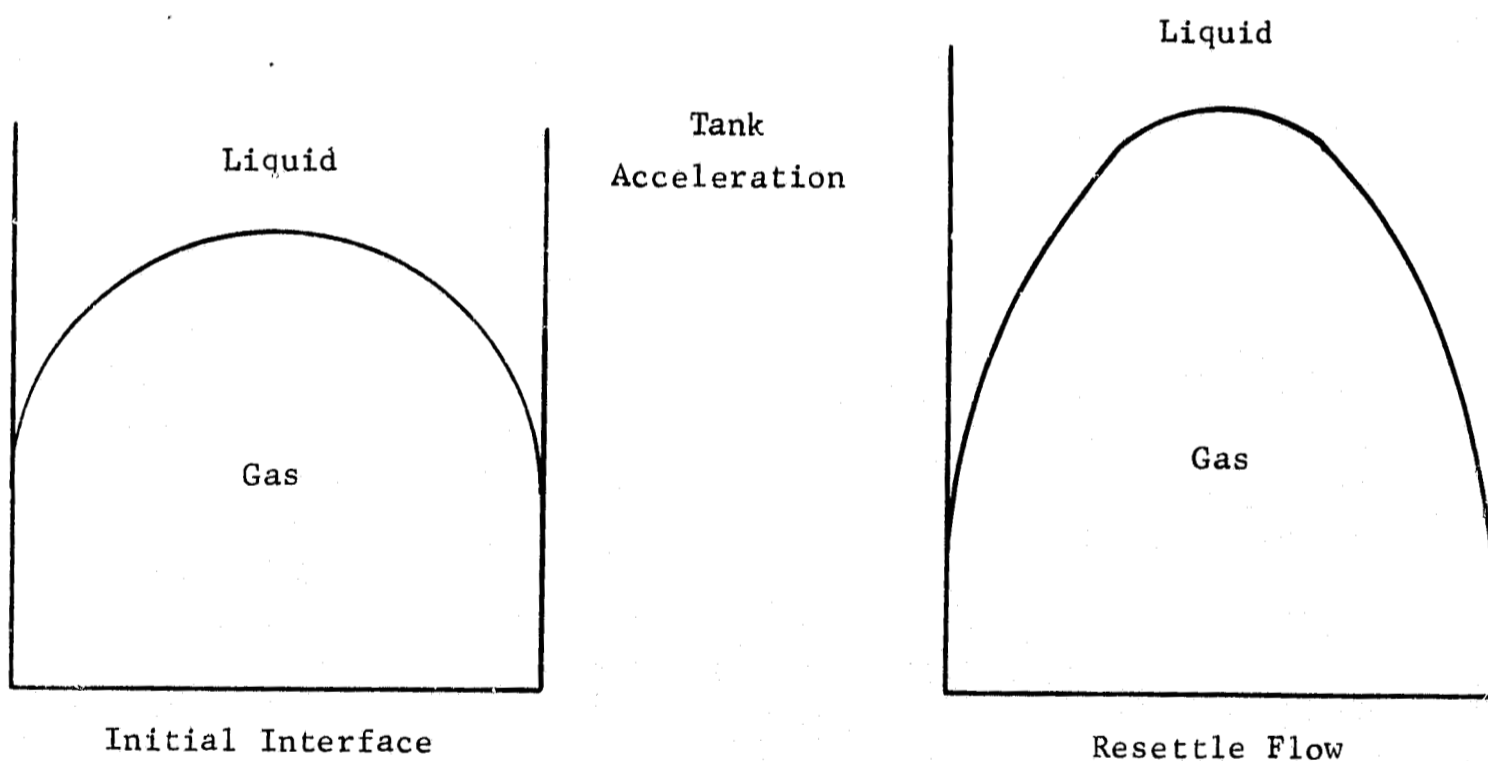be expected.

Fig. III-20 Liquid Reorientation Flow

The presence of the geyser phenomena makes the estimation of liquid collection rate extremely difficult. For the high resettle Bond numbers and the geometric shape involved in the capillary design, no analytical treatment is known and any such effort would by necessity involve extensive experimental observation. However, maximum collection rates can be estimated for the reorientation conditions assuming no geyser formation.

For a cylindrical tank with wall flow only, Gille and Gluck conducted an experimental program to determine the interface velocity. Starting with the potential flow theory developed by Davies and Taylor (Ref III-14) for the ullage velocity

$$v = 0.464 \ (aR)^{\frac{1}{2}}$$

[III-26]

An experimental program was conducted to determine the effect of viscosity (Reynolds number) and surface tension (Bond number) on the resettling flow (Froude number). The settling equation suggested by this correlation is:

$$v = 0.51 \ aR^{\frac{1}{2}} \left[1 - \frac{1.13}{Bo} \right] \left[f \ (Re) \right], \ \text{for Bo} > 4.75$$

[III-27]

As this equation shows, for large Bond numbers the function $\left[1 - \frac{1.13}{Bo} \right]$ approaches 1. An evaluation of the Reynolds number also suggested that for Re > 500 the term $f(Re)$ approaches 1. For the large Reynolds numbers (>>500) and Bond numbers (>>1100) encountered during thrusting in the SPS, the equation reduces to:

$$v = 0.51 \ \left(aR \right)^{\frac{1}{2}}$$

[III-28]

Additional experimental work to relate the Froude number and Bond number was conducted by Masica and Petrash. Their data indicate that for a Bond number greater than 12 the ullage velocity can be described by the relationship:

$$v = 0.48 \ (aR)^{\frac{1}{2}}$$

[III-29]

This relationship appeared to be valid for both low (0.01 to 0.08 g: $1 \leq Bo \leq 70$) and 1-g ($1 \leq Bo \leq 2000$) resettle conditions. An analysis of the leading edge displacement characteristics of these data resulted in the relationship:

$$a_L = \frac{3.8v^2}{R}, \ Bo > 1.7$$

[III-30]

where a_L is the magnitude of the leading edge acceleration. For large Bo (>12) the equation reduces to:

$$a_L = 0.875a \qquad\qquad [III-31]$$

This correlation was restricted to experimental data for distances of approximately two times the cylinder diameter.

If the profile of the ullage interface remains constant throughout the orientation mode, the relationship of Eq [III-29] can be used to determine the liquid collection rate (X_L) for a no-rebound condition:

$$X_L = (0.48)(aR)^{\frac{1}{2}} \cdot \pi(R-\delta)^2 \qquad\qquad [III-32]$$

where δ is the minimum thickness of the wall flow. Based upon this ideal condition, the collected volume versus time is shown in Fig. III-21 for nitrogen tetroxide. As shown, this collection rate exceeds the steady-state flow condition by orders of magnitude; so once the resettle flow is established, the containment device will no longer be required to supply propellant feed to the engine.

As mentioned earlier, geyser flow would be expected at the resettle Weber numbers for the prototype system. This geyser flow would, in effect, lower the collection rate by the quantity of rebounding liquid. Since the ideal collection rate is orders of magnitude above the outflow requirement, the actual collection rate should be sufficient to supply engine feed shortly after impingement of the leading liquid edge. Therefore primary consideration for resettle feed in the SPS appears to be a function of the velocity of the liquid leading edge rather than the collection rate.

Based on Eq [III-31], the time for the leading edge to impinge on the upper coverplate as a function of the vehicle acceleration for a straight cylindrical tank is presented in Fig. III-22. This plot shows if the end effects and initial transient effects are ignored, the liquid will begin to feed the containment reservoir in less than 0.9 sec for all cases.

While the above analysis is at best a crude approximation of the actual conditions for the system, the design margin is large enough that a more rigorous treatment does not appear necessary.

Propellant resettle for the no-hardware-modification design is complicated by the presence of internal hardware in the tank as shown in Fig. II-2. In addition to the central standpipe, the
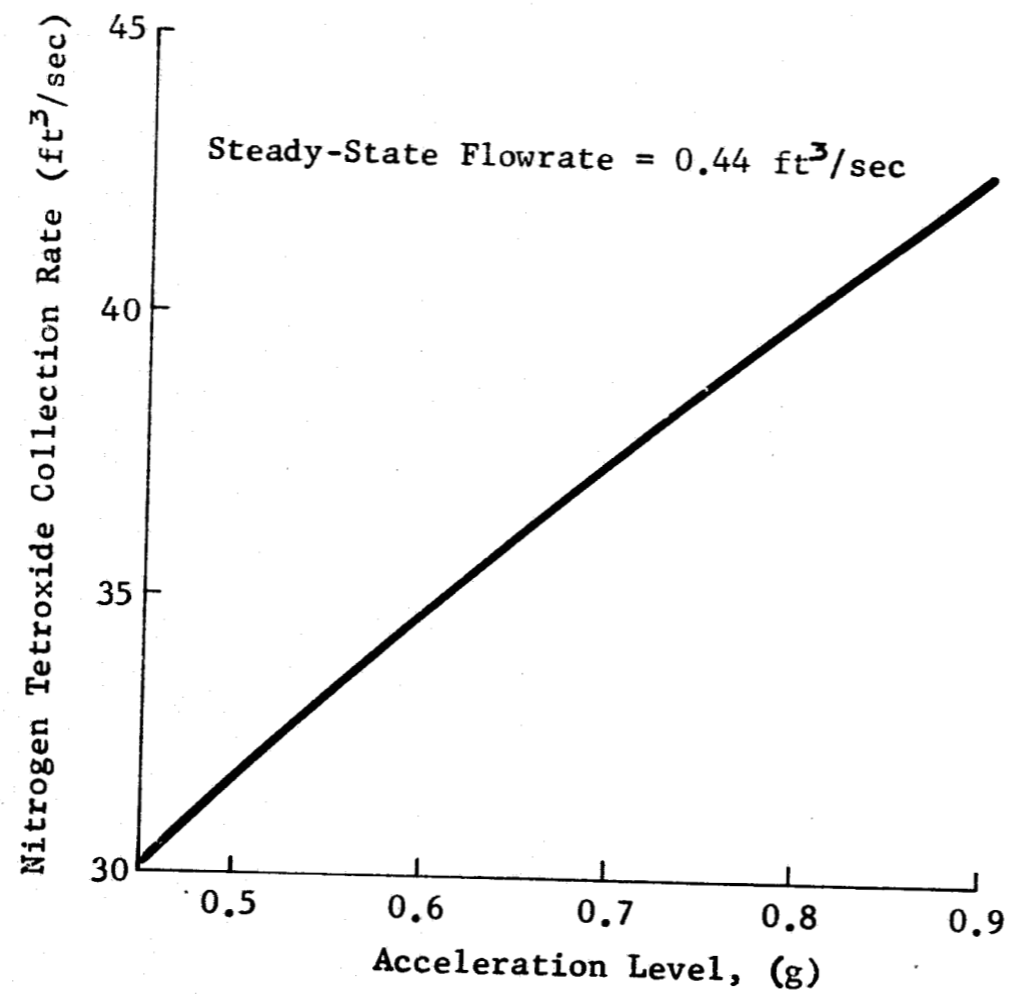
Fig. III-21 Propellant Collection Rate on Capillary Compartment Coverplate
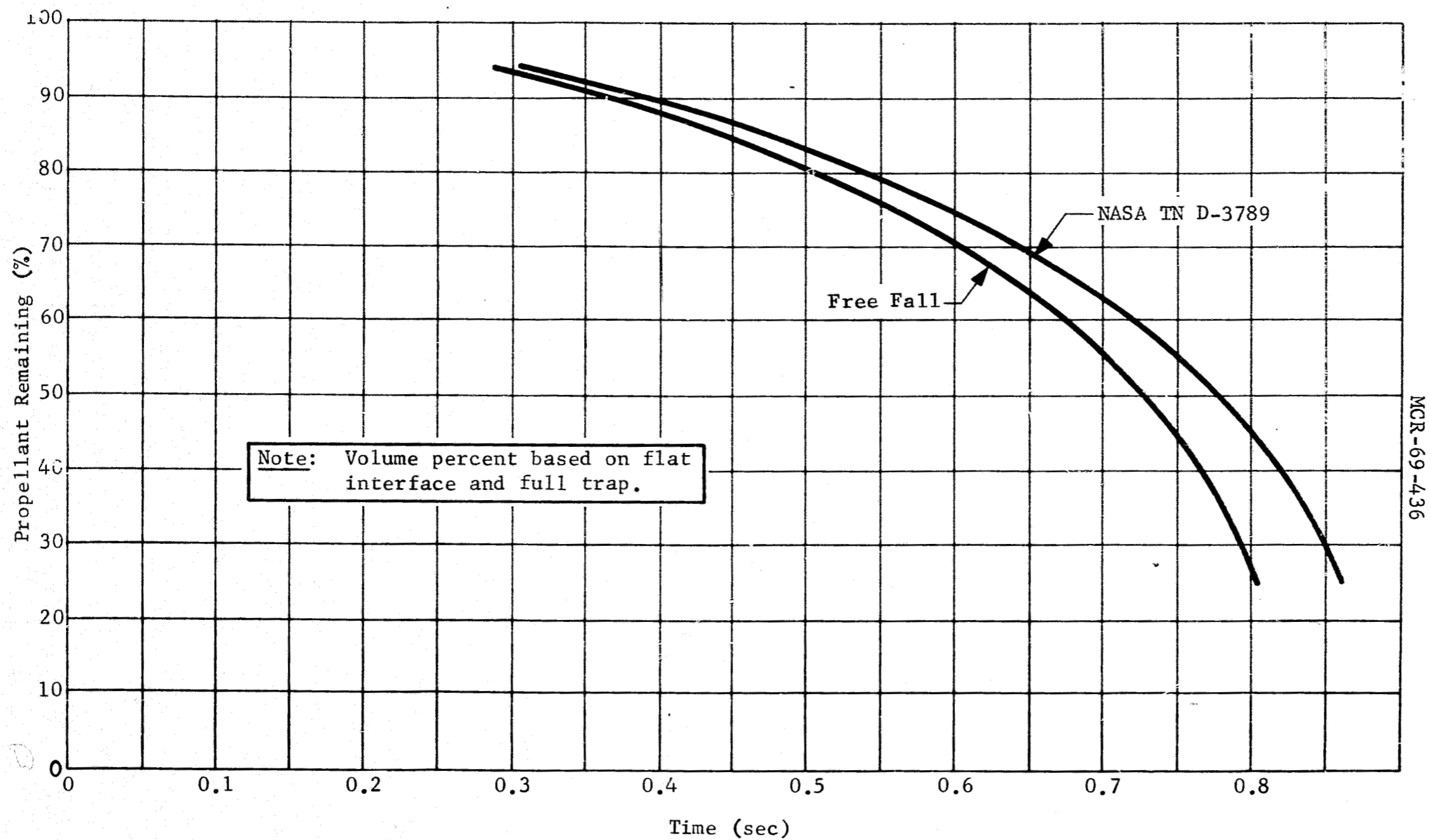
Fig. III-22 Propellant Resettle Time

deflection ring near the capillary barrier redirects the propel-
lant traveling down the center and the rebounding propellant from
the wall flow. With this geometry a great deal of liquid/gas
mixing and turbulence results. This turbulence would be expected
to disrupt and attenuate the geyser phenomena.

Resettle tests were conducted to establish the general char-
acteristics of the flow accumulation at the capillary barrier.
Froude number was selected as the scaling parameter for the set-
tling mode in the 1/5-scale model. Seventeen resettle tests were
conducted. The majority of the 17 tests were used in checkout to
establish flowrates and to synchronize liquid resettle and outflow
initiation. The first configuration of the resettle test appara-
tus is pictured in Fig. III-23. The barrel section of the 1/5-
scale model was lengthened to provide additional fall height for
the resettling liquid. Ethanol was used for the test fluid. The
liquid to be resettled was stored in the upper compartment, which
contained a coarse, square weave screen covering the base. Liquid
was retained in the compartment by pressure-supported, surface
tension stabilized pores of the screen. Liquid was released by
venting the top coverplate of the container. Wall flow of the
settling liquid was achieved by the conical deflector located at
the top of the barrel section below the screen. The barrel sec-
tion was vented to atmosphere to eliminate back pressure effects.
Liquid outflow from the compartments under the conical barriers
was achieved by opening the outflow valve to an evacuated catch
tank. The flowrate was controlled by the vacuum level in the catch
tank. The catch tank had sufficient volume for total outflow with
negligible pressure increase providing essentially constant liquid
outflow for the test duration. Resettle and outflow were initiated
by venting the upper reservoir and opening the outflow valve simul-
taneously. Liquid behavior in the vicinity of the coverplates was
documented on 16 mm film exposed at 200 and 64 fps. Two cameras
were used; one covered the tank outlet and one covered the upper
coverplate area. Tests were made using resettle liquid volumes of
10% and 20% of the bulk propellant, excluding the trap volume.
Some ullage gas entered the compartment under the top coverplate
before adequate resettling occurred, but complete draining of gas-
free liquid was achieved. The liquid settling heights used during
the tests were larger than required in conserving the Froude num-
ber. Heights approximately twice the required values were used to
promote geysering and to increase the required settling time. The
performance of the system under these conditions was satisfactory.

Collection rates and lower compartment refill were adequate to
ensure gas-free liquid withdrawal at the scaled outflow rate. A
sequence of single frame enlargements taken from 16 mm film used
to document test results, presented earlier in Fig. II-14, show
the resettle characteristics in the model. A higher confidence
level for reliable performance was achieved by demonstrating gas-
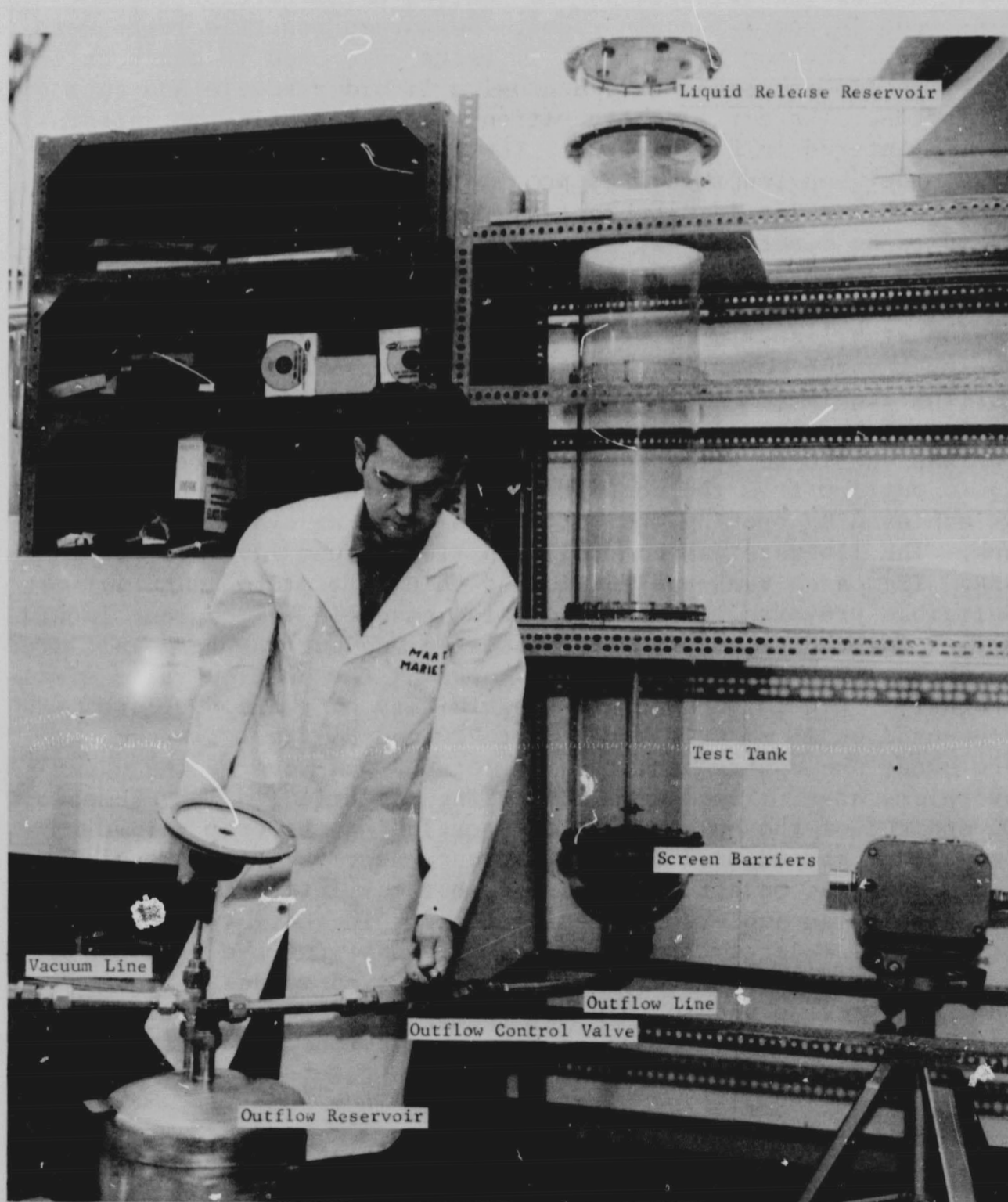free liquid expulsion at flowrates four times the scaled outflow
rate.

Fig. III-23 Liquid Resettle Test Setup

E. ZERO-G INTERFACE ANALYSIS

The screen liner in the lower compartment must prevent gas penetration into the liner during propellant outflow. The most critical period is when the compartment is in a near-empty condition. At this time, the liquid/liner contact area is decreasing, which results in an increase in the flow resistance across the liner, and hence, a higher driving pressure that must be supported by the screen. For positive axial thrust the liner will drain completely before gas ingestion at the outlet.

A critical period that may result in premature gas ingestion through the liner is during a low-g start transient with a low percent of propellant remaining. If the propellant does not contact sufficient liner area at the time of valve opening the resistance across the liner could result in gas ingestion until the propellant was oriented over the outlet due to main engine thrust buildup.

An analysis was conducted to establish the low-g equilibrium interface shape for the lower compartment geometry so the liquid/liner contact area could be established. The system environment of 10^{-5} g was used to establish the initial interface shape. The expected liquid configuration will be a function of the liquid location before entering the low-g environment. This is illustrated in Fig. III-24, where the liquid location is shown for similar quantities of fluid starting with the liquid oriented from a negative acceleration and from a positive acceleration. For the system with the liquid initially over the outlet, Fig. III-24(c), the liner contact area is large even for small percentages of liquid since the tendency is for the liquid to spread on the liner surface. The limiting case is that where the liquid is initially located in the conical barrier section [Fig. III-24(a)]. The equilibrium interface conditions for different liquid quantities were calculated for this propellant configuration until the liquid interface became discontinuous within the container boundaries. At this point it is not possible to predict the location from a minimum energy consideration since the elements of fluid can be independent of each other and have different interface curvatures.
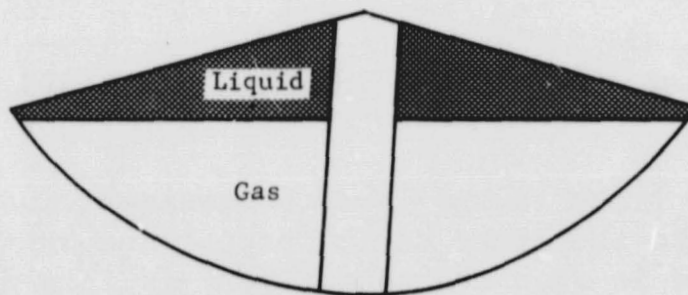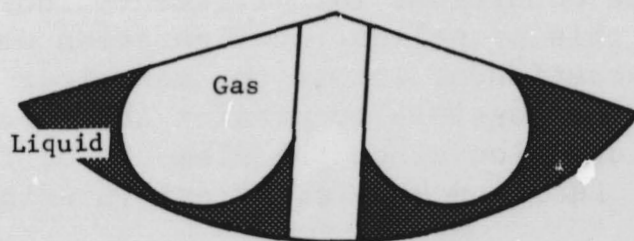
(a) Initial Configuration, Liquid on Top
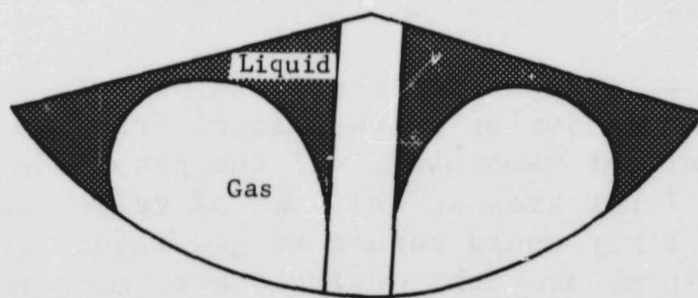
(b) Low-g Configuration, Liquid on Top
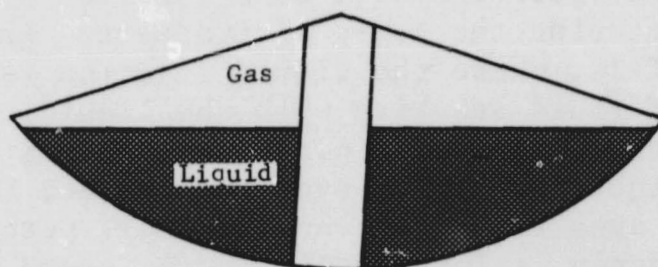
(c) Initial Configuration, Gas on Top

(d) Low-g Configuration, Gas on Top

Fig. III-24 Lower Compartment Interface Dependence on Initial Liquid Location

Two approaches were used to bracket the surface area covered
by the propellant as a function of the amount of liquid in the
compartment. One was to start with a small ullage bubble at the
outlet end of the center standpipe and progressively increase
the size of the ullage volume until the ullage contacts the wall
at which point the solution is no longer meaningful. The computer
solutions of several interface locations for different liquid
quantities are shown in Fig. III-25. This solution was used to
determine the liner contact area curve presented earlier in Fig.
II-18. To determine the maximum quantity of liquid that could
remain in a stable equilibrium position in the compartment at 10^{-5}
g and not contact the liner, a second series of calculations were
performed starting with a small liquid quantity at the central
standpipe in the apex of the conical barrier (i.e., very large
ullage bubble at the outlet end). The liquid quantity was in-
creased until contact with the liner surface was established.
Additional liquid would result in capillary pumping into the corner
formed by the conical barrier and the screen liner resulting in
liquid/liner contact. The maximum value that could exist without
contact was determined to be 17.6% of the propellant in the com-
partment. Two computer interface positions are shown in Fig.
III-26. Since the 17.6% liquid quantity is nearly identical to
the discontinuity point for the interface solution starting with
the small ullage bubble, it can be postulated that for a liquid
quantity in excess of 18% the fluid will be pumped into the con-
figurations shown in Fig. III-25. Therefore, the equilibrium
position interface contact area plot shown in Fig. II-18 is valid
for the range shown regardless of the liquid distribution at ini-
tiation of the low-g environment. The computer solution involved
solving for the axisymmetric liquid free surface shape inside a
volume of revolution bounded by the outside of a circular cylinder,
the inside of a cone, and the inside of a hemisphere as shown in
Fig. III-27. The boundaries of the volume of revolution are:

Cylinder: $r = r_1$ [III-33]

Cone: $z_c = (r - r_2) \tan \beta$ [III-34]

Sphere: $z_s = h_1 + (\sqrt{r_3^2 - r^2} - r_3)$ [III-35]
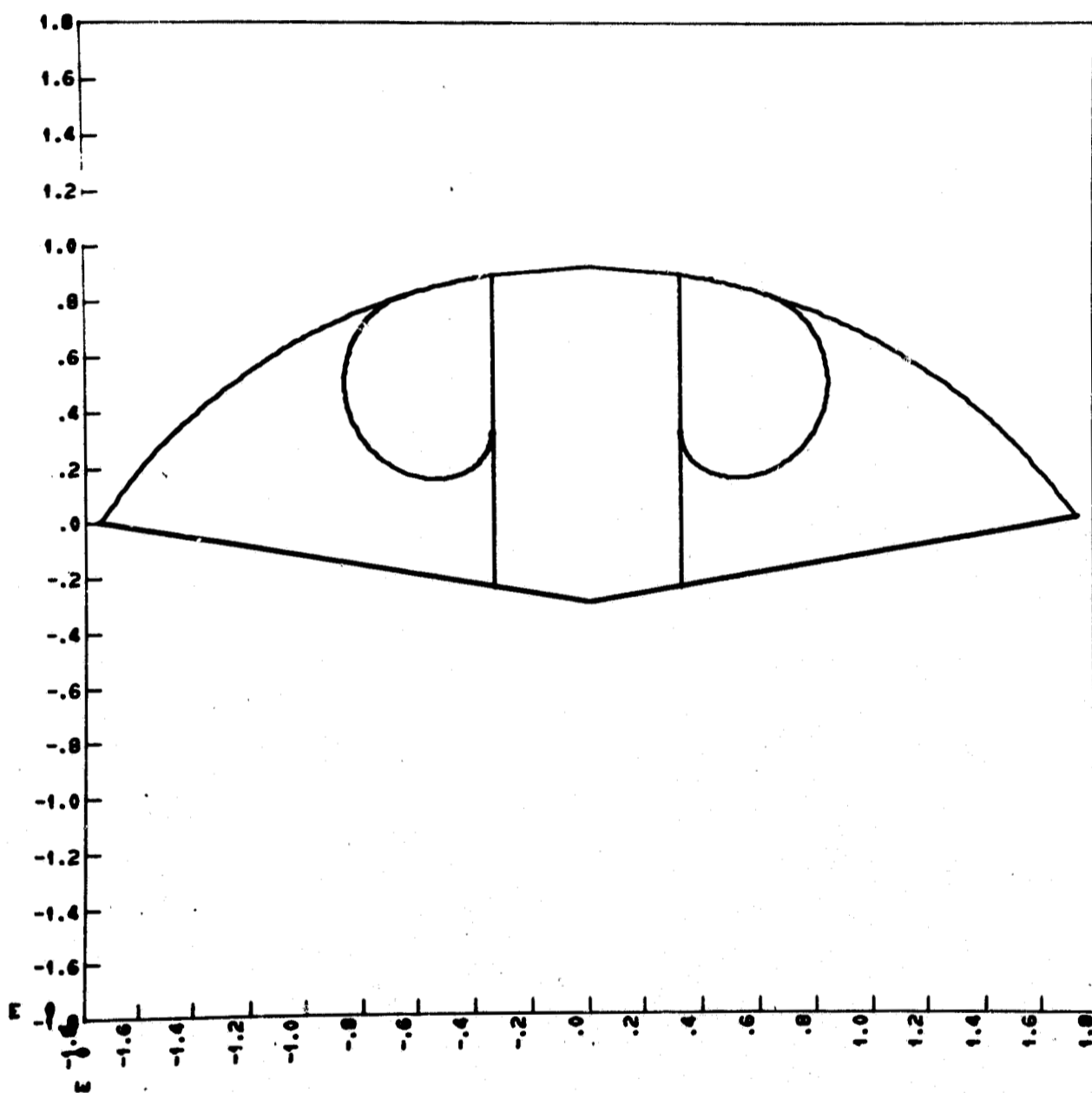
(a)   66% Liquid in Trap

Fig. III-25 Computer Solutions of Free Interface Configuration
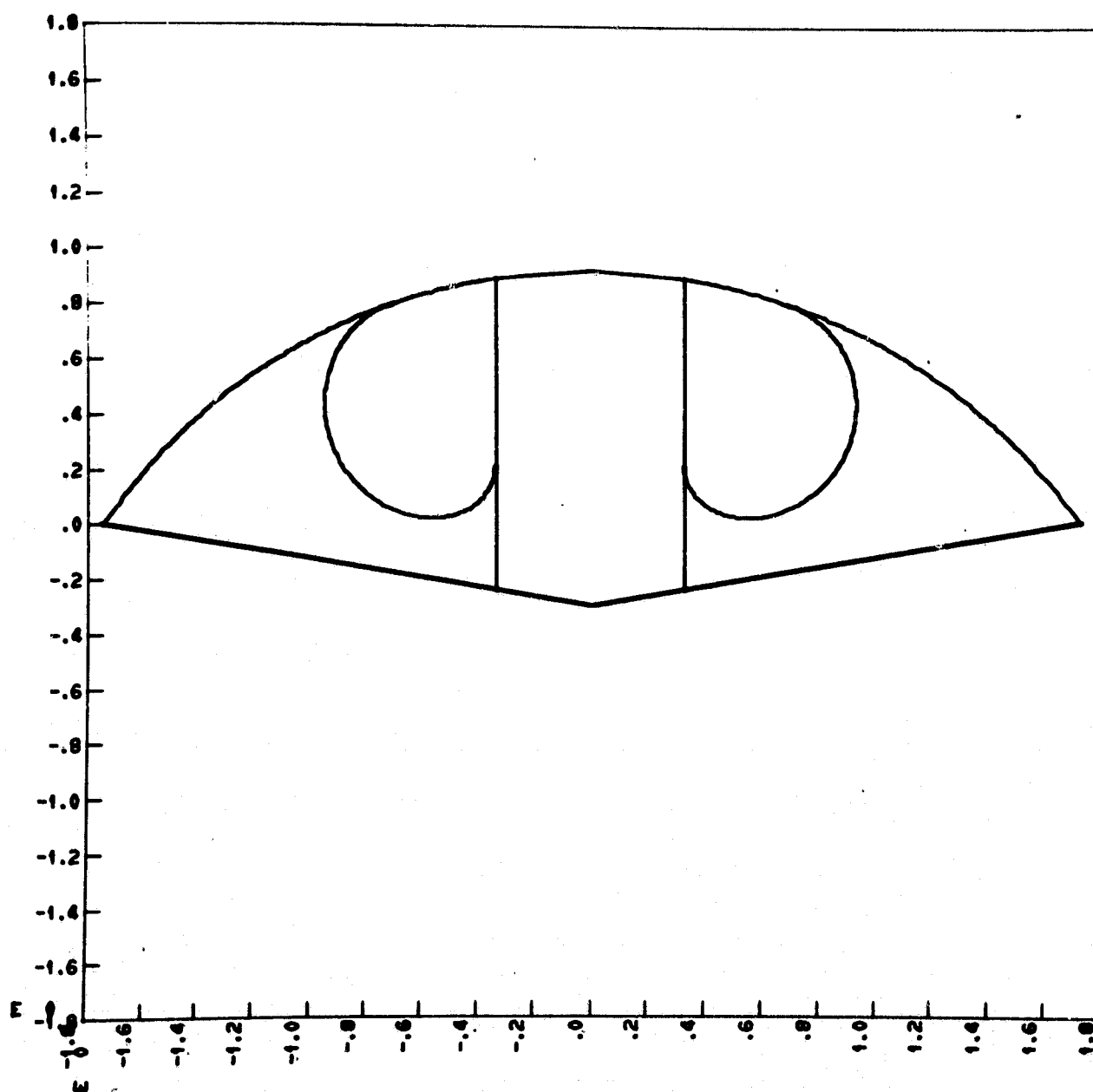
(b) 53% Liquid in Trap

Fig. III-25 (cont)

(c)   36% Liquid in Trap

Fig. III-25   (cont)

(d) 17% Liquid in Trap

Fig. III-25 (concl)

(a)   9% Liquid in Trap

Fig. III-26   Computer Solution of Free Interface Configuration

(b)   17% Liquid in Trap

Fig. III-26   (concl)
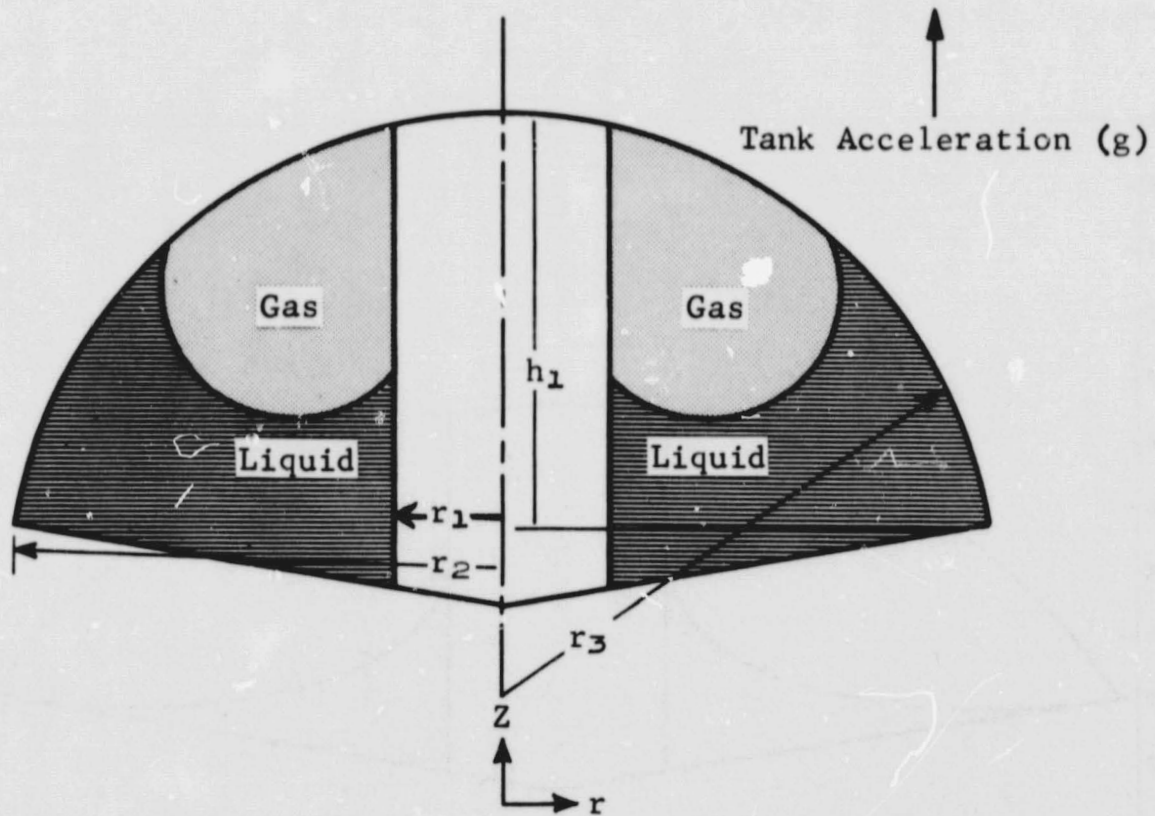
Fig. III-27 Configuration for Computer Analysis

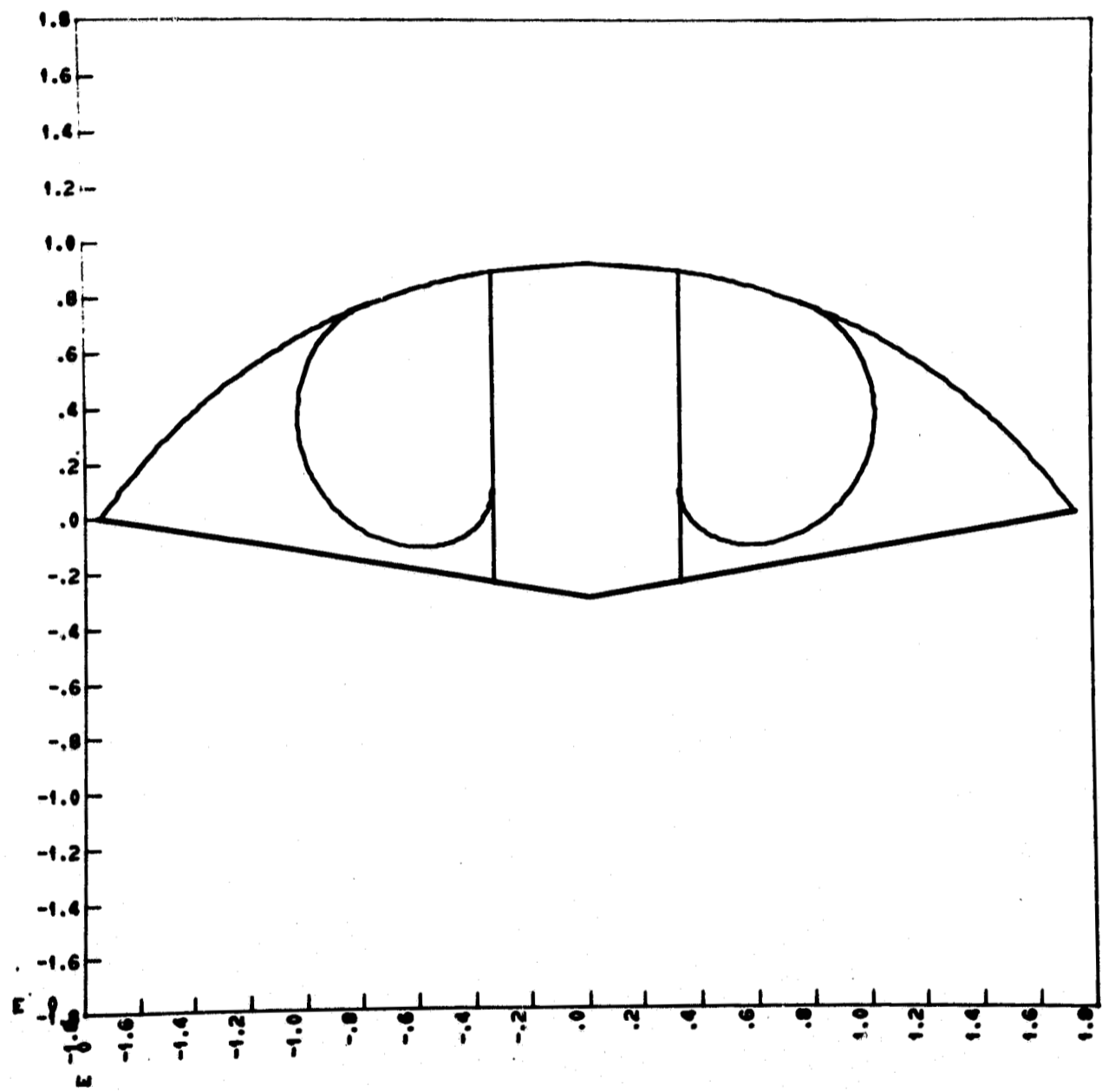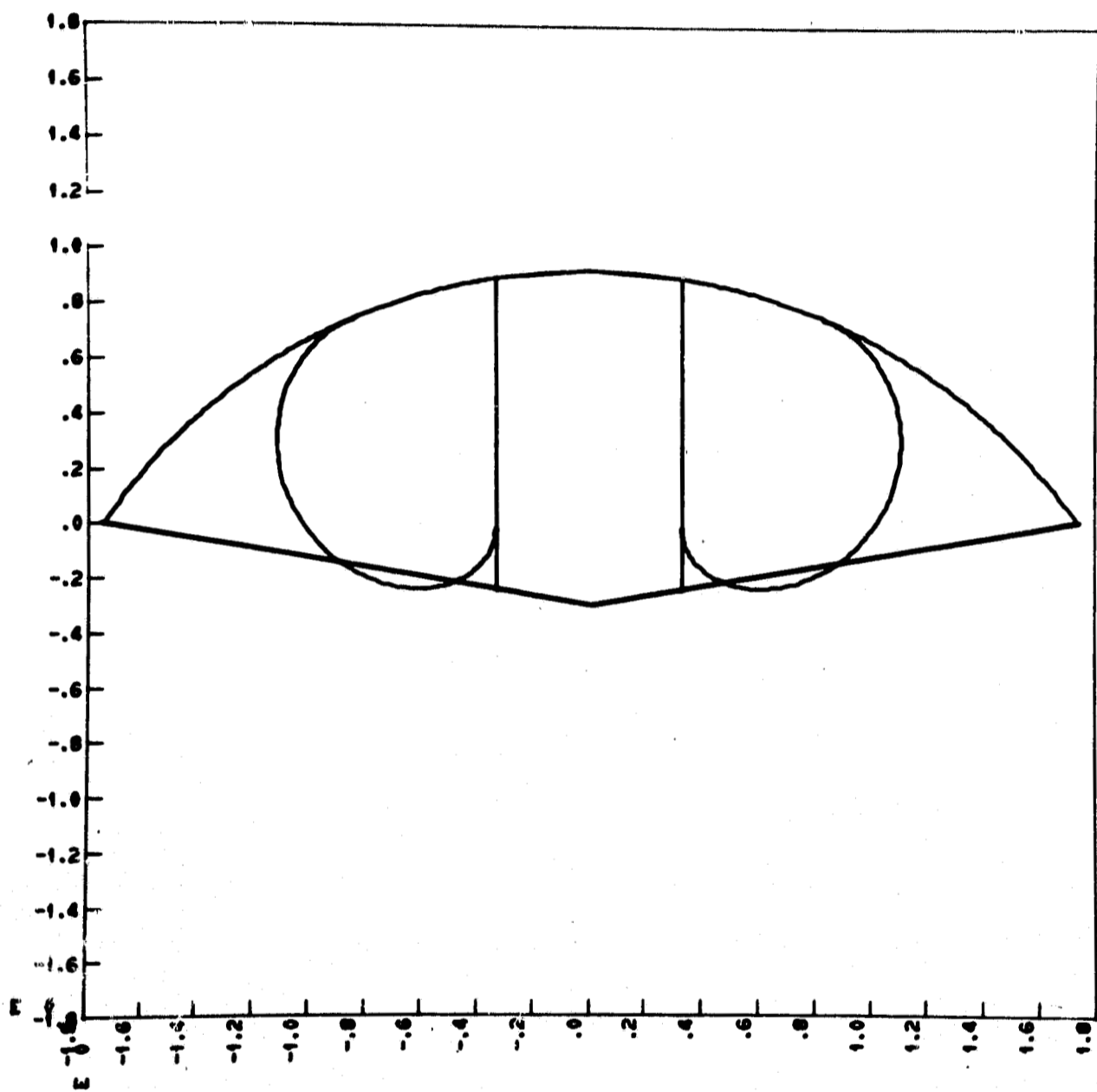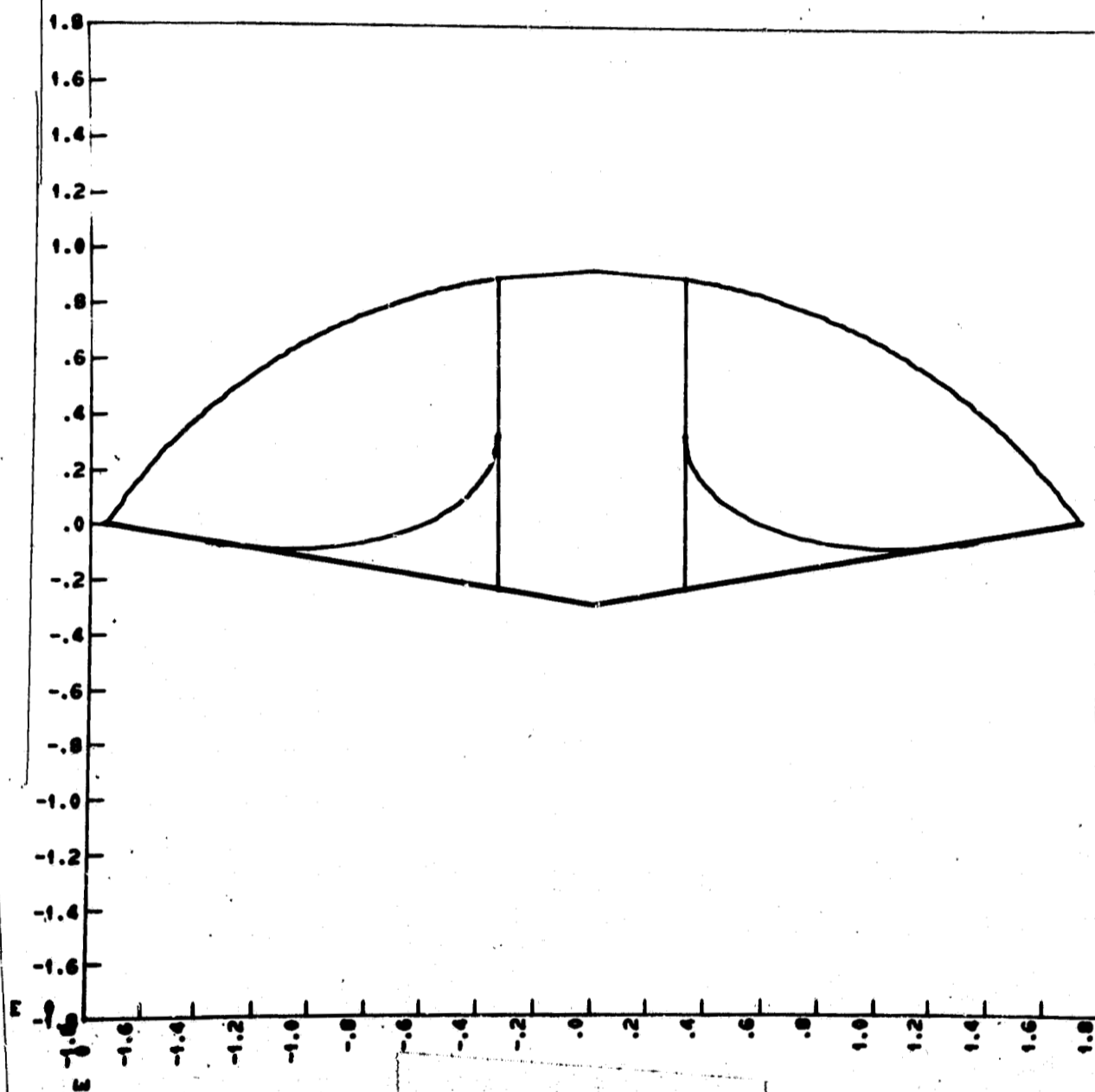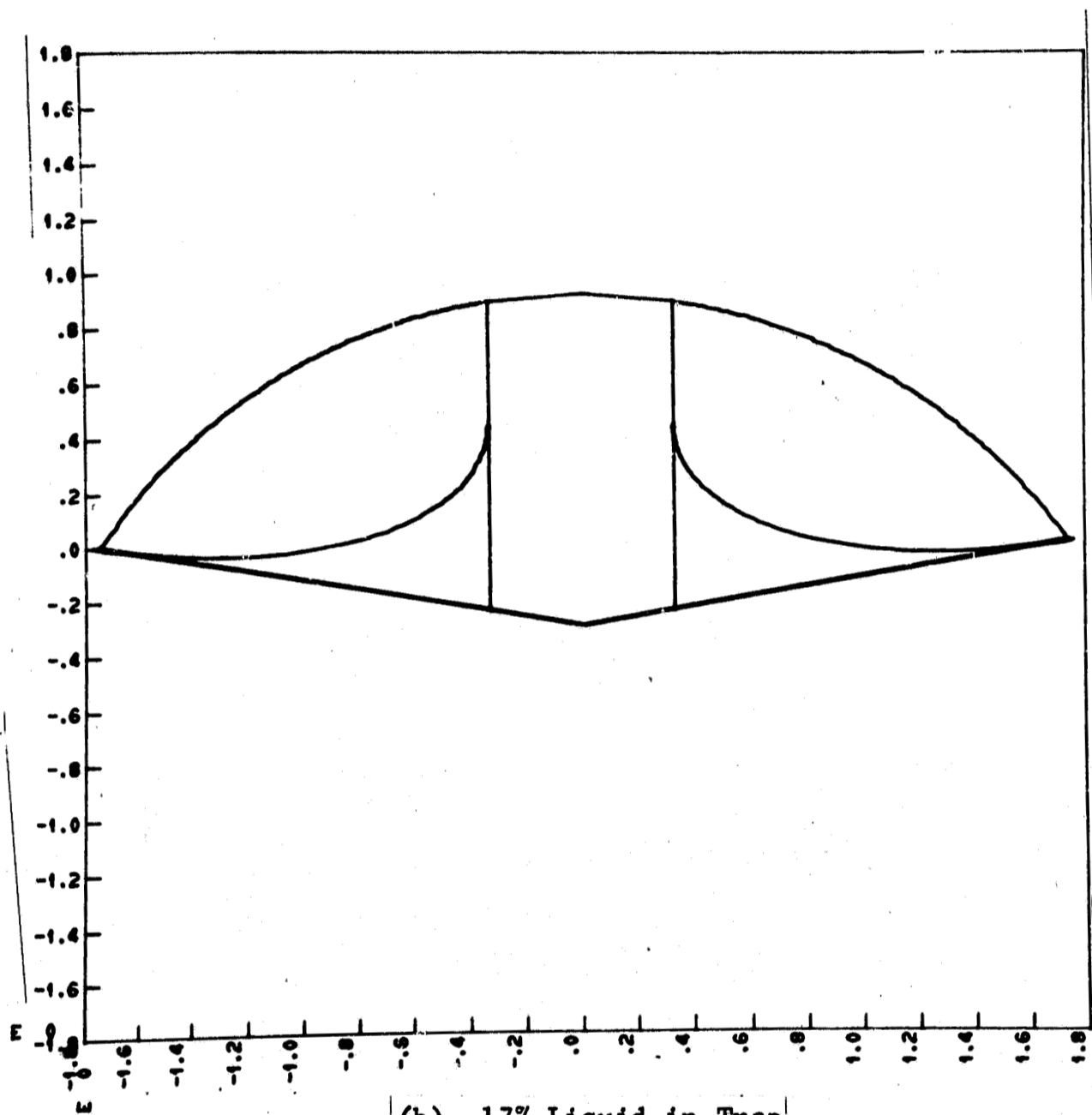The liquid position in the region is governed by a balance between surface tension and gravity forces, as expressed in the Young-Laplace equation. Written in parametric form, $r_L(\varphi)$ and $z_L(\varphi)$ represent the coordinates of the free surface, where φ is the slope of the surface dz_L/dr_L. The nonlinear Young-Laplace equation is then also expressed in parametric form as

$$dr_L = \cos\varphi \, d\varphi \bigg/ \left[b + \left(\frac{\rho g}{\sigma}\right)\left(z_L - h\right) - \sin\varphi/r_L \right] \qquad [\text{III-36}]$$

$$dz_L = \cos\varphi \, d\varphi \bigg/ \left[b + \left(\frac{\rho g}{\sigma}\right)\left(z_L - h\right) - \sin\varphi/r_L \right] \qquad [\text{III-37}]$$

b is the curvature at $r_L = r_1$, $z_L = h$; h is the liquid height at $r_L = r_1$. Nondimensional forms based on r_1 are as follows

$$r = r_L/r_1 \qquad\qquad\qquad z = z_L/r_1$$

$$B = \rho g \, r_1^2/\sigma \qquad\qquad\qquad C = b r_1 \qquad [\text{III-38}]$$

$$z_1 = h/r_1$$

and

$$dr = \left[\cos \varphi \Big/ \left(C + B(z - z_1) - \sin \varphi/r \right) \right] d\varphi \qquad \text{[III-39)}$$

$$dz = \left[\sin \varphi \Big/ \left(C + B(z - z_1) - \sin \varphi/r \right) \right] d\varphi \qquad \text{[III-40)}$$

The integration of φ is between the slopes at the solid walls of contact, reflecting the physical contact angle. The integration is performed from one wall to another. h is an input item, b is an unknown to be determined from the boundary conditions. b is first estimated from linear theory; then the integration is performed. If the opposite wall is not reached when the appropriate wall slope is reached, then the value of b is adjusted until this happens.

There are four liquid positions of possible interest: the configuration drawn in Fig. III-27, the liquid in the top corner, the liquid between the cylinder and the cone, and the liquid between the cone and sphere.

The liquid volume has been computed from the location of the free surface. The volume integral is composed of three parts in general,

$$V_L = 2\pi \int_{r_1}^{r_L(\pi/2)} \left(z_L - z_c \right) r\,dr$$

$$+ 2\pi \int_{r_L(\varphi_s)}^{r_L(\pi/2)} \left(z_s - z_L \right) r\,dr \qquad \text{[III-41]}$$

$$+ 2\pi \int_{r_L(\pi/2)}^{r_2} \left(z_s - z_c \right) r\,dr$$

To support the equilibrium interface analysis a series of low-g drop tests were conducted. Both 1/5-scale and 1/12-scale models of the lower compartment were used. Tests were conducted with 20, 40, and 60% of the compartment volume filled. The results are shown in Fig. III-28 thru III-30.

MCR-69-436
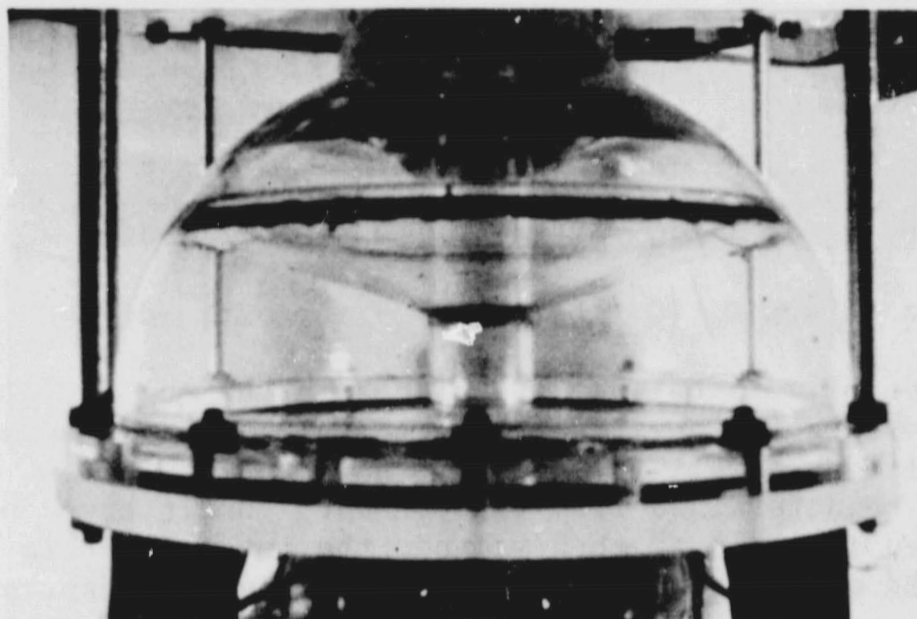
(a) Test 15, 25% Compartment Fill
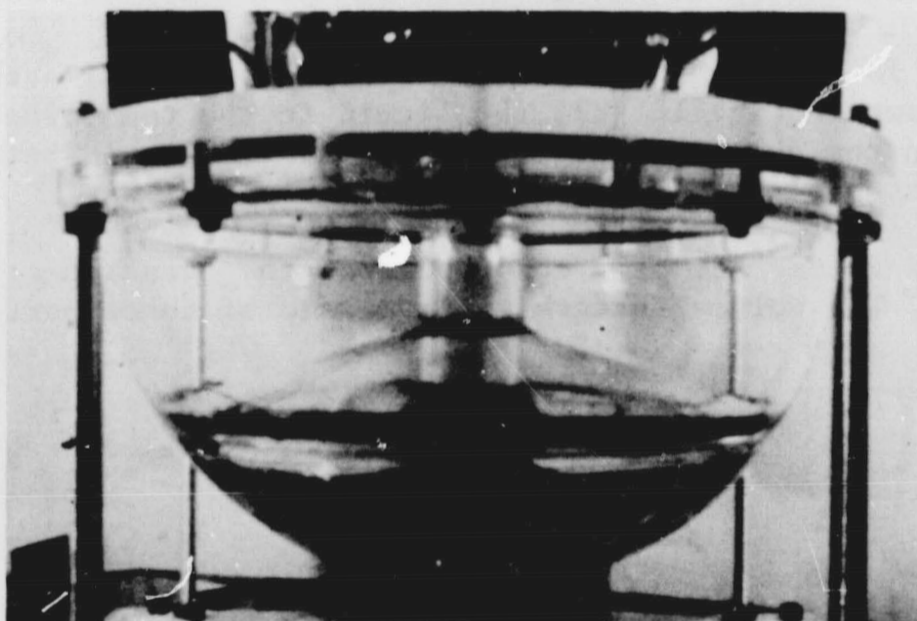
(b) Test 16, 50% Compartment Fill
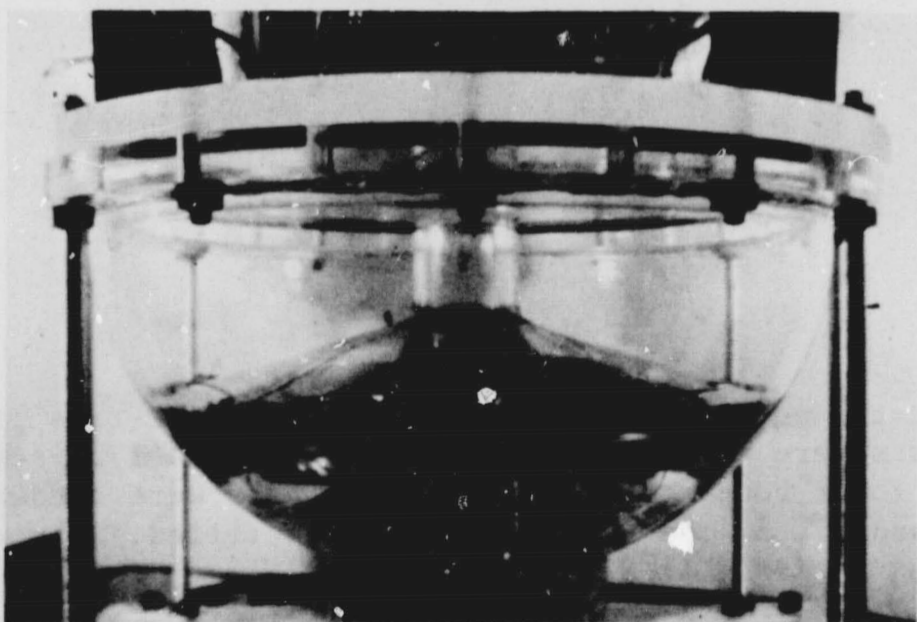
(c) Test 17, 75% Compartment Fill

Fig. III-28   1/5-Scale Low-g Interface Starting with Liquid over Outlet
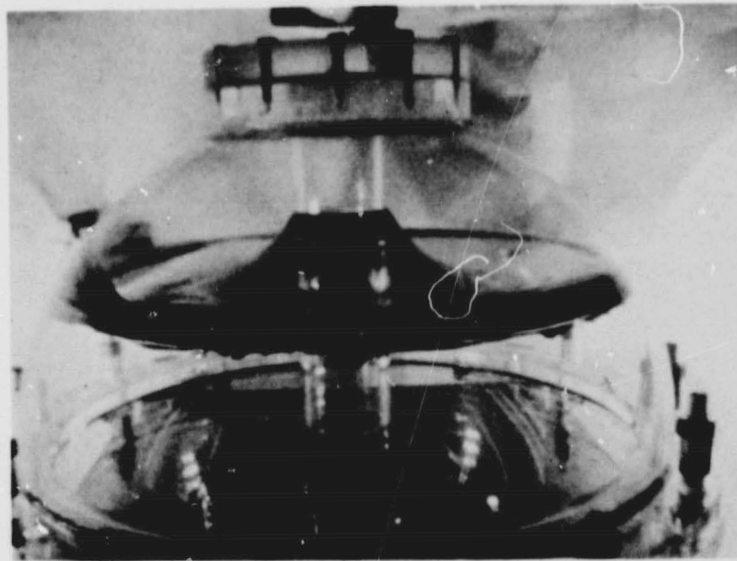
(a)   Test 11, 25% Compartment Fill
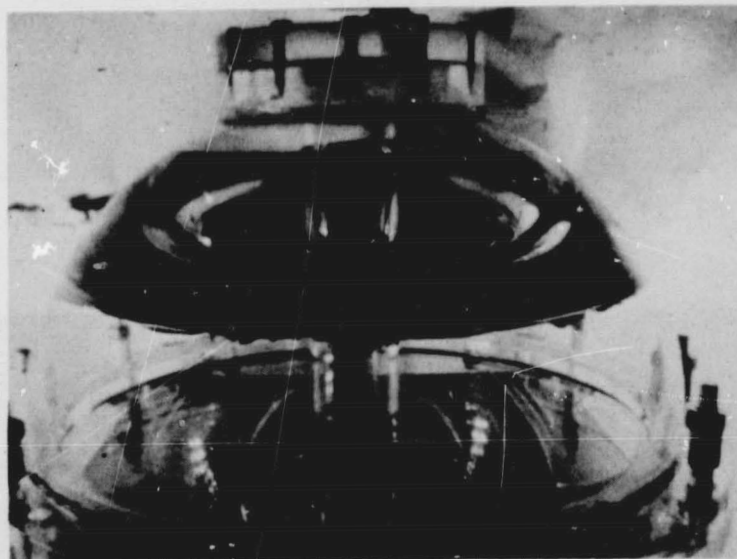
(b)   Test 12, 50% Compartment Fill
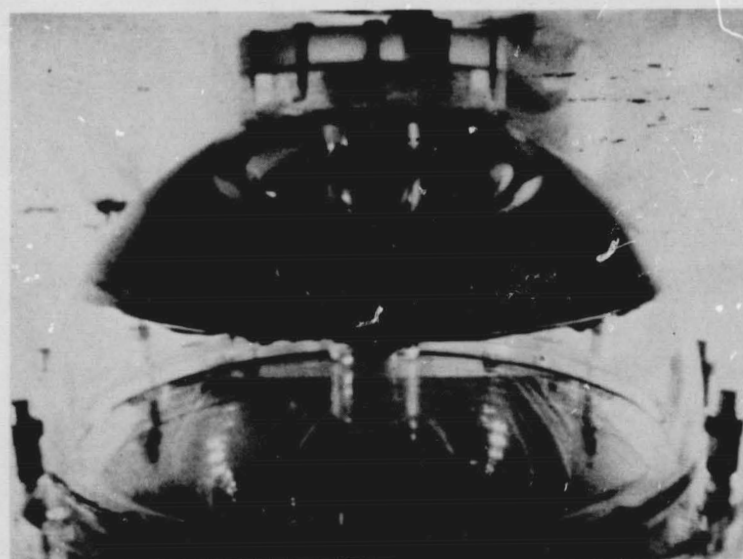
(c)   Test 13, 75% Compartment Fill

Fig. III-29   1/5-Scale Low-g Interface Starting from Inverted Position
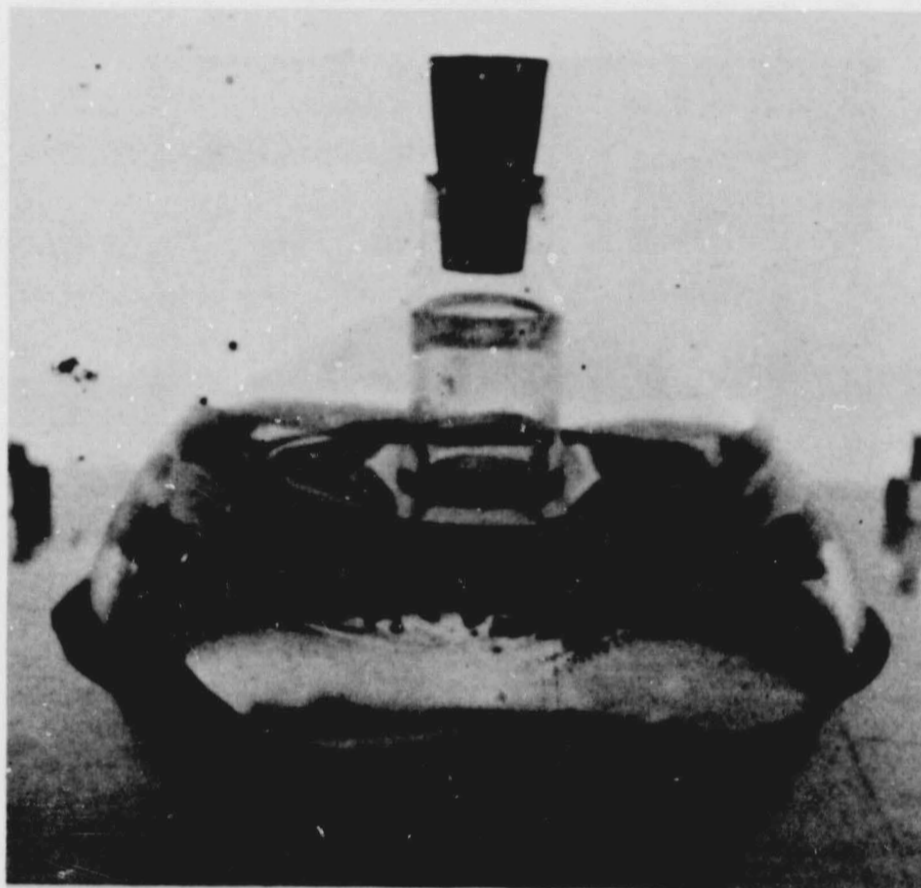
(a)   Test 18, 25% Fill, Inverted Position
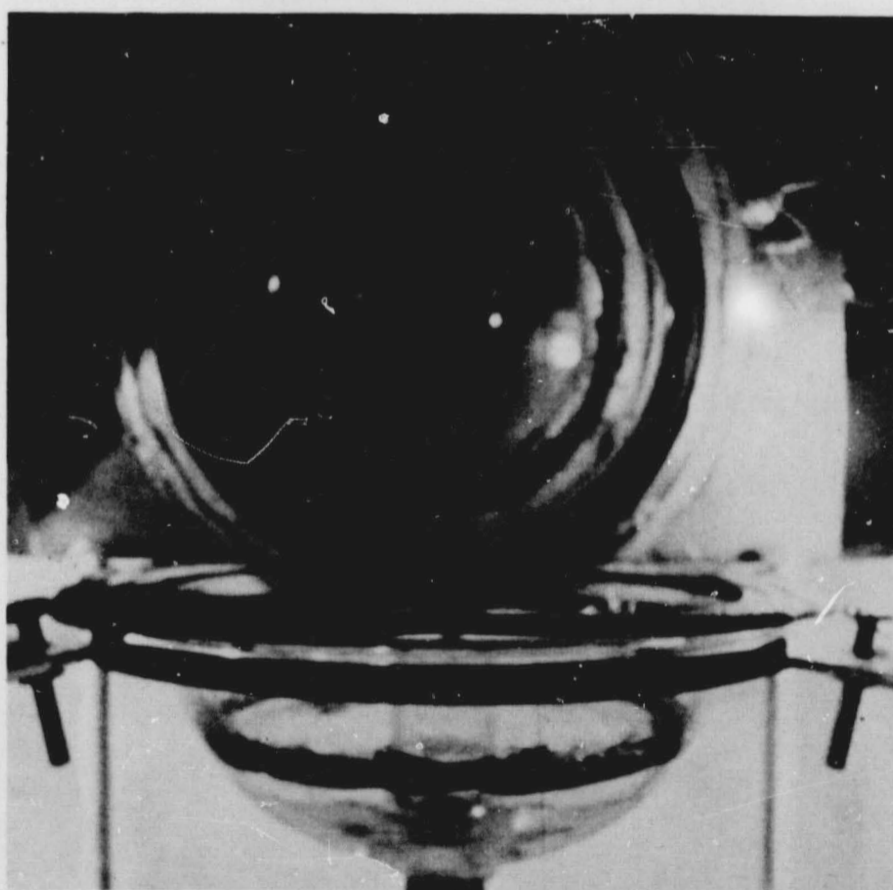
(b)   Test 18, 25% Fill, Initial Liquid over Outlet

Fig. III-30   1/12-Scale Model Low-g Interface Tests

All low-g tests were conducted in the Low-g Drop Tower. The zero-g condition is achieved by shielding the experimental package from drag forces encountered during the drop. An evacuated drag shield containing the experimental capsule provides a zero-g environment by allowing relative vertical displacement between capsule and shield as the drag forces act.

A total of 19 zero-g tests were conducted using 1/5- and 1/12-scale plexiglass models. The lower compartment of the acquisition device was used for these tests. The conical screen and perforated plate was replaced by a plastic cone so the liquid-vapor interface could be observed through film coverage from above as well as from the side. Color film exposed at 200 fps was used to record the liquid-vapor interface history during the tests. Both top and side views were recorded on the same film using a mirror (Fig. III-31). The attitude of the models was set to simulate both a positive and negative acceleration environment before zero-g entry, i.e., liquid bottomed in the hemisphere and against the conical coverplate, respectively. The model was mounted with the outlet down for the former condition and inverted for the latter.

The test liquid selected for these tests was FC-43, a fluoro-chemical liquid produced by Minnesota Mining and Manufacturing Co., St. Paul, Minnesota. This liquid is relatively inert and simulates N_2O_4 fairly well in the pertinent physical properties, surface tension, and density.

The 1/5-scale model was used in both the upright and inverted attitudes with the liquid quantities of 75, 50, and 25% of the total compartment volume. These represent approximately 2.3, 1.5, and 0.8% of the total tank volume. The zero-g time available, 2.1 sec, was marginal for the interface to form in the transition from gravity dominated to zero-g for the 25% case. Tests using the 1/12-scale model were also used to investigate the interface formation in this case.

The results from these tests indicate sufficient liquid-to-screen-liner contact area to provide gas free liquid withdrawal during the engine restart transient.
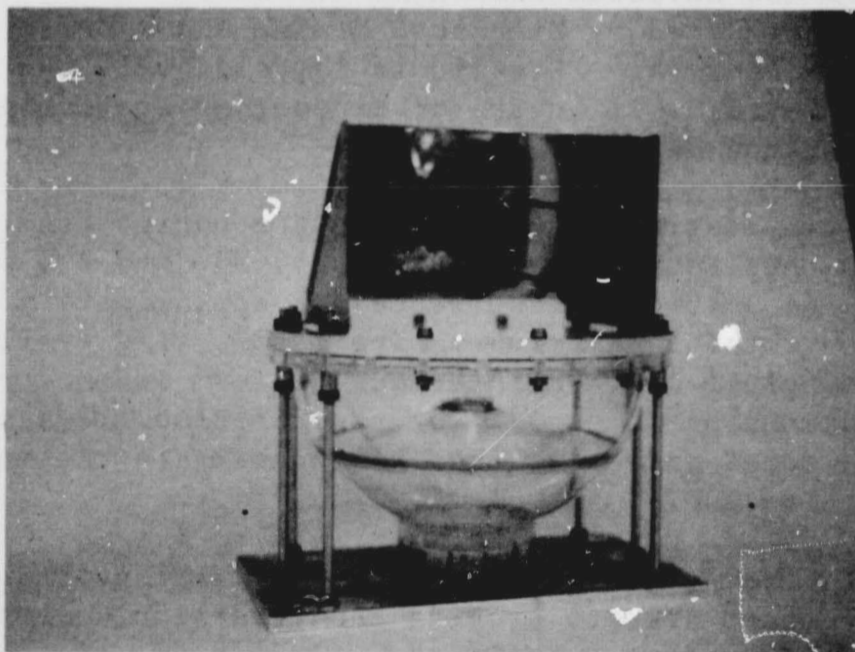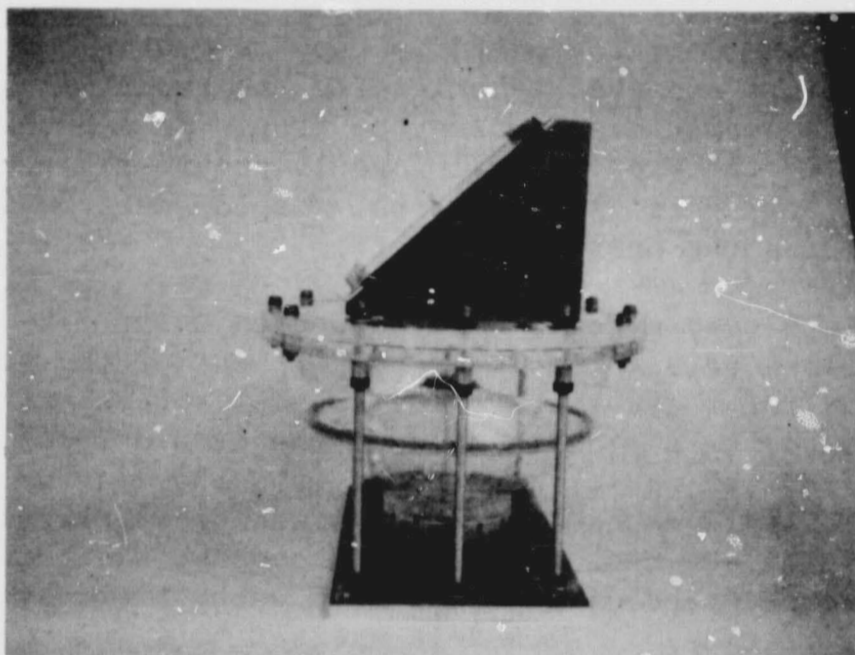
Fig. III-31 Low-g Interface Test Apparatus

F. SIPHONING

One of the problems associated with the presence of the gaging system stillwell in the no-hardware-modification design is the possibility of the stillwell acting as a siphon during negative accelerations and pumping liquid from the compartments. Several design innovations were included to relieve this problem. However, under the high negative accelerations some propellant loss is possible. A schematic of the system is shown in Fig. II-20. The design is such that liquid loss from the compartment will no longer occur once the annular reservoir has been cleared of fluid. The analysis was separated into two parts; the surface draining from the annular cavity around the stillwell, and the siphoning of the liquid from the base of the annulus.

The primary mode for liquid drainage from the annulus is due to siphoning through the stillwell. The driving potential for siphoning is the difference in column height of fluid in the stillwell and the liquid in the annulus, ZT, in Fig. II-20. The draining potential from the capillary compartment is caused by the liquid column height differences less the retention capability of the barrier. Once the annulus liquid is completely drained, as shown in Fig. III-32, the liquid drainage potential from the compartment reverses and gas attempts to enter the lower screen cylinder. The pore size of this screen is sized to prevent gas entering for the negative 0.2 g condition and the liquid column height, h, in Fig. III-32.

1. Siphoning Analysis Method

The potential magnitude of the stillwell siphoning problem was evaluated with an existing computer program, with modifications to accommodate system geometry, initial conditions, and functional requirements. The program is in FORTRAN IV and is run on the CDC 6400 and 6500 computers at Martin Marietta Corporation.

The original mathematical model was derived to simulate low g and capillary controlled liquid motion in a standpipe coaxially located in a closed cylinder. This geometry is analogous to the stillwell/annular reservoir arrangement in the recommended SPS propellant retention system design, so the major task in program modification was addition of the necessary equations and logic to simulate pertinent pressure differences and flow rate induced in the propellant retention compartment. The resulting three conduit flow system necessitated an iterative solution for pressure drop and flow, in lieu of the explicit solution used for the direct coupled two conduit system.
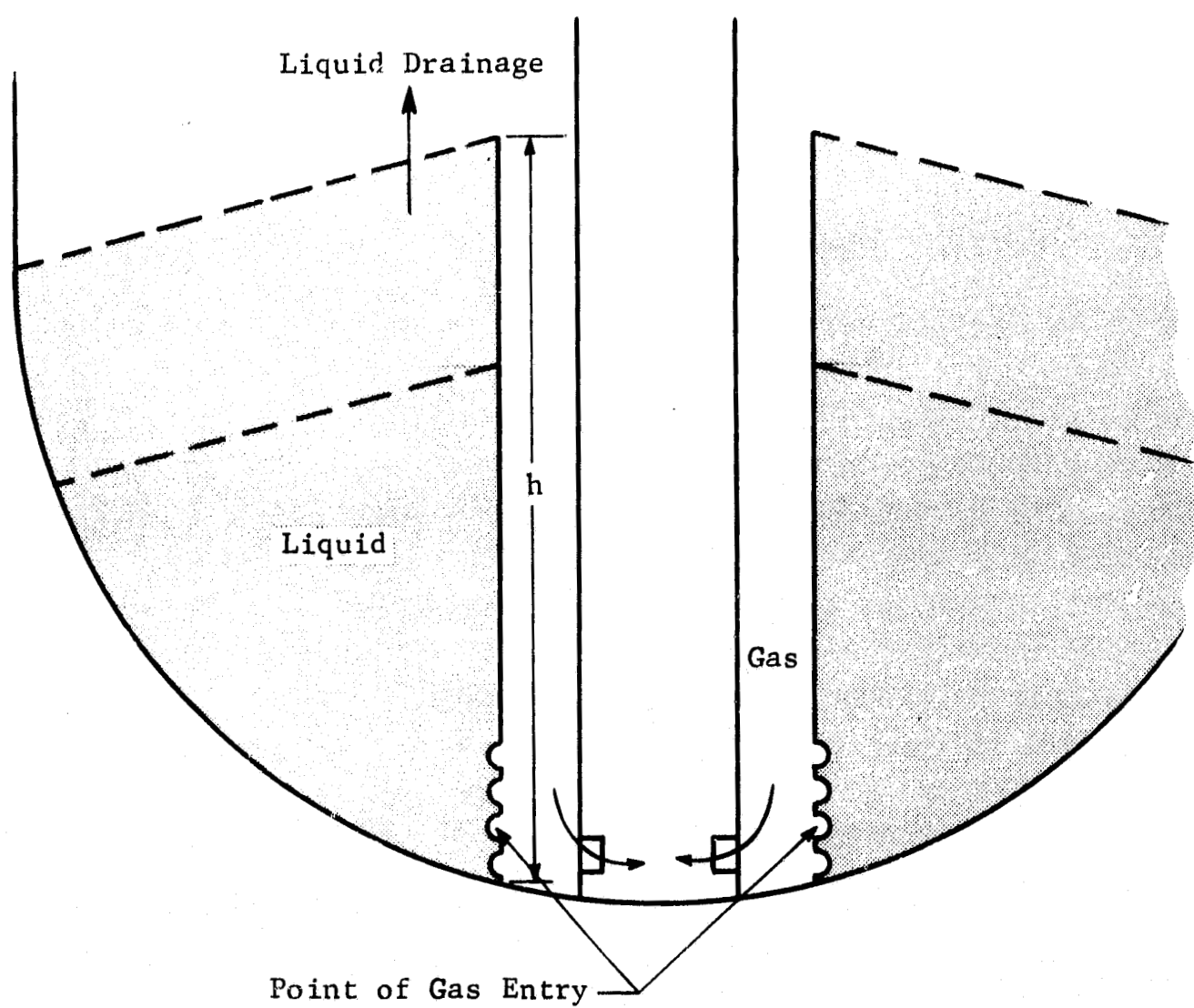
MCR-69-436

Fig. III-32   Stabilized Compartment Annulus Draining

The mathematical model represents the system shown in Fig. II-20. The forward differencing technique is used to obtain solutions for successive time increments. Acceleration of liquid in the stillwell and in the annular reservoir are calculated from pressure differences. The method of Milne is then used to integrate these accelerations over the time increment to get velocity and displacement. If the difference in pressure across the upper screen (or plate) exceeds the respective bubble point, liquid flow through the annular reservoir screen is calculated. Pressure drops, accelerations, and flows are then recalculated until the continuity equation is satisfied. The determination of liquid lost from the retention compartment is conservative, since the only resistances to flow in the reservoir considered are the bubble point of the upper screen or plate and the flow loss across the annular reservoir screen.

Using this model a parametric study was conducted to determine under what conditions propellant loss would occur and what the magnitude of the loss would be. The results are shown in Fig. II-21. While some liquid loss at high negative accelerations will occur, the amount is less than a fourth of a cubic foot for the worst-case situation for the selected design with a 2-in.-high annulus screen. This is only about 0.1% of the total contained propellant volume.

2. Annulus Draining

There are two approaches in analyzing the draining of liquid from the annular region between the central tube and the screen trap. The first consists of seeking an explicit solution for the steady-state outflow of liquid from such a region, and the second amounts to a numerical solution of the complete time-dependent, nonlinear Navier-Stokes equations.

The explicit approach assumes a semi-infinite annulus, closed at one end, with liquid draining steadily away toward infinity. A coordinate system is selected that moves with the interface. Because of the assumption of steady state, the coordinate system moves with constant velocity relative to the annulus, and the interface (which extends to infinity as it approaches the cylindrical boundaries) does not move or change shape relative to the coordinate system.

Assuming the liquid flows without rotation and incompressibly down the annulus, the problem becomes one of solving Laplace's equation ($\nabla^2 \varphi = 0$) within a region bounded by two concentric circular cylinders and a third unknown boundary appropriate to a

gaseous "obstacle" in the annulus. The usual boundary condition,
$\nabla \varphi \cdot \vec{n}$, applies to all the boundaries. In addition, pressure must
be constant along the unknown boundary. It is apparent, on the
basis of either physical or mathematical considerations, that all
of these conditions cannot be satisfied for arbitrary flow speed
for upstream of the gaseous obstacle. Consequently, solution of
the problem will yield an equilibrium flow velocity at which the
assumed steady-state draining is possible.

Since the liquid free surface is being treated as a fixed but
unknown boundary, a straightforward solution of Laplace's equation
to obtain a velocity potential with enough unknown parameters to
allow the free surface conditions to be satisfied is probably not
the most convenient procedure to follow. A simpler approach in
this sort of problem is to work with Stokes' stream function.

Unlike the ordinary stream function in rectangular coordinates,
Stokes' stream function does not satisfy Laplace's equation, but
rather a slightly different equation:

$$\frac{\partial^2 \psi}{\partial r^2} - \frac{1}{r} \frac{\partial \psi}{\partial r} + \frac{\partial^2 \psi}{\partial z^2} = 0 \qquad\qquad [\text{III-42}]$$

if we assume axial symmetry. We are looking for a solution in the
form

$$\psi = -\tfrac{1}{2} u_o r^2 + \psi_*, \qquad\qquad [\text{III-43}]$$

where the first term on the right side represents a uniform stream,
speed u_o, throughout the annulus, and the perturbation function
ψ_* must satisfy the following conditions:

$$\psi_* = 0 \text{ on } r = r_1, r_2 \qquad\qquad [\text{III-44}]$$

where r_1, r_2 are the radii of the walls of the annulus, and

$$\psi_* \to 0 \text{ as } z \to \infty \qquad\qquad [\text{III-45}]$$

(i.e., the perturbation function vanishes far upstream). Finally,
since the radial and axial velocity components are $\frac{1}{r} \frac{\partial \psi}{\partial z}$ and $\frac{1}{r} \frac{\partial \psi}{\partial r}$,
respectively, Bernoulli's equation requires

$$\left[\frac{\partial \psi}{\partial r}\right]^2 + \left[\frac{\partial \psi}{\partial z}\right]^2 = -2gr^2 z \qquad\qquad [\text{III-46}]$$

on the free surface (g is gravity or system acceleration).

The appropriate solutions of Eq [III-42] (satisfying Eq [III-45]) will be in the form

$$\psi_{*n} = r \left[A_n\, e^{-k_n z/r_1}\, J_1 \left(k_n \frac{r}{r_1} \right) + B_n\, e^{-k_n z/r_1}\, Y_1 \left(\ell_n \frac{r}{r_1} \right) \right]. \quad [III-47]$$

For $\psi_* = 0$ on any $r = $ constant, $k_n = \ell_n$. Introducing the cylinder function

$$\zeta_{\nu n}\left(\lambda_n \frac{r}{r} \right) = J_{\nu n}\left(\lambda_n \frac{r}{r_1} \right) + \zeta_{\nu n}\left(\lambda_n \frac{r}{r} \right) \quad [III-48]$$

then, we have

$$\psi_* = \sum_n A_n\, \zeta_{\ell_n}\left(\lambda_n \frac{r}{r_1} \right)\, r\, e^{-\lambda_n z/r_1}, \quad [III-49]$$

where the eigenvalues ζ_{ℓ_n}, $\wedge_n$ are determined from Eq [III-44]:

$$\zeta_{\ell_n}\left(\lambda_n \right) = \zeta_{\ell_n}\, \lambda_n^{r_2/r_1} = 0 \quad [III-50]$$

The A_n's and u_o can then be determined from the fact that there must be a stagnation point at the uppermost point on the free surface, and the requirement that the pressure condition, Eq [III-46], must be satisfied on the appropriate two branches of the stagnation streamline.

Two difficulties render a complete solution of the problem unlikely. One is the nonlinearity of the boundary condition expressed in Eq [III-46]. The other is the fact that the nature of the other boundary conditions is such that the orthogonality properties of the solutions cannot be readily exploited. Consequently, a computer program was written to obtain a one-term approximation to the solution, along the lines of Davies and Taylor's successful solution to the problem of emptying tubes (Ref III-14). With such a solution it is of course possible to satisfy the pressure condition (Eq [III-46]) at only a single point on the free surface.

Results of the computer program indicated that the one term approximation is much less satisfactory in this case than in the case investigated by Davies and Taylor, no doubt because of the more complex geometry. It was impossible to find any point on the surface for which the pressure condition could be satisfied without producing a grossly erroneous pressure distribution over the rest of the surface.

The second approach taken was to adapt Martin Marietta's version of the Marker and Cell computation scheme to the problem of liquid outflow from a cylindrical annulus closed at one end. This adaptation consisted primarily of introducing concentric cylindrical boundaries and a calculated low Bond number initial interface configuration. The Marker and Cell computer program essentially performs a numerical experiment on the described system in a manner described in some detail in the section on propellant reorientation (Section C of this chapter). Calculation of the initial interface is also described in that section.

Propellant configuration in the annulus, assuming no withdrawal into the screen reservoir, is shown in Fig. III-33 for a few of the time steps. The central "empty" cylinder is 5 in. in diameter, and the outer screen boundary is 8 in. in diameter. The top of the liquid surface is initially positioned just below the top of this outer boundary. Reorientation acceleration was taken as 0.5 ft/sec. Computational cells were 1/4 in. square.

For this case, it was found that little draining forward out of the annulus had occurred even after 0.35 sec, a time at which withdrawal into the reservoir would actually have emptied the annulus. For this reason, the portion of the analysis dealing with inertial draining was not pursued further.

G. EXPULSION EFFICIENCY

An analysis of the capillary system under steady-state outflow conditions was conducted to determine the quantity of residual propellant at screen liner breakdown. Single-phase liquid feed cannot be assured after gas has penetrated the liner. Even though the gas on the outlet side of the liner may not be carried to the outlet during the burn period in which the leakage occurs, it could migrate to the outlet between burns and be ingested during subsequent burns. If all of the propellant in the bottom compartment is expelled before gas penetration the expulsion efficiency can be calculated based upon geometric considerations. For the designs shown in Fig. II-4 and II-6, the trapped liquid and the liner volume represents less than 0.5% of the total tank volume.

Flushing Annulus
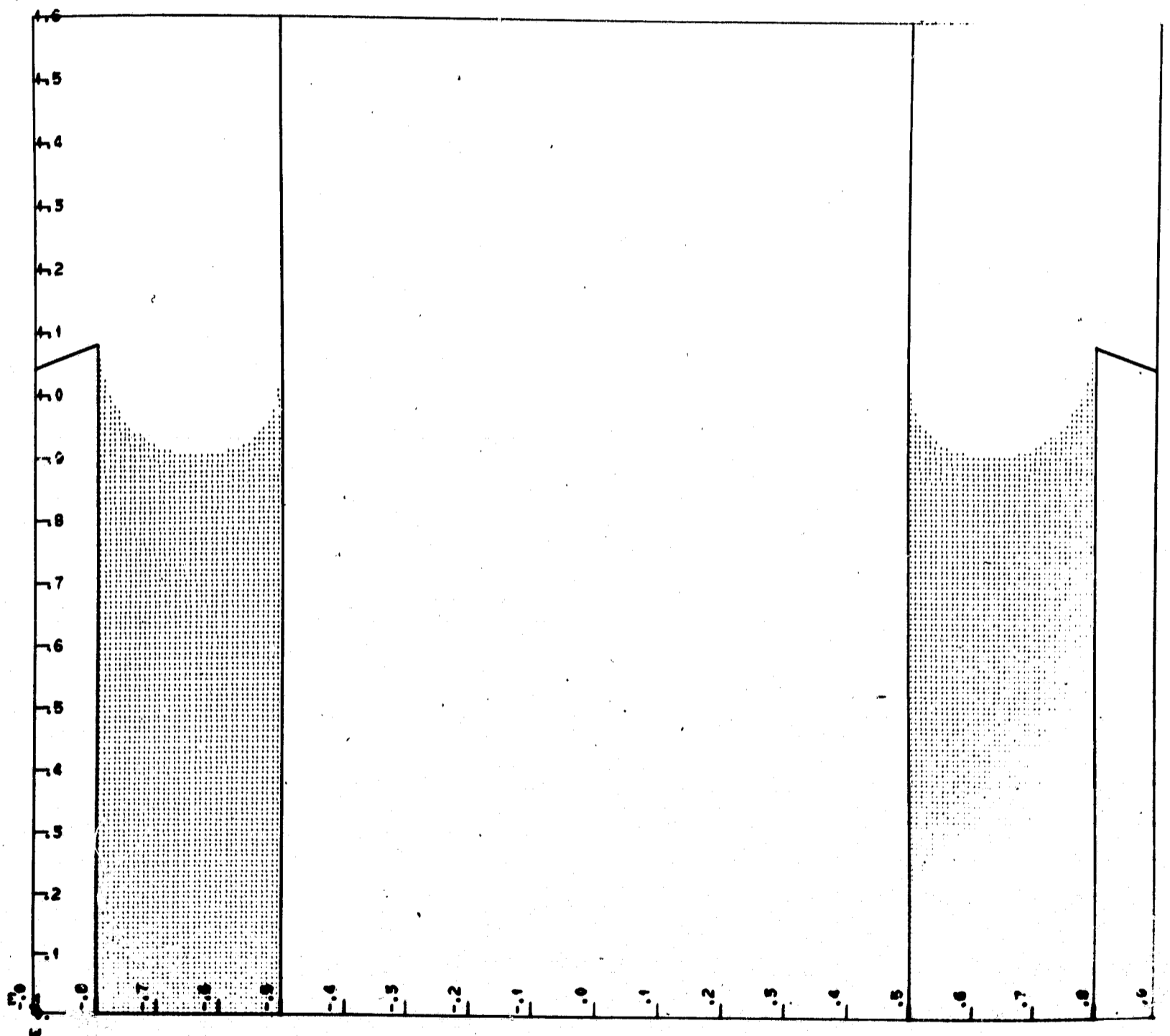
Flushing Annulus
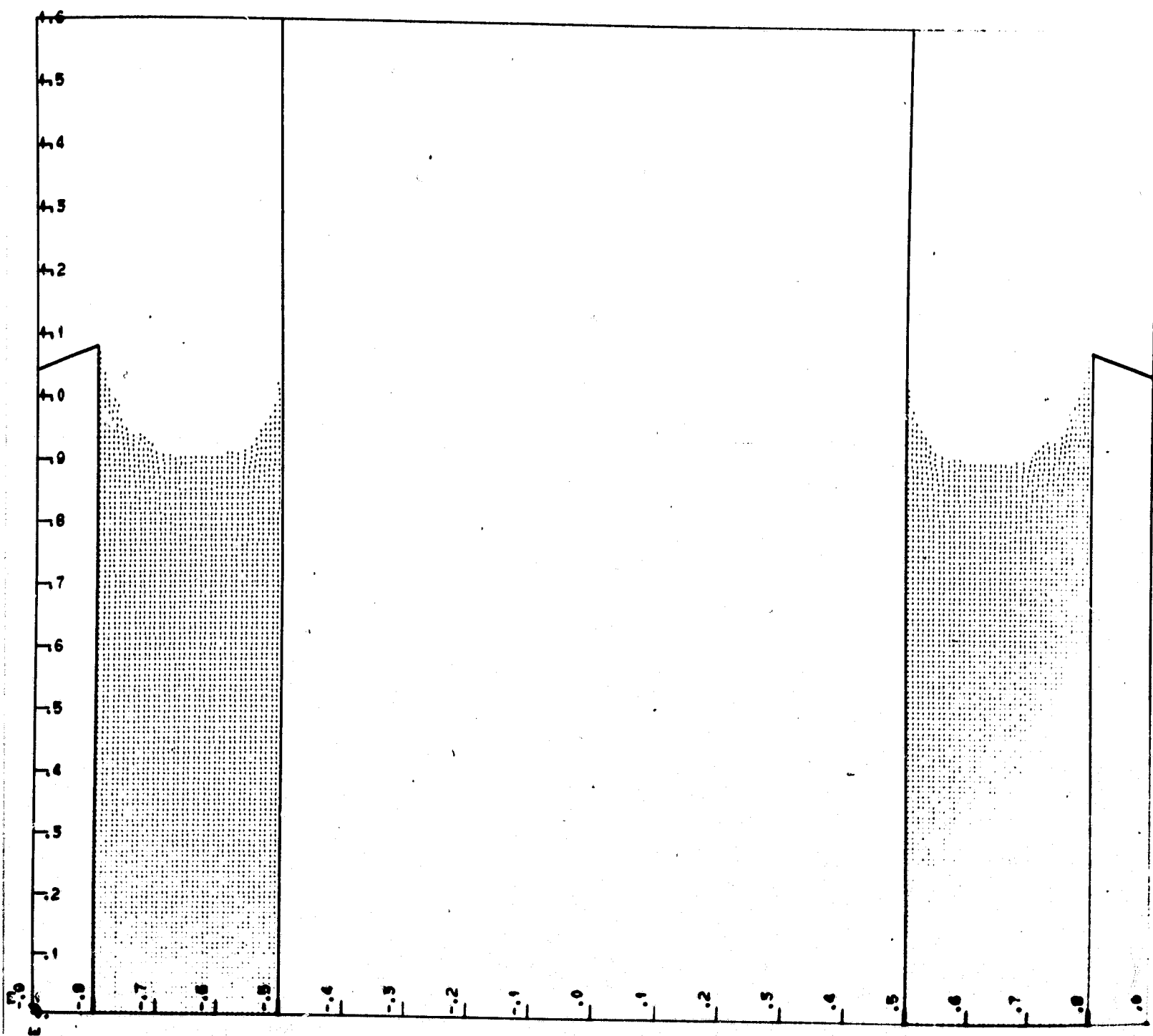
(b)   0.150 sec

Fig. III-33   (cont)

Flushing Annulus

(c) 0.237 sec

Fig. III-33 (cont)

Flushing Annulus

(d)   0.303 sec

Fig. III-33   (cont)

Flushing Annulus

(e)   0.345 sec

Fig. III-33   (cont)

Flushing Annulus

(f)   0.362 sec

Fig. III-33   (concl)

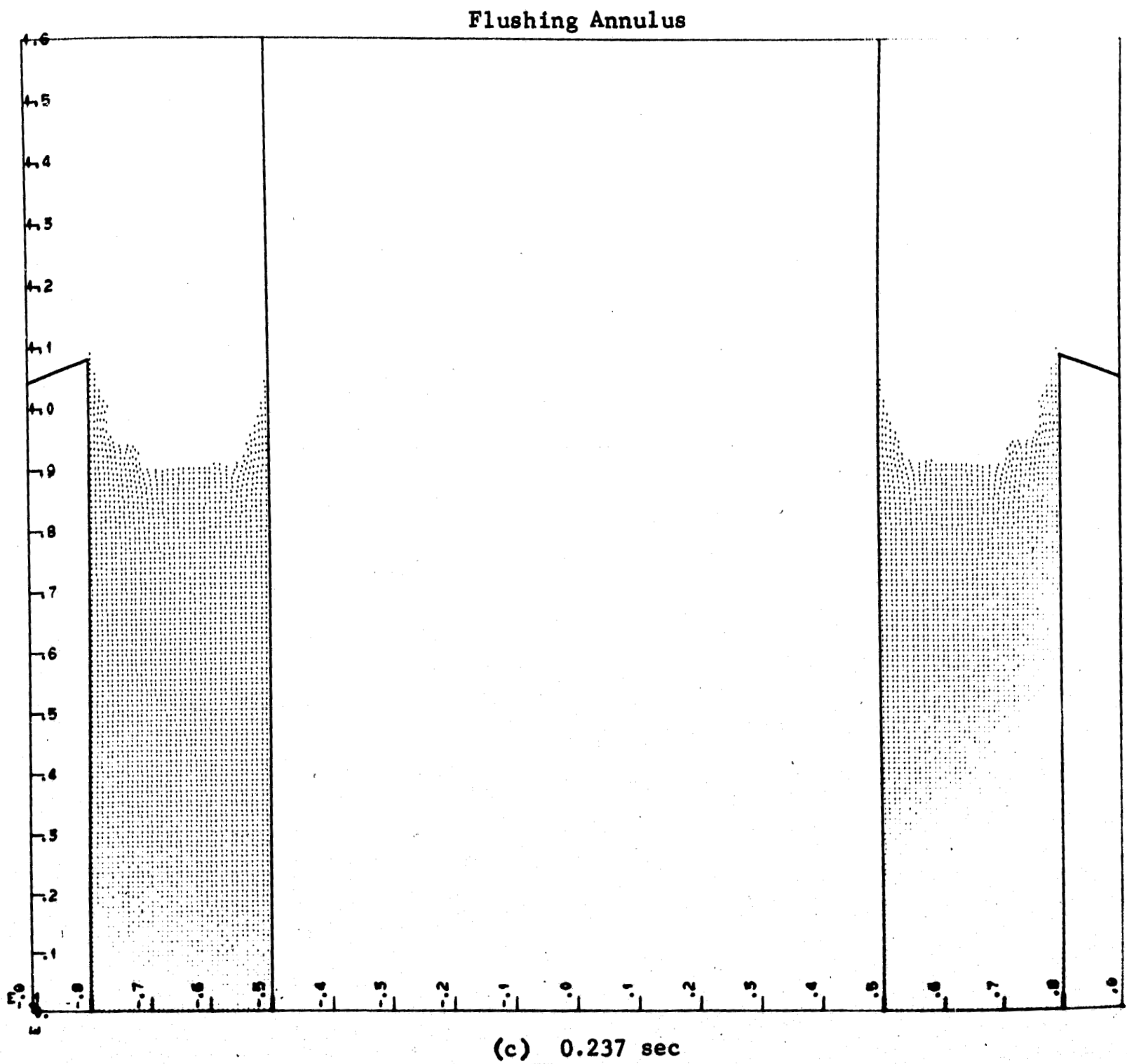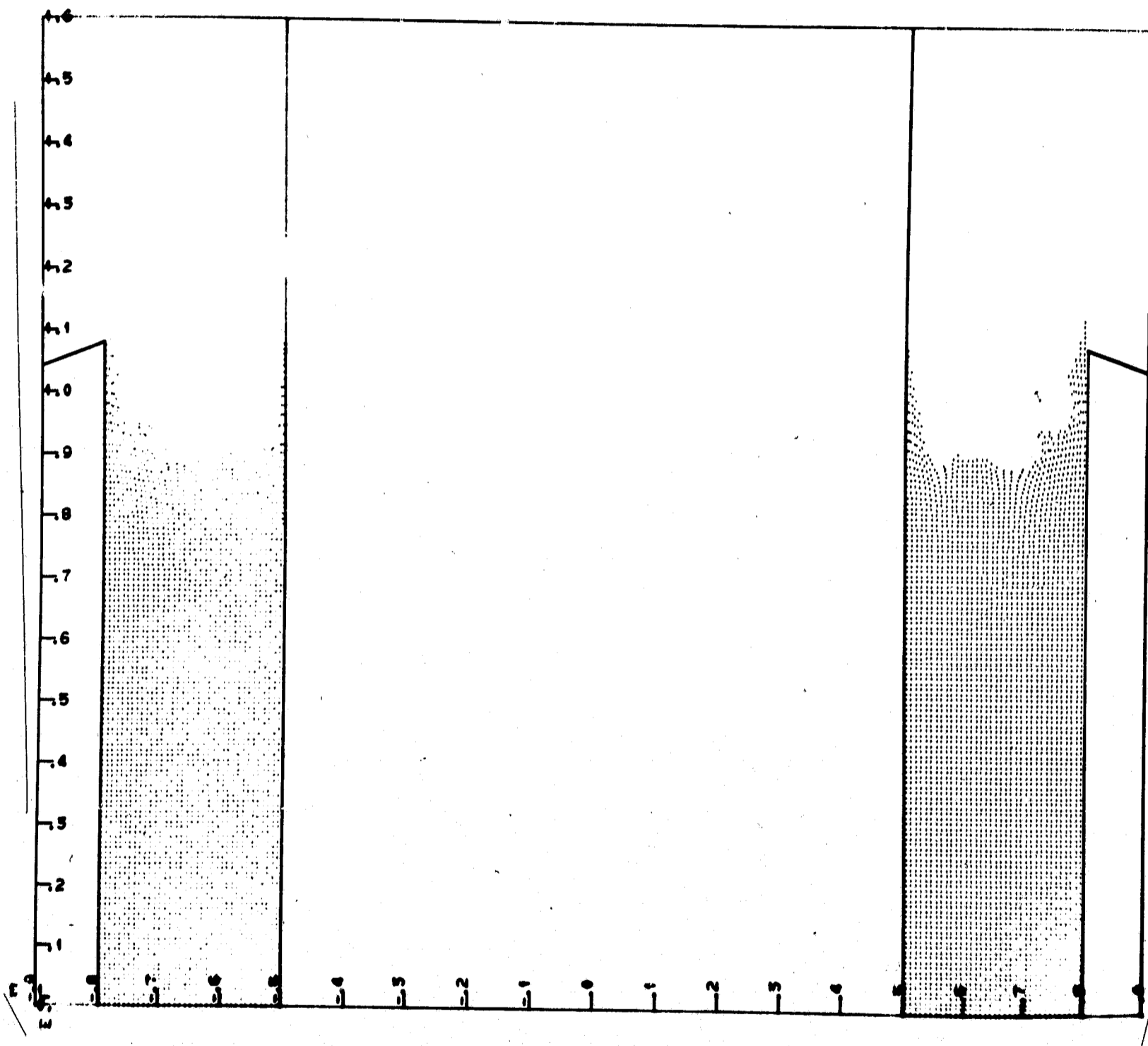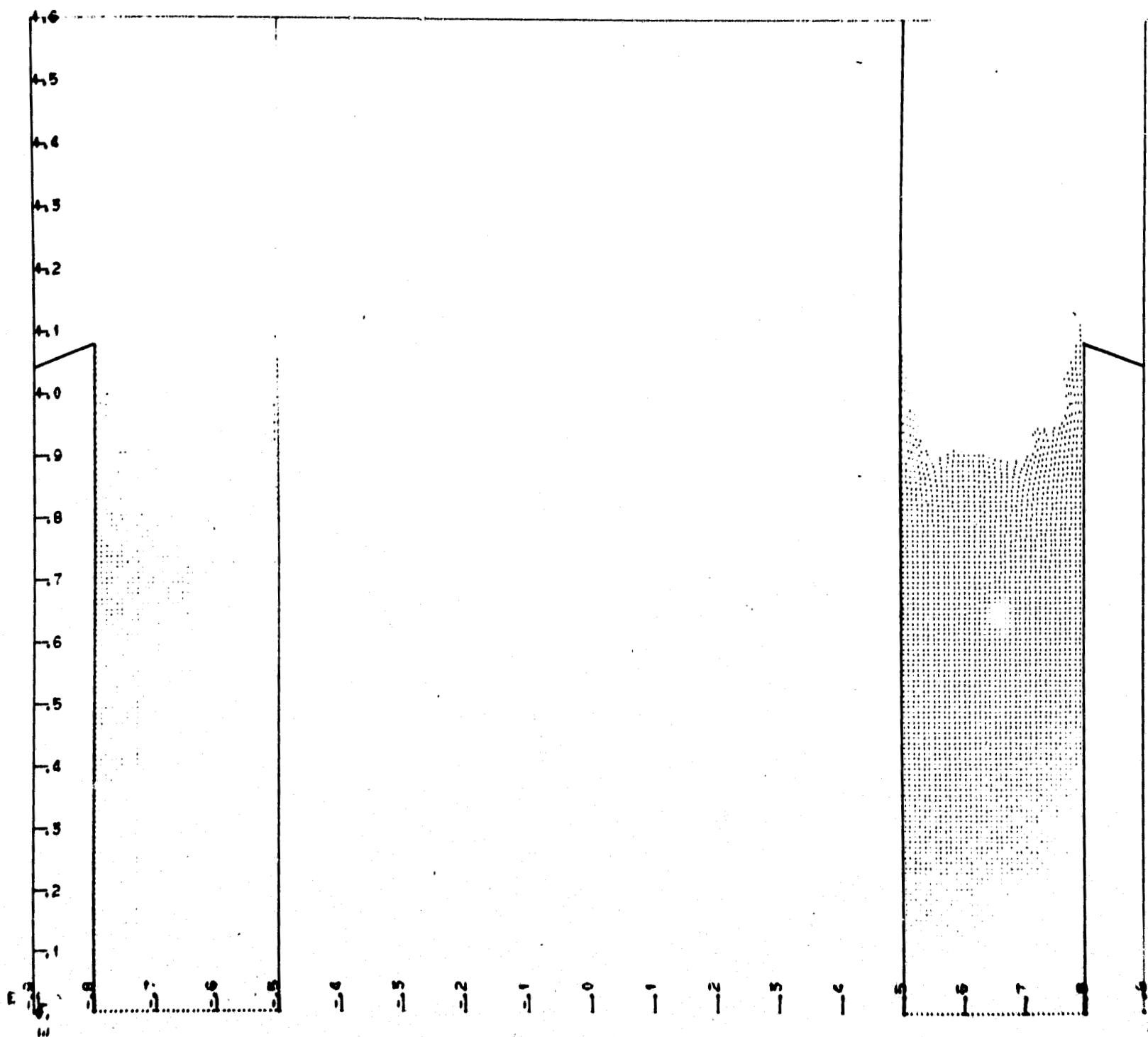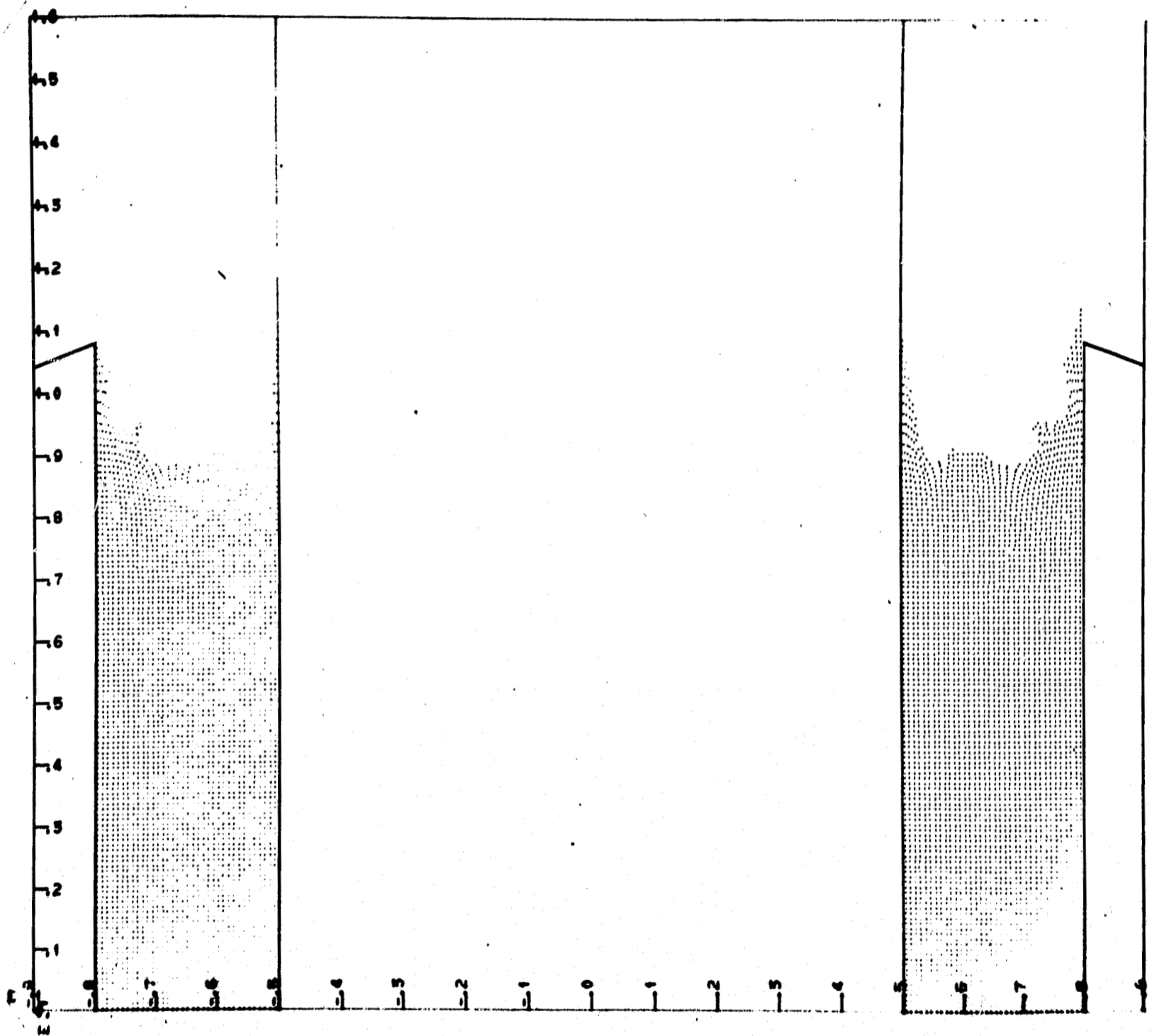An analysis of the terminal drain condition for the lower res-
ervoir was conducted to determine the quantity of propellant re-
maining in the compartment at liner breakdown. The variables con-
sidered are:

$$\Delta P_B = P_u - P_a = \Delta P_H + \Delta P_V + \Delta P_{f_1} + \Delta P_{f_2} \leq \Delta P_C \qquad \text{[III-51]}$$

where

ΔP_B = breakdown pressure,

ΔP_C = maximum capillary retention pressure,

ΔP_H = hydrostatic head pressure,

ΔP_V = velocity head in annulus,

ΔP_{f_1} = pressure drop in annulus due to outflow,

ΔP_{f_2} = pressure drop across screen liner (includes entrance
      and exit losses),

P_u = ullage pressure,

P_a = minimum exposed annulus liquid pressure.

For a positive g field draining condition several variables
drop out of the analysis, namely, the ΔP_V and ΔP_{f_1} terms. For the
terminal condition the liquid interface will be as shown on Fig.
II-17. For a worst-case assumption that there is no pressure gra-
dient in the annulus (i.e., flow per unit area of covered screen
is constant) the stability is defined as:

$$\Delta P_C \geq \Delta P_B = P_u - P_a = \Delta P_H + \Delta P_{f_2} \qquad \text{[III-52]}$$

Based on the pressure drop data presented in Appendix B and the
geometries of Fig. II-4 and II-6, the liner retention pressure re-
quired $\left(P_u - P_a\right)$ to expell all of the propellant does not exceed
the capillary retention capability. Therefore the expulsion effi-
ciency of the device would be 99.5% or greater depending on the
volume of liquid expelled from the liner.

Scaled draining tests were not conducted to provide experimental verification of the system performance. To simulate the hydrostatic and viscous heads would require scaled outflow testing in an increased acceleration environment. While this is possible by centrifuge testing it was not considered necessary for a high confidence design. Both the retention capability of the liner and the viscous flow losses for the capillary liner material have been verified through testing. These data permit ready calculation of the positive g field draining capability.

Demonstration outflow tests were conducted using ethanol in the 1/5-scale plexiglass tank and screen liner in both a positive and negative one-g orientation for volumetric flow rates of up to 1/8 the prototype outflows (maximum test setup capability) without any premature breakdown. Expulsion efficiency from the lined volume was near 100% (i.e., no measurable liquid volume was left within the liner) for all the test cases.

An analysis of dropout due to draining for the capillary liner was not attempted **because of the complexity and experimental nature** of the problem. However draining tests conducted under scaled outflow conditions demonstrated that dropout or gas ingestion due to coring was not a problem for the proposed design. These tests are discussed below with results of a typical outflow shown in Fig. III-34.

In determining tank draining dropout, four primary considerations must be included:

1) Acceleration environment;

2) Tank geometry, i.e., shape, outlet location, and configuration ratio of tank characteristic dimension to outlet dimension;

3) Liquid interface velocity;

4) Liquid physical properties (viscosity, density, and surface tension).
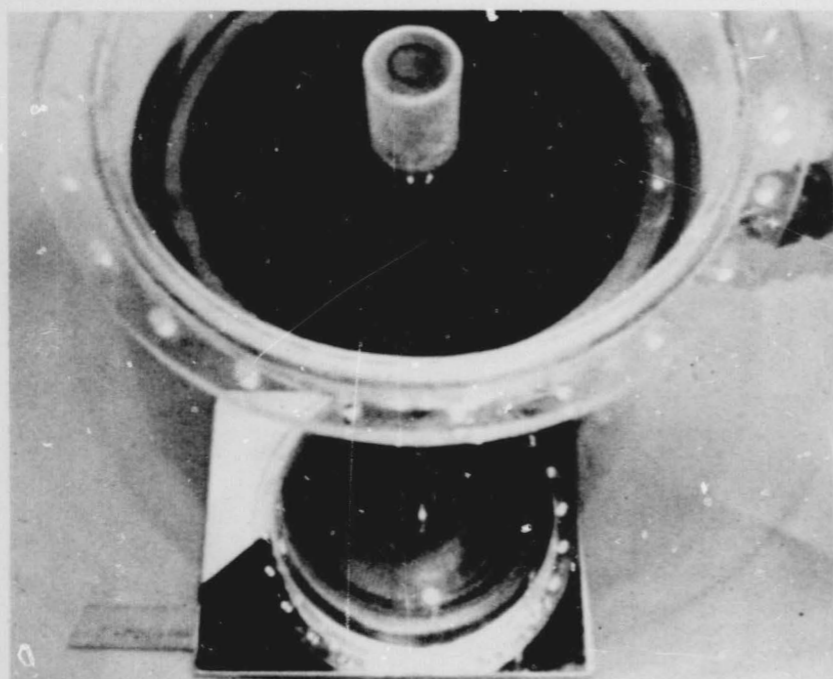
(a) Liquid Level above Liner, 0.32 sec after
Outflow Initiation, Test 3
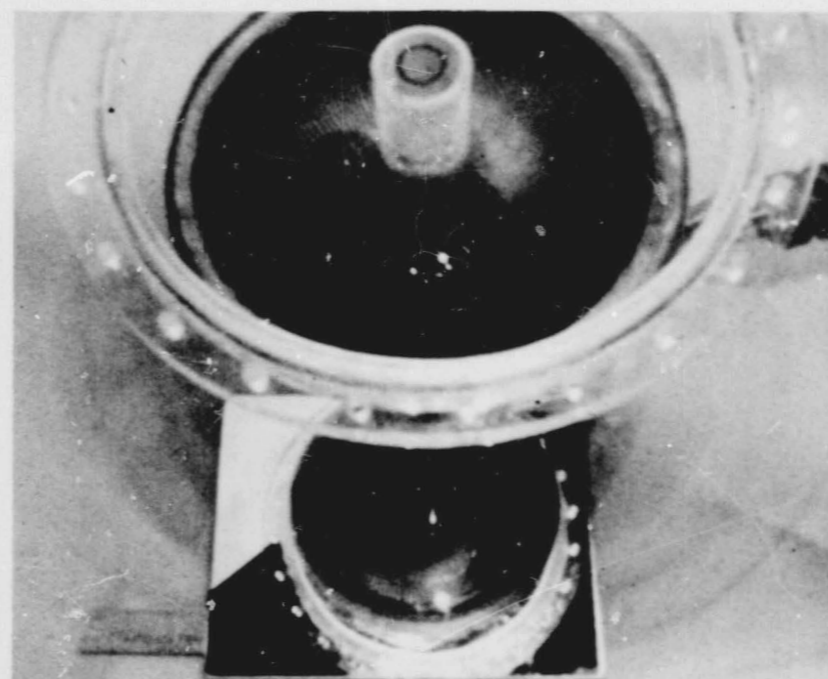
(b) Liquid in Liner Nearly Depleted, No Liner Annulus
Breakdown, 0.43 after Outflow Initiation, Test 3
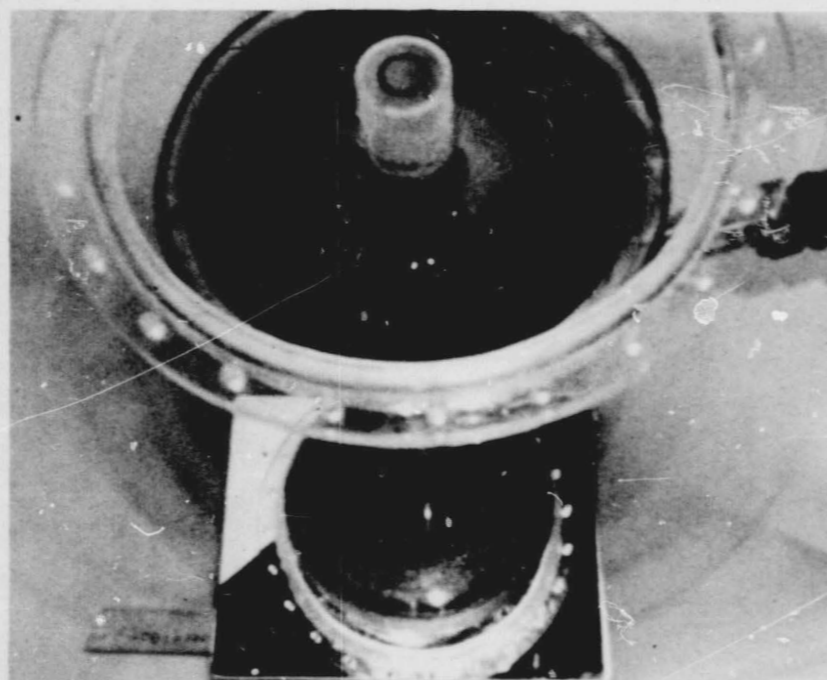
(c) Liquid in Liner Depleted, Liner Breakdown just
Initiated as Shown by Bubbles in Annulus

Figure III-34   Screen Liner Outflow Sequence

In the model testing conducted, the model and prototype maintain
geometric similitude, the acceleration environments at the termi-
nal drain condition are similar (0.94 g versus 1 g). Therefore,
a reasonable approach to experimental verification seems to be to
use the prototype propellants and scale the model to simulate the
same liquid interface velocity during liquid draining. Since the
test model materials of construction were not compatible with the
propellants, a simulant fluid, ethanol, was required. However,
this is not a severe limitation since inspection of the outflow
problem indicates that for the high Reynolds number involved in
flow across the liner (>>500) and the high system Bond number
(>1000), the test liquid physical properties are not important
parameters in the simulation.

To maintain the same average liquid interface velocity requires
scaling to an equivalent flow per unit area between the prototype
and the model. Therefore, for the 1/5-scale model the flow rate
would be 1/25 of the prototype or about 0.018 ft^3/sec. Model out-
flow tests were conducted to flow rates of 0.05 ft^3/sec (the maxi-
mum capability of the test setup) without any gas ingestion into
the liner before complete draining of the fluid in the liner res-
ervoir.

H.   COVERPLATE DRAINING

Propellant outflow characteristics through an acquisition de-
vice are important from the standpoint of gas-free propellant with-
drawal and expulsion efficiency. Liquid draining rates from the
various compartments formed by the devic must be large enough to
deplete all upstream compartments before the outlet compartment
is depleted. Complete draining of the proposed no-hardware-modi-
fication system was investigated experimentally using a 1/5-scale
model. A computer program describing the outflow characteristics
was used to predict full-scale performance of the prototype sys-
tems. The computed results for the model were first compared to
the experimental results using ethanol as the working fluid.

The program looks at the flow characteristics in each of the
two conical coverplates in terms of liquid and ullage gas veloci-
ties; pressure drop across the double perforated plate and screen
sections; and both gas and liquid volumetric flow rates through
the coverplates. The acquisition device is divided into five com-
partments, i.e., 3, 5, 7, 4, and 6 (Fig. III-35). The volume in
each compartment is determined as a function of time based on a
constant liquid withdrawal rate. Analytical and model outflow re-
sults are compared in Fig. III-36. The liquid height values, h_2,
h_3, and h_4, pertain to the volumes above the top coverplate, be-
tween the two conical plates, and below the bottom plate, respec-
tively. The predicted results are somewhat conservative because
the computed liquid levels are above those determined experimen-
tally. One exception is the level in the outlet compartment, com-
partment 6, in Fig. III-35, where better agreement was achieved.
Draining of the various compartments was demonstrated experimen-
tally using the 1/5-scale model. Enlarged pictures taken from 16
mm film used to document the outflow tests show the liquid level
in the various compartments during outflow, Fig. III-37. As shown,
satisfactory draining of all compartments prior to outlet compart-
ment depletion was achieved. The pleated screen liner was not
used during the tests and was not considered in the analysis be-
cause it does not have any affect on the coverplate draining re-
sults.

Flow losses in the coverplate screens were determined using
the approach presented by Armour and Cannon (see Appendix B). The
double perforated plate areas were treated as orifices. Incom-
pressible flow equations were used to describe the gas flow char-
acteristics through these areas. The initial liquid level at time
= 0 was set at the junction of perforated plate and Dutch twill
screen in the top coverplate. The perforated plate was assumed
wet offering an initial pressure retention value equal to the
bubble point. All flow from compartment 2 under this condition
is through the screen. During outflow, the ΔP across the screen
exceeded the bubble point of the double perforated plate in less
than 0.01 sec under steady-state outflow conditions. Once the
perforated plates break down, i.e., ΔP = bubble point, the pres-
sure retention capability was assumed to be zero. Laboratory
tests supported this assumption. Orifice flow theory was then
used to compute ullage gas flow through the double perforated
plate. An overall flow coefficient of 0.03 was used to obtain
the curves shown in Fig. III-36.
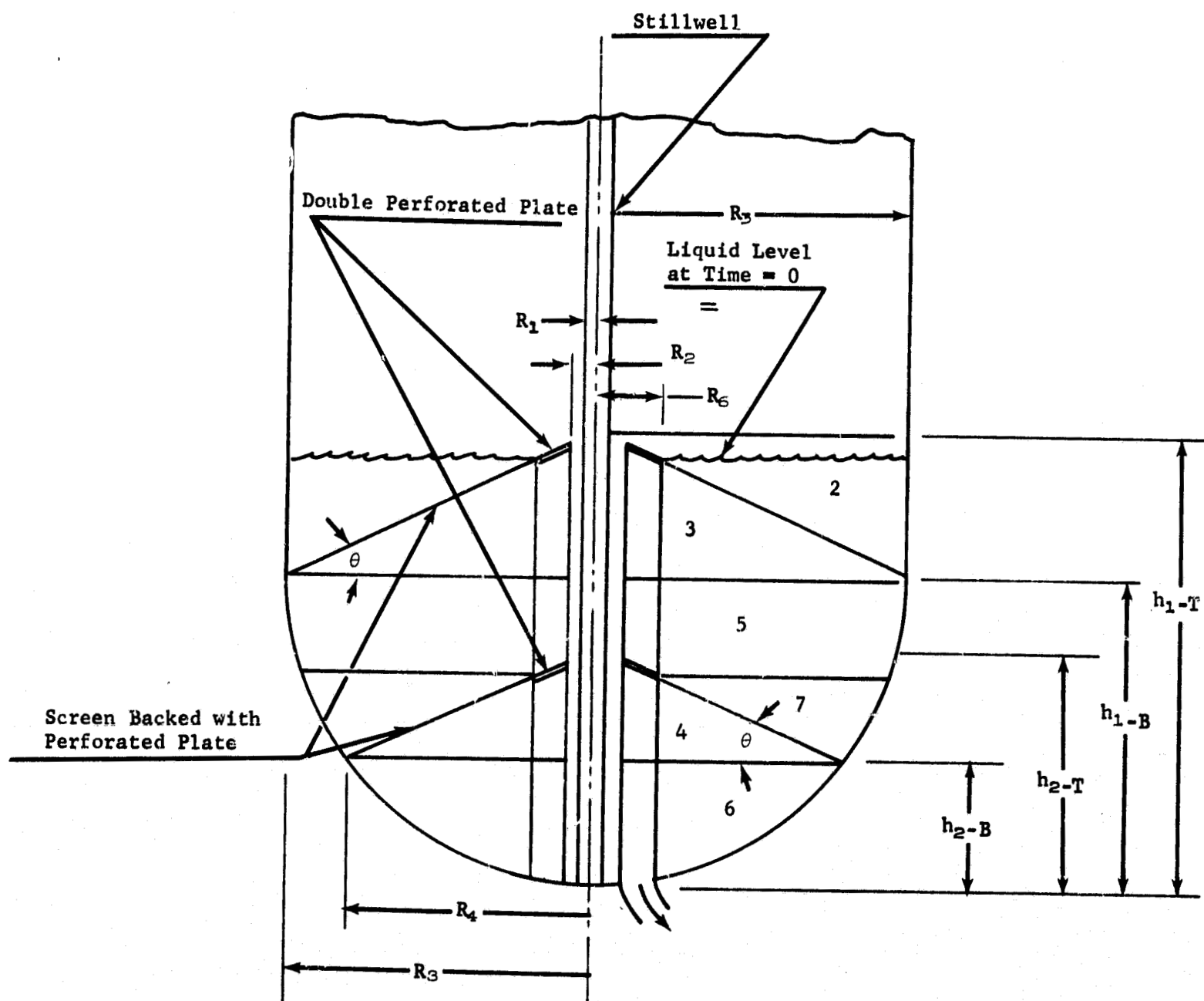
Fig. III-35 Dimension Identification for Coverplate Outflow Characteristic Analysis
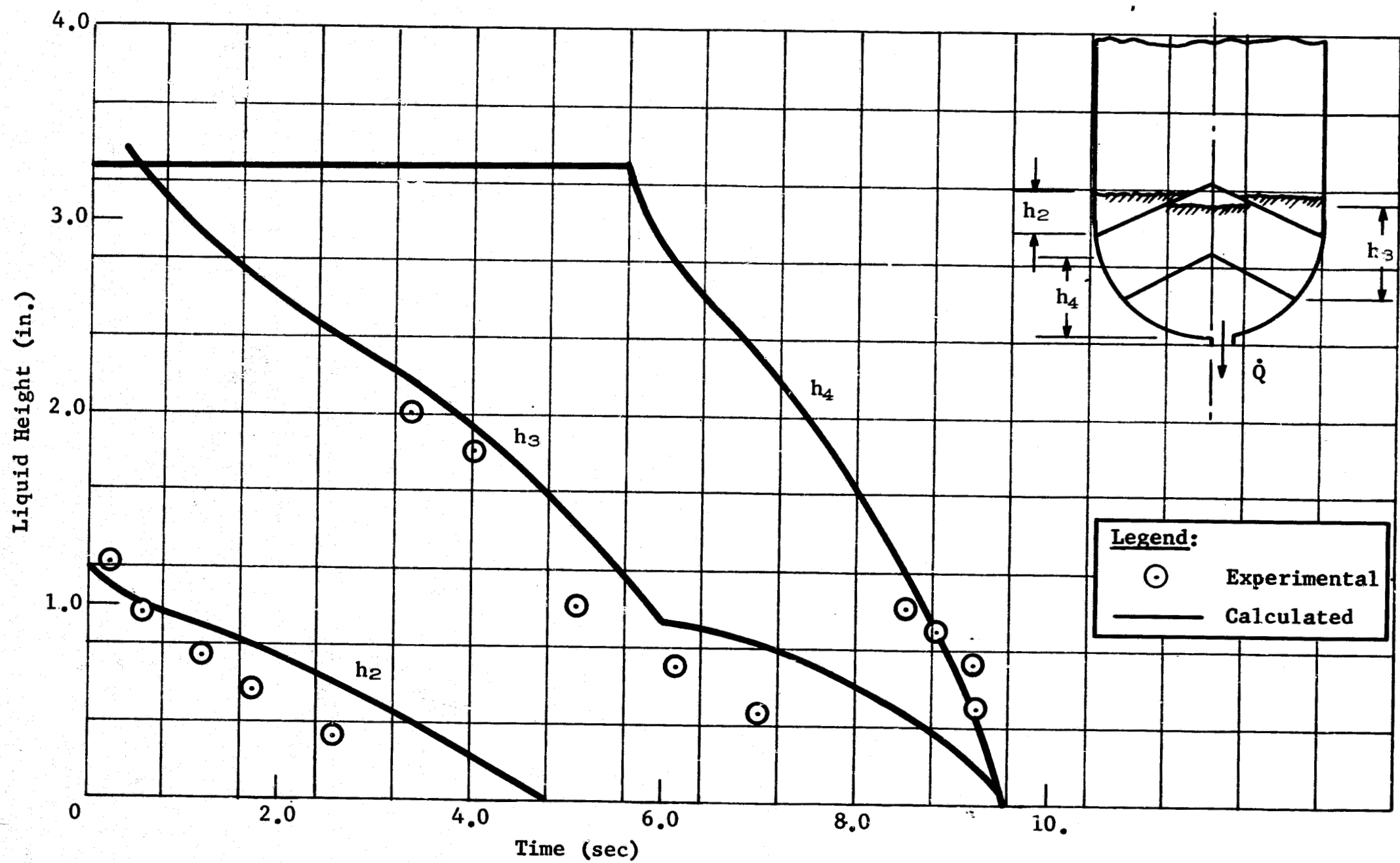
Fig. III-36 Analytical and Experimental Results Comparison
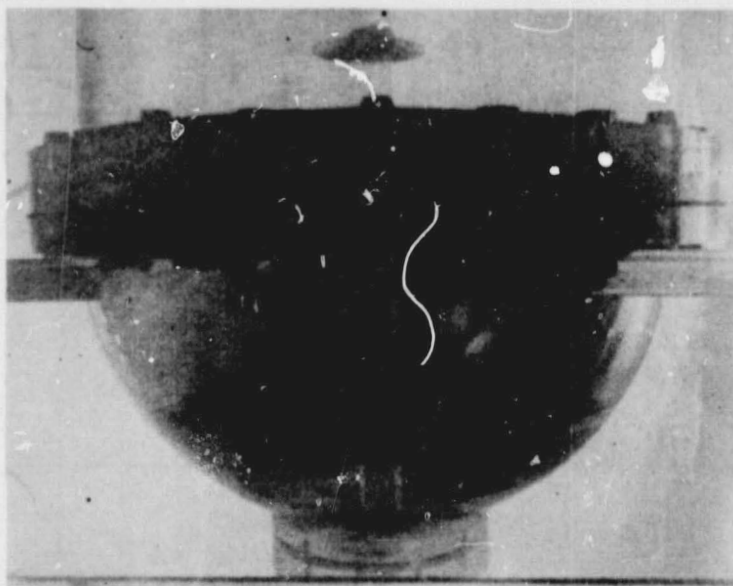
(a) Liquid above Both Barriers
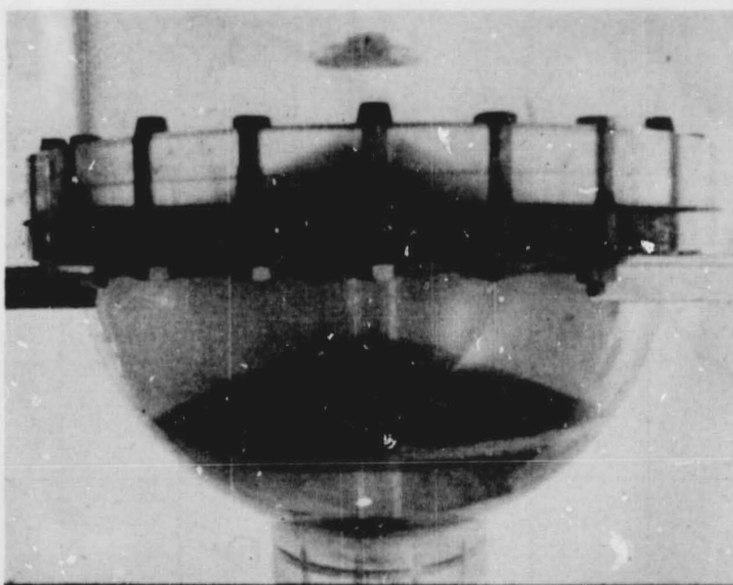
(b) Liquid Drained from above Top Barrier
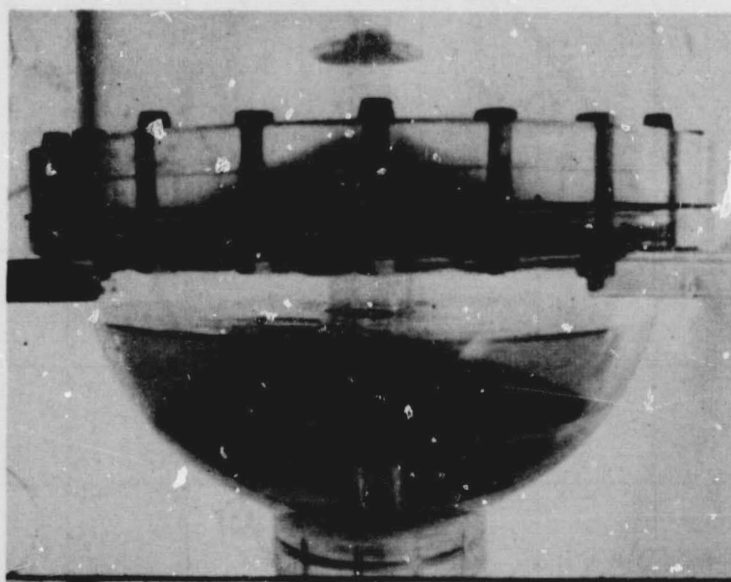
(c) Liquid Level at Top of Lower Barrier

Fig. III-37 Capillary Compartment Draining Sequence from Test 13
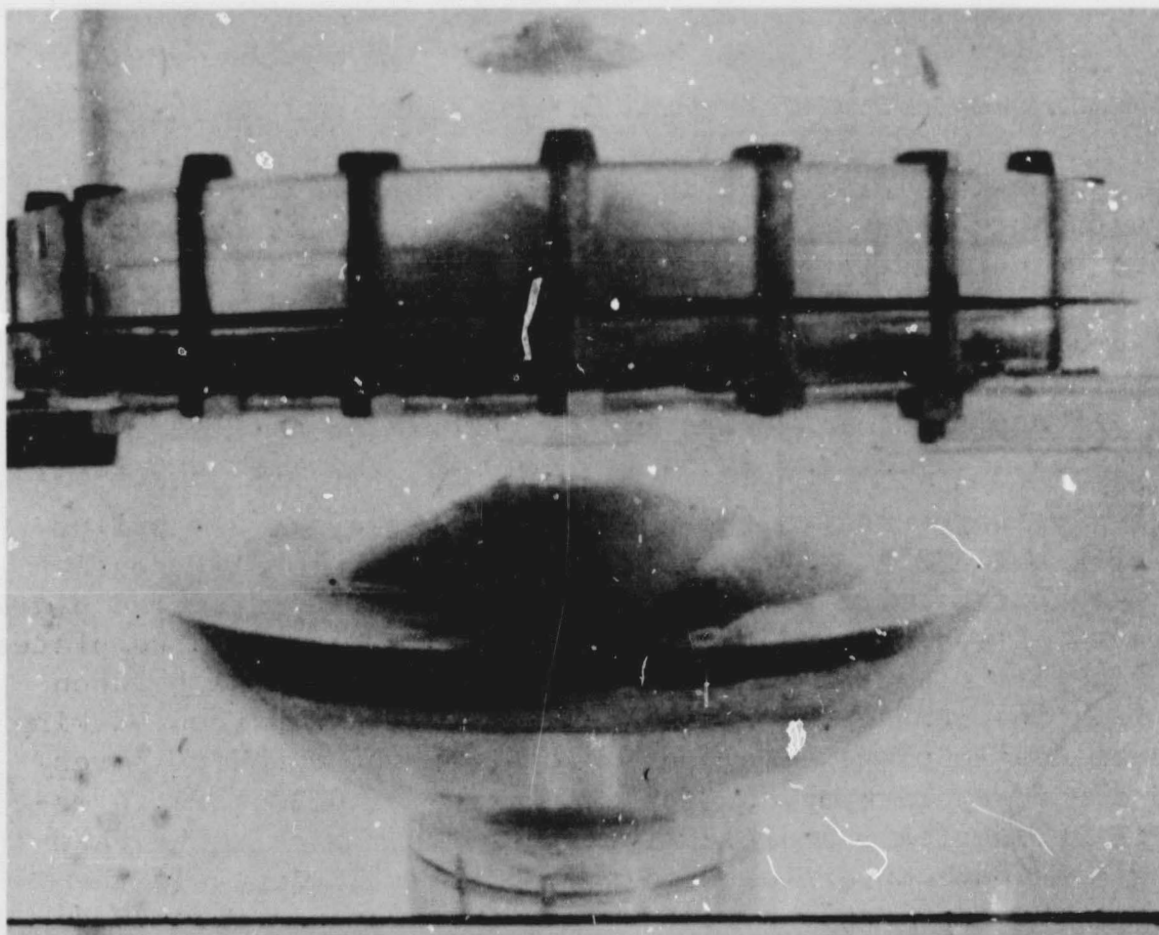
(d)   Liquid Level below Bottom Barrier
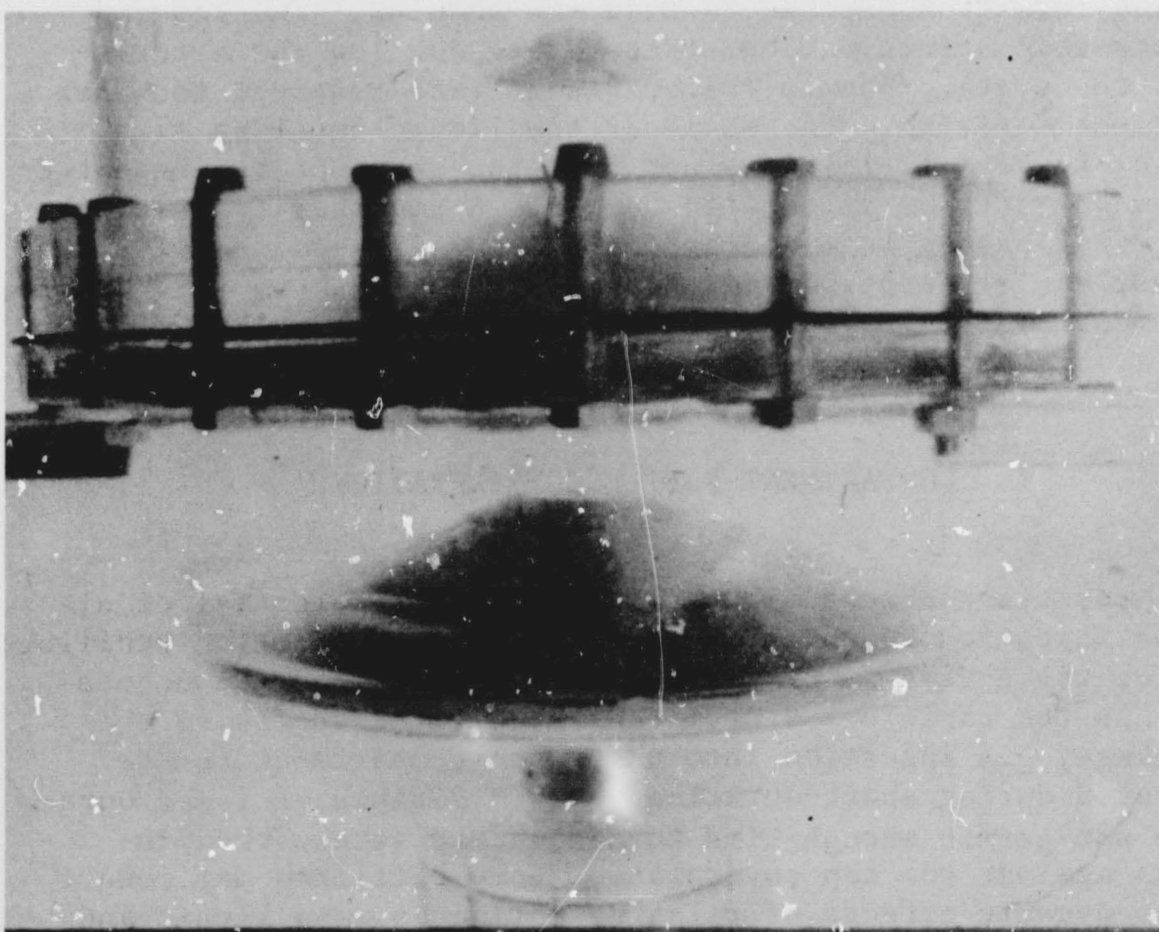
(e)   Liquid Level Entering Outlet at Bottom
      (Note complete drainage from both barriers.)

Fig. III-37 (concl)

The hydrostatic head used to calculate the driving potential for flow through the Dutch twill screen was taken as the difference in liquid heights between adjacent compartments. Characteristic curves for the full-scale system using both fuel and oxidizer propellants (presented in Fig. II-15) show that the upper compartment in the device drains completely before the outlet compartment is depleted, achieving maximum expulsion efficiency. Outflow rates of 39.26 and 24.54 lb_m/sec for oxidizer and fuel, respectively, were used in the analysis. Ullage gas was helium at 175 psia and 530°R. Both upper and lower coverplates contain 30x250 mesh Dutch twill weave screen supported by perforated plate in the area between R_6 and the tank wall and two perforated plates spaced ½ a pore diameter (0.013-in.) apart in the areas between R_2 and R_6. The perforated plate used for both the screen backing and in the double plate area contained 0.026-in.-diameter pores in a 60 deg array forming an open area ratio of 0.33. Plate material is 300 series stainless steel 0.020-in. thick. The base cone angle of both coverplates in the model is 20 deg. In the prototype, the base angle of the upper coverplate is also 20 deg, but this angle in the lower plate was reduced to 10 deg to provide a more desirable geometry for low negative-g liquid-vapor interface formation desired to feed the annulus. The reduced angle has some effect on the steady-state outflow characteristics of the system, but is insignificant with resepect to upper compartment draining. The shape of the liquid level vs time curve (h_3 in Fig. II-15) does not have the sharp break presented in the model outflow calculated curves. A smoother transition as the level passes from compartment 5 to 7 is obtained with the cone base angle reduction. As previously stated, complete upper compartment draining precedes outlet compartment depletion.

I. COMPARTMENT REFILL CONSIDERATIONS

All capillary acquisition devices have the potential of ullage gas ingestion depending on the mission acceleration profile. Refilling the device is of prime concern if gas ingestion does occur. In the capillary system suggested for retrofit in the SPS tankage, gas ingestion into the upper compartment can be anticipated during short-duration burns. Firings of 1-sec duration do not permit enough time to adequately settle the propellants against the top coverplate. Some refilling may result from the dynamic effects of relative motion between liquid and

tank under this condition, but burn periods of longer duration
are required for substantial refilling. Refilling the volume be-
low the coverplates in the suggested configuration is achieved
when liquid enters the compartment under sufficient hydrostatic
head to raise the gas pressure in the compartment to a level
which exceeds the bubble point of the double perforated plate near
the center of the coverplate cone. When the pressure exceeds the
bubble point, gas is expelled from the compartment through the
double perforated plate into the bulk liquid above. The maximum
refill height is a function of the positive acceleration magnitude
and the liquid head difference between the compartments above and
below the screen. The maximum head difference is the product of
the radii difference (R_3 - R_6 in Fig. III-35) and the tangent of
the coverplate cone base angle. The head difference as a function
of positive acceleration magnitude presented in Fig. III-38 and
III-39 represent the maximum refill heights achievable for fuel
and oxidizer, respectively, in the full size system. Refill of
the oxidizer system is more complete than in the fuel system be-
cause of the higher kinematic surface tension of the fuel.

Refill rates as function of time and acceleration level for
A-50 and N_2O_4 in the full scale tank are presented in Fig. II-16
and II-17. These curves resulted from calculations based on the
following conditions:

1) At time = 0, the bulk liquid level has been settled
on the top coverplate;

2) Bulk liquid completely covers the top plate;

3) The liquid level in the compartment below the top
coverplate is located half-way between the two plates;

4) Compression of the gas between the plates is isother-
mal.

All the refill rates calculated at positive accelerations of
0.5, 0.6, and 0.7 g reached a steady-state value in less than 10
msec. Although the values presented are for a specific case, a
similar result would be expected over a wide range of initial con-
ditions. The steady-state values would not change until the re-
filling liquid level reaches the base of the coverplate cone. As
the level increases above this point, the driving potential which
causes liquid flow through the screen decreases as the hydrostatic
head decreases. The refill rate then decreases with increased h
and approaches zero as h approaches the maximum heights presented
in Fig. III-38 and III-39. Transient conditions during ingested
gas pressure build-up are also volume dependent.
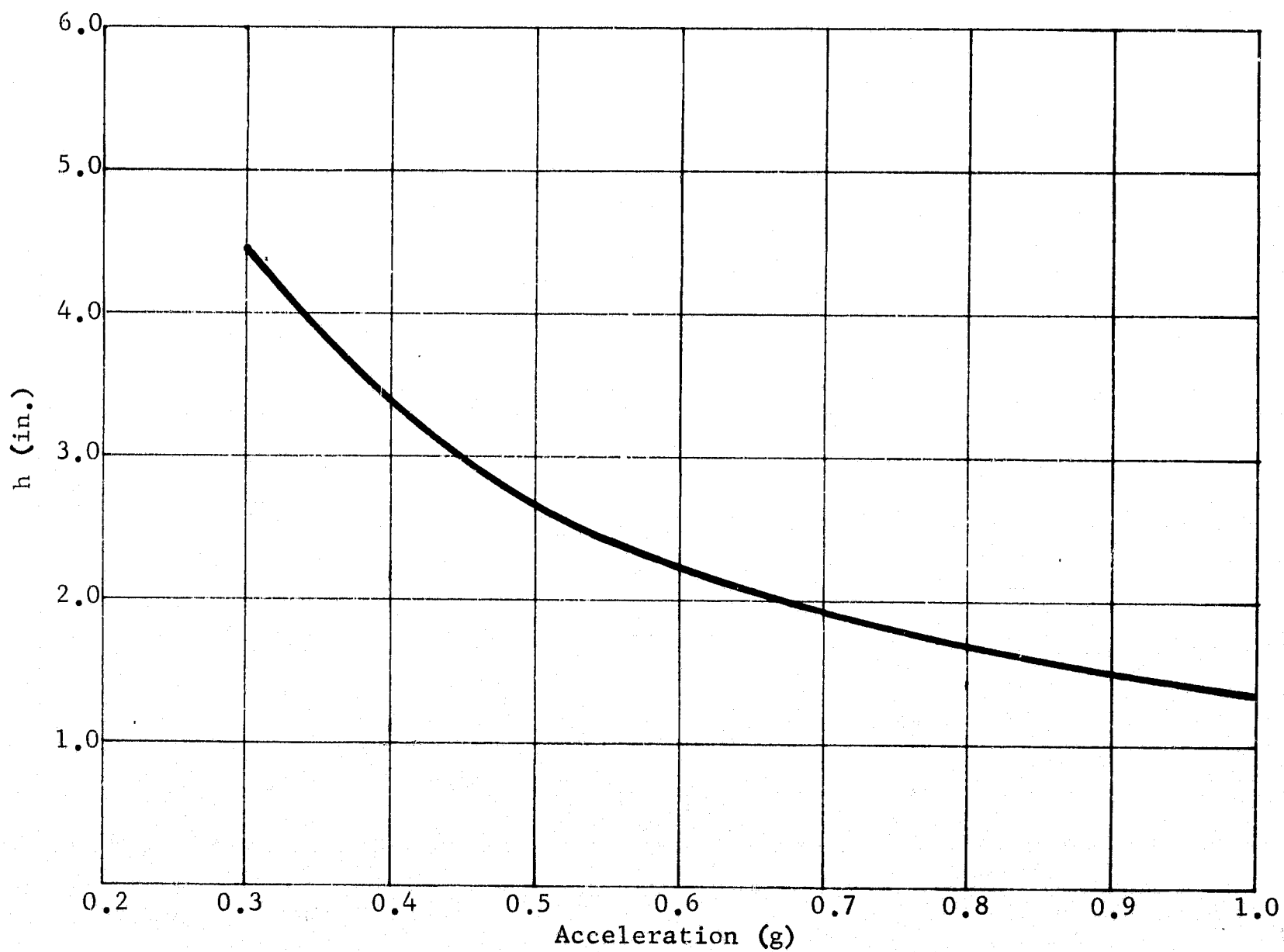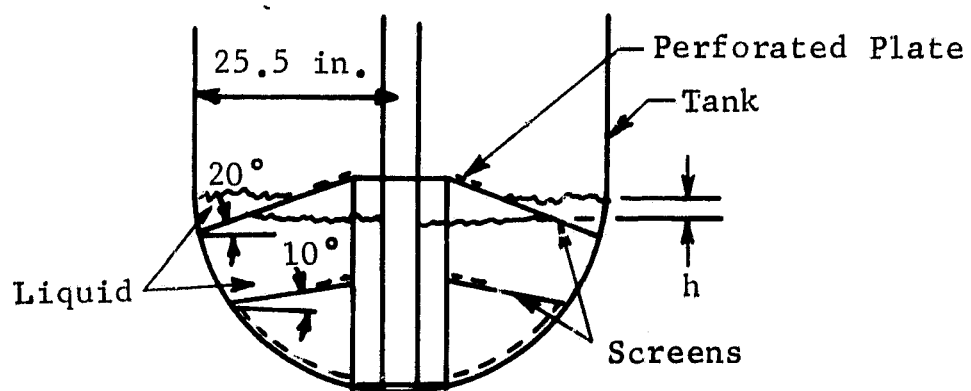
Fig. III-38   Maximum Refill Height vs Acceleration for A-50
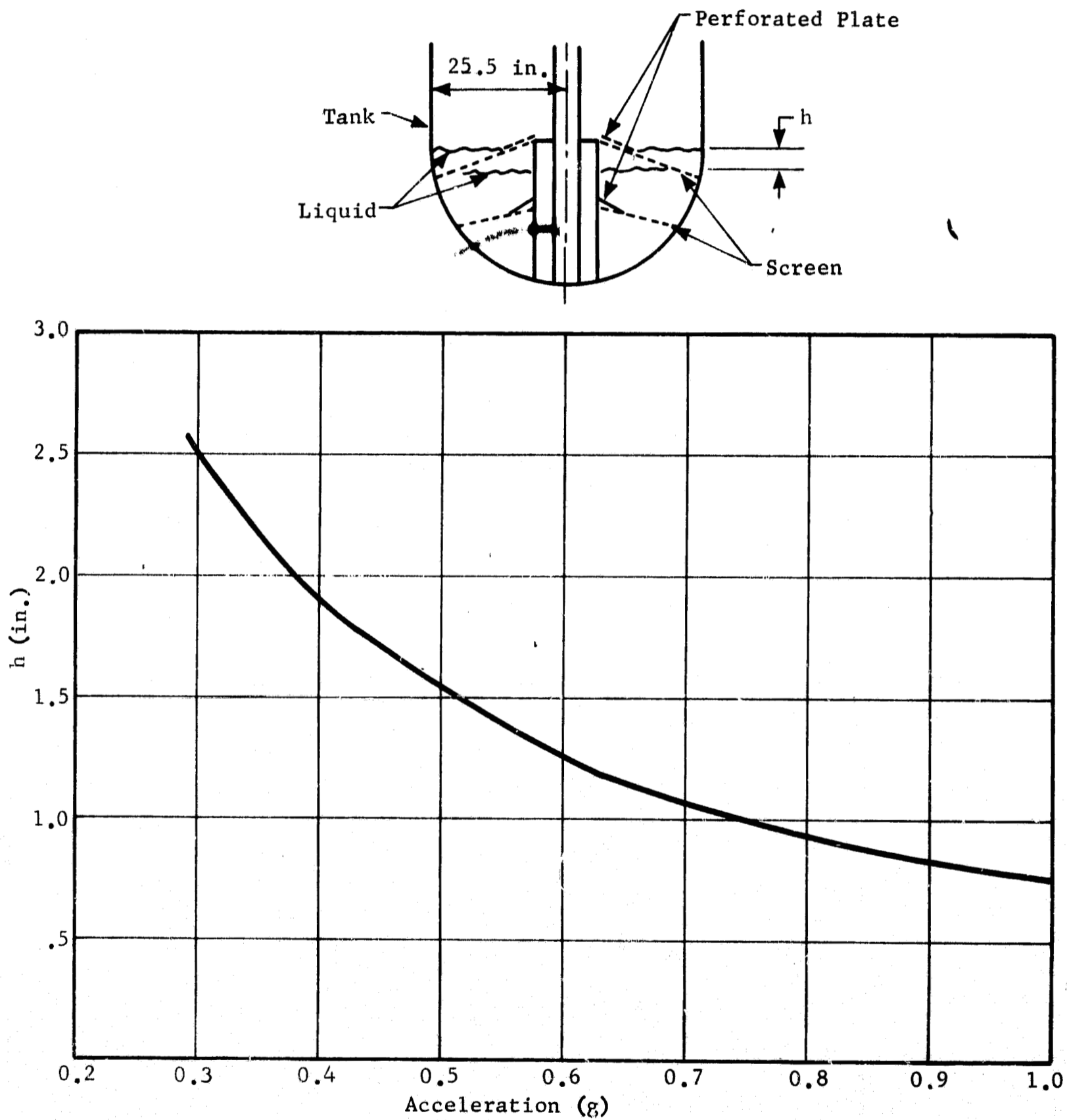
Fig. III-39   Maximum Refill Height vs Acceleration for N_2O_4

As the ingested gas volume increases, the time for pressure build-
up to reach the bubble point of the double perforated plate also
increases because the refilling liquid flowrate is essentially
constant at constant acceleration if the gas volume is greater
than the coverplate cone volume.

This set of curves show that the acquisition device does have
the capability of refilling. Refilling potential was also demon-
strated during the 1/5-scale model tests using ethanol as the work-
ing fluid at 1 g (Fig. III-23). As stated previously, the refill
rate of this device is a function of the ingested gas volume,
positive acceleration level, and the propellant properties. For
the conditions used in the calculations, refill rates peak-out
rapidly after adequate resettling. Using a resettle time of 2
sec at an acceleration of 0.5-g, a 10-sec burn would provide re-
fill to accommodate five 1-sec burns assuming complete ingestion
with no refill during the short-duration burns.

IV. CONCLUSIONS

● The propellant management system designs shown in Fig. II-4 and II-6 are capable of meeting the propulsion system requirements as outlined in Table I-1.

● The no-hardware-modification design can be retrofitted into the existing Apollo tankage as presented in Fig. I-1.

● The no-hardware-modification design meets the Priority I and Priority II system design goals as presented in Table I-2 with the exception of weight of 19 lb/tank as opposed to the goal of 10 lb/tank.

● The no-hardware-limitation design meets all the design goals presented in Table I-2 with the exception of the 11 lb/tank weight and the no-hardware-change goal (Priority II, No. 3) which does not apply for this design.

V. REFERENCES

I-1   D. L. Balzer, et al.: Advanced Propellant Management Sys-
        tem for Spacecraft Propulsion Systems, Phase I -- Survey
        Study and Evaluation. MCR-69-87 (Contract NAS9-8939).
        Martin Marietta Corporation, Denver, Colorado, February 1969.

II-1   J. P. Gille: "Stability of Capillary Barriers When Sub-
        jected to Suddenly Applied Linear Accelerations." Master
        of Science Thesis, California State College at Long Beach,
        January 1969.

II-2   T. R. Barksdale and H. L. Paynter: Criteria for Passive
        Propellant Control Schemes. SR-1660-69-7. Martin Marietta
        Corporation, Denver, Colorado, April 1969.

II-3   H. L. Paynter and T. R. Barksdale: Criteria for Passive
        Propellant Control Schemes." AIAA Paper No. 69-531.
        AIAA 5th Propellant Joint Specification Conference,
        U. S. Air Force Academy, June 1969.

II-4   H. L. Paynter, et al.: Experimental Investigation of Ca-
        pillary Propellant Control Devices for Low Gravity Environ-
        ments. MCR-68-199. Martin Marietta Corporation, Denver,
        Colorado, December 1968.

II-5   D. F. Gluck: "Propellant Position Control by Capillary
        Barriers During Spacecraft Rotational Maneuvers." AIAA
        Paper No. 69-529. AIAA 5th Propellant Joint Specification
        Conference, U. S. Air Force Academy, June 1969.

II-6   Apollo SPS Propellant Position Control In Low- and Zero-G
        Environment. SD67-655. NAA, Inc., 21 July 1967.

II-7   W. H. T. Lott: Jet, Rocket, Nuclear, Ion and Electric Pro-
        pulsion: Theory and Design. Springer-Veslag, Inc., New
        York, 1968.

II-8   J. E. Welch, F. H. Harlow, J. P. Shannon, and B. J. Daly:
        The MAC Method: A Computing technique for solving viscous,
        incompressible, transient fluid-flow problems involving free
        surfaces. Report LA-3425. Los Alamos Scientific Labora-
        tory, Los Alamos, New Mexico, 1966.

III-1   G. A. Lyerly and H. Peper: Summary Report, Studies of In-
        terfacial Surface Energies. NASA CR-54175. Harris Research
        Laboratories, Inc., December 1964.

III-2   D. E. Gilmore and T. R. Barksdale: <u>Low-G Laboratory An-</u>
        <u>nual Progress Report: 1965, Development Task #605</u>.
        M-65-67. Martin Marietta Corporation, Denver, Colorado,
        December 1965.

III-3   F. H. Harlow and J. E. Welch: "Numerical calculation of
        time-dependent viscous incompressible flow of fluid with
        free surface." <u>Physics of Fluids</u>. 8, 2182-2189, 1965.

III-4   F. H. Harlow and J. E. Welch: "Numerical study of large
        amplitude free-surface motions." <u>Physics of Fluids</u>.
        9,842-851,1966.

III-5   C. W. Hirt and F. H. Harlow: "A general corrective pro-
        cedure for the numerical solution of initial value prob-
        lems." <u>Journal of Computational Physics</u>. 2, 114-119, 1967.

III-6   C. W. Hirt and J. P. Shannon: "Free-surface stress condi-
        tions for incompressible flow calculations." <u>Journal of</u>
        <u>Computational Physics</u>. 2, 403-411, 1968.

III-7   C. W. Hirt: "Heuristic stability theory for finite-dif-
        ference equations." <u>Journal of Computational Physics</u>.
        2, 339-335, 1968.

III-8   B. J. Daly and W. E. Pracht: "A numerical study of den-
        sity-current surges." <u>Physics of Fluids</u>. 11, 15-30,
        1968.

III-9   B. J. Daly: "A technique for including surface tension
        effects in hydrodynamic calculations." (to be published
        in <u>Journal of Computational Physics</u>).

III-10 B. J. Daly: "A numerical study of the effect of surface
        tension on interface stability." (to be published in
        <u>Physics of Fluids</u>).

III-11 D. F. Gluck and J. P. Gille: "Fluid Mechanics of Zero G
        Propellant Transfer." Paper 862A, SAE-ASME Air Transport
        and Space Meeting, New York, N. Y., April 1964.

III-12 J. A. Salzman and W. J. Masica: "Experimental Investiga-
        tion of Liquid-Propellant Reorientation." NASA TN D3789,
        Lewis Research Center, Cleveland, Ohio, January 1967.

III-13 M. P. Hollister, H. M. Satterlee, and H. Cohan: <u>A Study</u>
        <u>of Liquid Propellant Behavior During Periods of Varying</u>
        <u>Accelerations</u>. LMSC-A874728. Lockheed Missiles and Space
        Company, Sunnyvale, California, 30 June 1967.

III-14 R. M. Davies and G. I. Taylor: "The Mechanics of Large
        Bubbles Rising Through Extended Liquids and Through Liquids
        in Tubes." Proc. Roy. Soc. A, 200, pages 375-390, 1950.

APPENDIX A

NOMENCLATURE

NOMENCLATURE

a	Acceleration
Bo	Nondimensional Bond number
D	diameter
g	acceleration (thrust/weight)
g_c	gravitational constant (32.2 ft/sec^2)
h .	distance
L	characteristic dimension
$\dot{Q}$	volumetric flow rate
r,R	radius
Re	nondimensional Reynolds number
s	safety factor
v	velocity
$\dot{v}$	acceleration
We	nondimensional Weber number
We*	nondimensional modified Weber number
X	liquid collection rate, quantity/time
z	distance
Z	dimensionless retention stability parameter
ΔP	differential pressure
β	kinematic surface tension
δ	liquid film thickness
μ	microns
ρ	density
σ	surface tension
φ	nondimensional correlation factor
ω	angular velocity
$\dot{\omega}$	angular acceleration

SUBSCRIPT

a	annulus
B	breakdown value
C	maximum
crit	critical value
f_1	viscous loss in annulus
f_2	viscous loss across liner
H	hydrostatic head
L	liquid
m	model
p	pore
P	prototype
u	ullage
V	velocity head

APPENDIX B

PRESSURE LOSS DUE TO FLUID FLOW THROUGH WOVEN SCREENS

Prediction of the expulsion capability of a capillary screen propellant control device requires knowledge of the pressure drop across the screen under low flow conditions. This pressure drop is particularly significant for systems that are required to expel liquids in adverse gravity environments.

While several correlations have been developed to predict the pressure drop across rectangular mesh screens based on fractional open area as a major parameter, these are not applicable to the complex weaves often required in the design of capillary expulsion systems. Armour and Cannon,* expanding on the work of Ingenson, et al. have adapted a packed bed model to develop a general correlation applicable to the flow of Newtonian fluids through all types of woven metal screen. The result of the analysis yields a screen friction factor that is defined as a function of a screen Reynolds number. The form of the final equation is

$$f = \frac{\alpha}{N_{Re}} + \beta \qquad\qquad [B-1]$$

$$f = \text{friction factor} = \frac{\Delta p \; gc \; \epsilon^2 D}{L\rho \; u^2} \qquad\qquad [B-1a]$$

$$N_{Re} = \text{Reynolds Number} = \frac{\rho \; u}{\mu \; a^2 D} \qquad\qquad [B-1b]$$

α = Viscous resistance coefficient,

β = Inertial resistance coefficient,

Δp = Screen pressure drop

gc = Gravitational conversion constant,

D = Screen pore diameter,

L = Fluid path length = QB,

u = Fluid approach velocity,

a = Surface area to unit volume ratio of screen,

---

* J. C. Armour and J. N. Cannon: "Fluid Flow Through Woven Screens." AIChE Journal. May 1968.

ϵ = Screen volume void fraction,

μ = Fluid viscosity,

ρ = Fluid density,

B = Screen thickness,

Q = Tortuosity factor to yield effective fluid path
    length for complex weaves. Q is 1 for rectang-
    ular weave, 1.3 for dutch weave.

Values of α and β were obtained by Armour and Cannon from non-
linear, least squares, regression analysis of pressure drop vs
velocity data collected for nitrogen over a velocity range of
0.1 to 30 ft/sec. The values of α and β are 8.61 and 0.52, re-
spectively. Therefore Eq [B-1] becomes:

$$f = \frac{8.61}{N_{Re}} + 0.52 \qquad\qquad [B-2]$$

Figure B-1 is a plot of Eq [B-2] together with the data points
for 18 screens representing five weave types that were the basis
of the correlation. To further validate the correlation, the
data of Ingmanson and Amneus for flow of water through fourdrinier
screens were plotted in accordance with the model. These data
along with additional data collected by Armour and Cannon for
helium flow through plain Dutch and twilled Dutch screens is
shown in Fig. B-2. Even though the bulk of the water data of
Ingmanson extends the Reynolds number range an order of magnitude
beyond that used for the correlation, Fig. B-1, the agreement is
quite good. In fact regression analysis applied to a combination
of the nitrogen and water data altered the values of α and β by
less than 1 and 4%, respectively. The range for application of
this correlation that is suggested by the authors is Reynolds
number of 0.1 to 1000, void fractions from 0.35 to 0.76, screen
pore diameters from 5 to 550 microns, mesh sizes from 30 to 2400
wires/in., and surface area-to-unit volume ratios from 1200 to
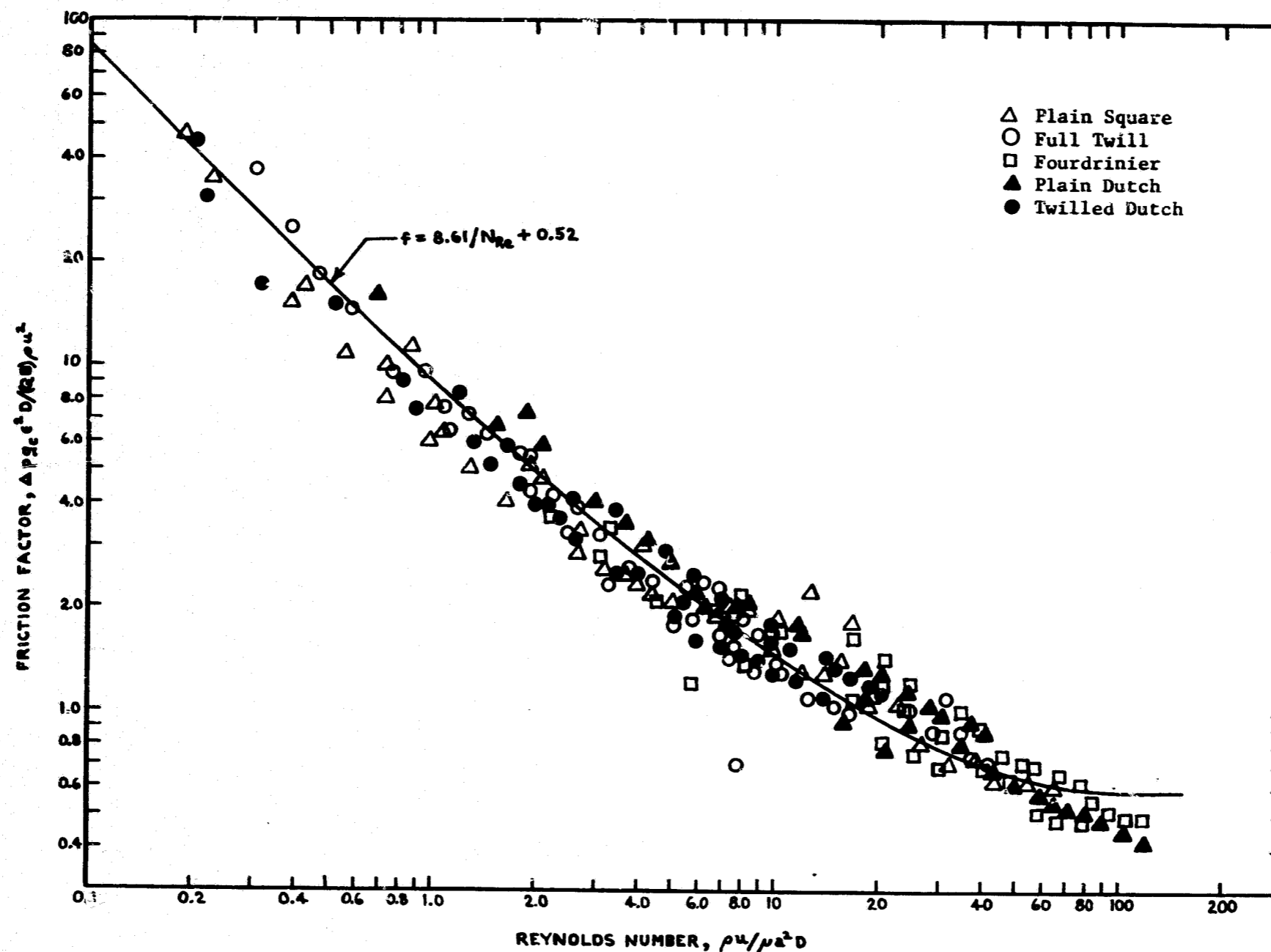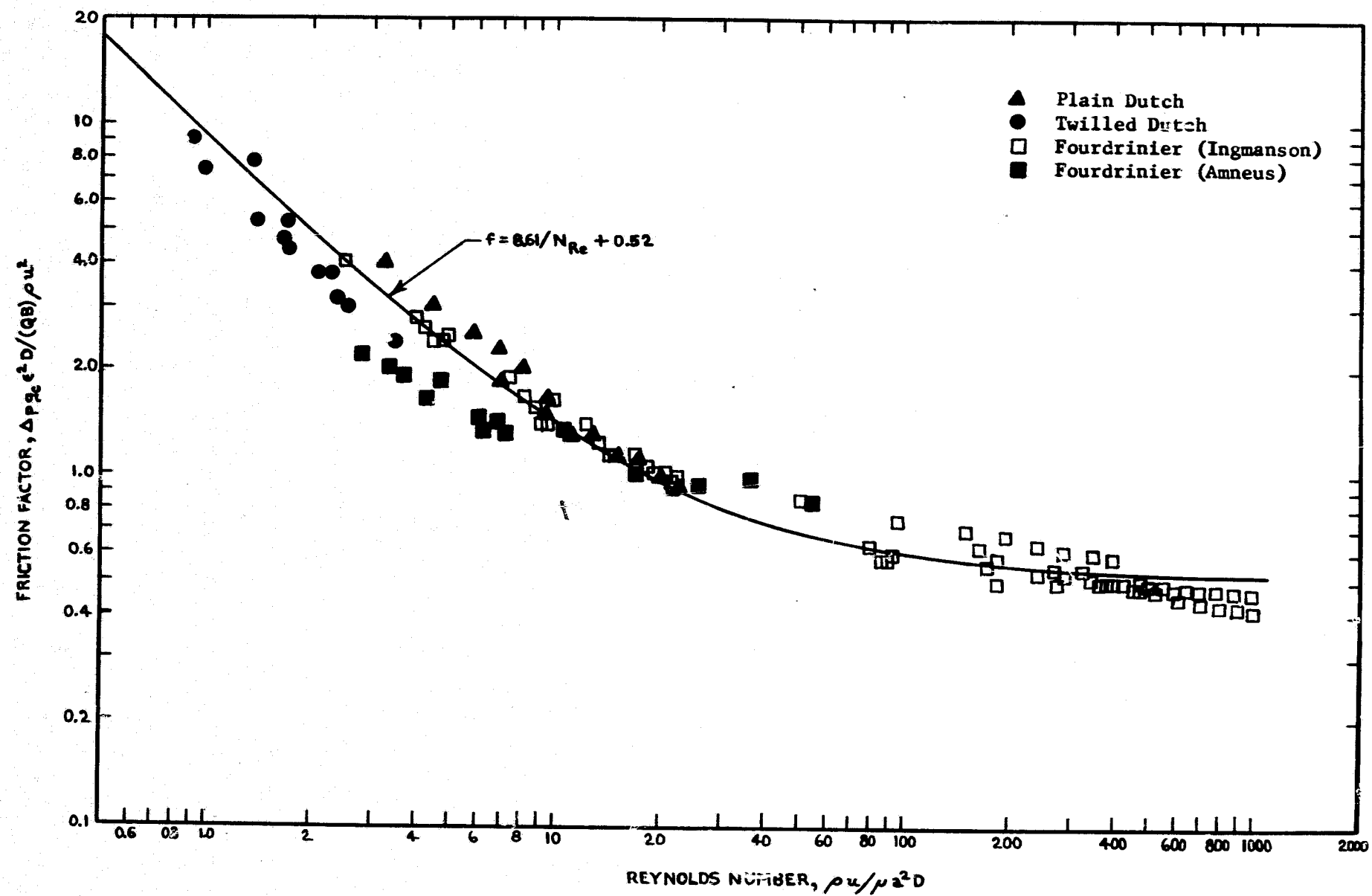29,000 ft^{-1}.

Fig. B-1 Screen Flow Data Correlation

Fig. B-2 Additional Flow Data Correlation

For most expulsion system applications, only the very small Reynolds number range is of interest, 0.01 to 10. While Armour and Cannon suggest a usable Reynolds number for their correlation down to 0.1, as Fig. B-1 and B-2 show, no data are presented below a N_{Re} of 0.2 and little data are given below a value of 1. To better define the low flow velocity regime, pressure drop tests were conducted under RA 631. The flow test set up is shown in Fig. B-3 with the screen test specimens presented in Table B-1. A plot of these data along with Eq [B-2] is presented in Fig. B-4. Although there is considerable data scatter, the correlation appears valid for the low Reynolds number regime (to 0.03). An error analysis was not performed on the data; however, it is believed that the inaccuracies in measuring the small pressure drops contributed significantly to the data scatter.

Table B-1 Screen Test Specimens

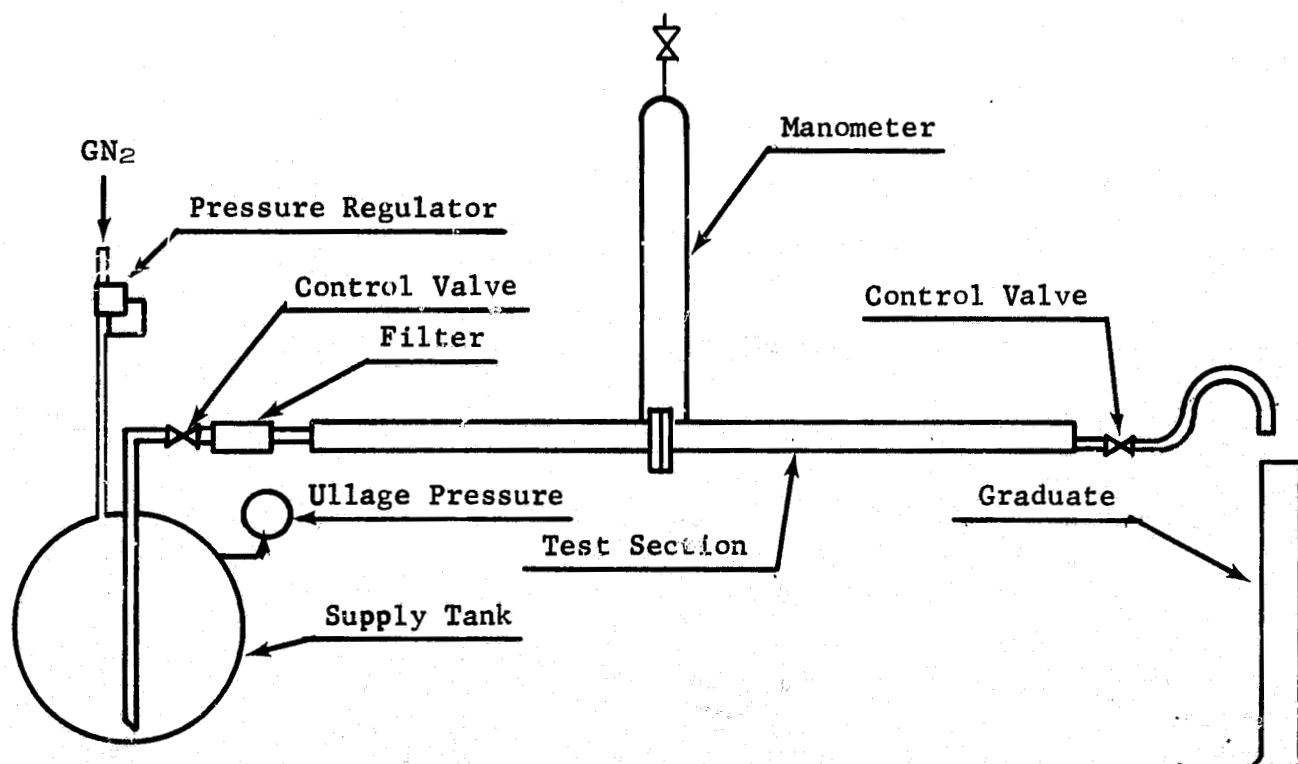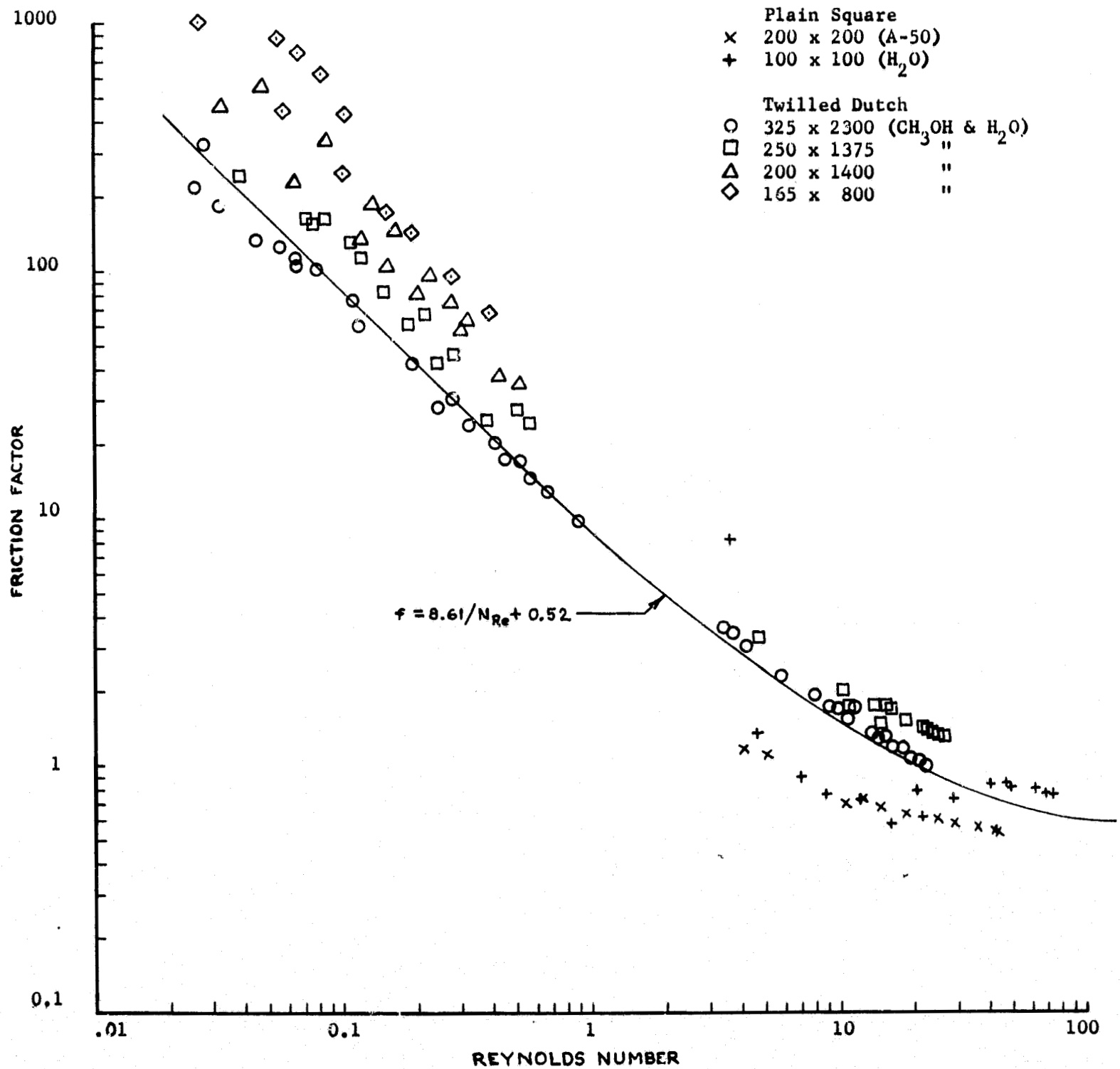| Screen No.	Weave	Mesh Size
1	Dutch-Twill	325 x 2300
2	Dutch-Twill	200 x 1400
3	Dutch-Twill	250 x 1375
4	Dutch-Twill	165 x 800
5	Square Weave	100
All specimens of stainless steel.		

Fig. B-3 Test Setup Schematic

Fig. B-4 Martin Marietta Screen Flow Data